

SIMULATION OF LAUNCHING AND SELF-UPENDING OF A SPAR HULL

A Thesis

by

SANGHUN SON

Submitted to the Office of Graduate and Professional Studies of  
Texas A&M University  
in partial fulfillment of the requirements for the degree of

MASTER OF SCIENCE

Chair of Committee,	Richard Mercier
Committee Members,	Robert Randall
	Achim Stössel
Head of Department,	Sharath Girimaji

May 2017

Major Subject: Ocean Engineering

Copyright 2017 Sanghun Son

## ABSTRACT

The goal of this research is to develop an effective and efficient plan for the installation of a spar using the barge launching method. Relative to the conventional method of installing spars, the barge launching method enables the elimination of some operations and therefore has the potential to reduce installation costs and schedule.

Through numerical simulations based on fundamental equations of motion, the trajectory analysis of the spar and barge during all stages of the launching and spar upending process is performed to verify that the spar, as designed, can be safely installed using the barge launching method.

The derivation of the equations motions based on conservation of momentum and use of free body diagrams is provided. The coupled equations of motion are integrated in time and the results are sufficiently reasonable to understand the global behavior of the dynamics of the spar and the barge on the sea. The numerical time integration of the matrix system of equations is performed using Matlab ODE solver based on fourth and fifth order Runge-Kutta formulas. A detailed flow chart for the simulation procedure is provided.

Two basic launching scenarios are considered: launching from the top of the spar and from the bottom of the spar. For each of these launch scenarios, three cases involving different trim angles and kinetic friction coefficients are investigated. Based on detailed analysis of the simulation results it is concluded that although both launch

scenarios may be feasible, the bottom launch scenario occurs at slower speed and is therefore preferable.

## DEDICATION

Thanks to my mother Younghee Won, father Jikhwan Sohn and younger brother Heegeun Sohn for their encouragement, patience and love.

I hope for my lovely niece Yeonwoo Sohn, my younger brother's daughter, happiness in life.

## ACKNOWLEDGEMENTS

I would like to thank my committee chair, Dr. Richard Mercier, for his guidance, inspiration and encouragement to realize my creative idea during my whole study.

I also would like to thank my committee members, Dr. Robert Randall and Dr. Achim Stössel, for their guidance and support throughout the course of this research.

I reserve special thanks to my previous company manager, Chungun Cho, for his continuous support and sharing his valuable knowledge and experience in the practical field.

Thanks are extended to my elder cousin sister, the head of a department of Samsung Electric Ltd, Co., Jonghee Sohn, for her guidance and sharing her experience in the practical field and my patent with this research.

Thanks also go to my friends and colleagues, Deogsang Bae, Woochul Jeong, Junho Lee, Junrak Son, Jinyoung Kim, Byungjin Kim, Dongyoung Lee, Soobum Bae and Jongsuk Shin for sharing their knowledge in numerical modeling analysis and mathematical theory.

## CONTRIBUTORS AND FUNDING SOURCES

### **Contributors**

This work was supervised by a thesis committee consisting of Professor Richard Mercier and Robert Randall of the Department of Ocean Engineering and Professor Achim Stössel of the Department of Oceanography.

All work for the thesis was completed by the student, under the advisement of Dr. Richard Mercier of the Department of Ocean Engineering.

### **Funding Sources**

There are no outside funding contributions to acknowledge related to the research and compilation of this document.

## NOMENCLATURE

$\phi$	Total velocity potential
$\eta$	Free surface elevation
$C_D$	Drag coefficient
$\Theta$	Pitch trim angle
$X_g$	X-axis of global coordinate system
$Z_g$	Z-axis of global coordinate system
$X_b$	X-axis of body coordinate system
$Z_b$	Z-axis of body coordinate system
FWD	Foreword of barge
AFT	Aft end of barge
M.S.L	Mean sea level
PSC	Portside center water ballast tank
SBC	Starboard center water ballast tank
PSO	Portside oil and lubricant tank
SBO	Starboard oil and lubricant tank
PSW	Portside water ballast tank
SBW	Starboard water ballast tank
C11	11th Center water ballast tank
CoG or CG	Center of gravity
CoB	Center of buoyancy

$X_{CoG}$	Center of gravity at X-axis
$Z_{CoG}$	Center of gravity at Z-axis
$X_S$	X-axis at spar fixed reference
$Z_S$	Z-axis at spar fixed reference
$X_L$	X-axis at barge fixed reference
$Z_L$	Z-axis at barge fixed reference
$\theta_S$	Pitch trim angle of spar hull at global coordinate system
$\theta_L$	Pitch trim angle of barge at global coordinate system
$M_{ij}$	Mass of body
$A_{ij}$	Added mass of body
$\ddot{\xi}_j$	Position coordinate or angle
$F_i$	External force
$C_i$	Coupling force
$F$	Force
$\rho$	Fluid density
$g$	Gravitational acceleration
$R$	Radius
$V$	Velocity
$t$	Time
$F_3$	Heave direction force
$A_{11}$	Added mass for surge
$A_{33}$	Added mass for heave



$A_{55}$	Added mass for pitch
$\forall$	Submerged volume
$h$	Submergence depth
$\delta$	Representation of $h/R$
$F_E$	Water entry force
$C_m$	Inertia coefficient
$Ca$	Added mass coefficient
$u$	Current velocity
$v$	Body velocity
$\dot{u}$	First order of $u$
$\dot{v}$	First order of $v$
$A_w$	Submerged area to normal velocity of body
$C_f$	Friction coefficient
$F_N$	Normal reaction force
$F_U$	Friction force of body
$W_S$	Weight of spar
$m_S$	Mass of spar
$W_L$	Weight of barge
$m_L$	Mass of barge
$m_R$	Mass of rocker arm
$m_{B1\sim B11}$	Each filled ballast water mass
$W_{B1\sim B11}$	Each filled ballast water weight

$X_{LgR}$	Barge-fixed $X_L$ -coordinate of rocker arm pivot point
$Z_{LgR}$	Barge-fixed $Z_L$ -coordinate of rocker arm pivot point
$X_{LB1\sim LB11}$	Barge-fixed $X_L$ -coordinates of ballast tank
$Z_{LB1\sim LB11}$	Barge-fixed $Z_L$ -coordinates of ballast tank
$F_W$	Hydraulic jack force
$F_{DSH}$	Horizontal drag force for spar
$F_{DSV}$	Vertical drag force for spar
$F_{DL}$	Drag force for barge projected area
$X_{DS}$	Spar-fixed $X_S$ -coordinate of line of action of vertical drag force
$Z_{DS}$	Spar-fixed $Z_S$ -coordinate of line of action of horizontal drag force
$X_{LN}$	Barge-fixed $X_L$ -coordinate of normal force
$Z_{LU}$	Barge-fixed $Z_L$ -coordinate of friction force
$X_{SBL}$	Spar-fixed $X_S$ -coordinate of spar buoyancy force
$X_{ES}$	Spar-fixed $X_S$ -coordinate of spar water entry force
$Z_{SU}$	Spar-fixed $Z_S$ -coordinate of line of action of friction force
$Z_{SW}$	Spar-fixed $Z_S$ -coordinate of line of action of hydraulic force
$B_S$	Buoyancy of spar
$B_L$	Buoyancy of barge
$I_S$	Inertial moment of spar
$I_L$	Inertial moment of barge
$\ddot{X}_S$	Second order of X-axis displacement for spar
$\ddot{Z}_S$	Second order of Z-axis displacement for spar

$\ddot{X}_L$	Second order of X-axis displacement for barge
$\ddot{Z}_L$	Second order of Z-axis displacement for barge
$\ddot{\theta}_S$	Second order of spar pitch trim angle
$\ddot{\theta}_L$	Second order of barge pitch trim angle
ODE	Ordinary differential equation
Stbd	Starboard

## TABLE OF CONTENTS

	Page
ABSTRACT .....	ii
DEDICATION .....	iv
ACKNOWLEDGEMENTS .....	v
CONTRIBUTORS AND FUNDING SOURCES.....	vi
NOMENCLATURE.....	vii
TABLE OF CONTENTS .....	xii
LIST OF FIGURES.....	xiv
LIST OF TABLES .....	xvii
1. INTRODUCTION.....	1
1.1 Motivation and Objectives .....	4
1.2 Literature Survey.....	5
1.3 Approach.....	8
1.4 Overview of Thesis .....	9
2. OVERVIEW OF SPAR LAUNCHING PROCEDURE.....	11
2.1 Launch Trajectory Analysis Procedure.....	11
2.2 Description of Structures.....	13
2.3 Design Parameters.....	17
2.4 Coordinate Systems.....	18
2.5 Scenarios and Initial Conditions .....	20
2.6 Ballasting Plan.....	22
3. MODEL FORMULATION.....	26
3.1 Equations of Motion.....	26
3.2 Free Body Diagram and Equations of Motion .....	27
3.3 Bearing Force and Friction Force.....	32
3.4 Hydrostatic Buoyancy .....	33
3.5 Hydrodynamic Forces .....	38

4. NUMERICAL SOLUTION PROCEDURE .....	43
4.1 Matlab ODE Solver .....	43
4.2 Matrix System of Equations .....	46
4.3 Runge-Kutta Method .....	48
4.4 Simulation Flow Chart .....	52
5. LAUNCHING AND UPENDING SIMULATION RESULTS .....	60
5.1 Added Mass for Spar Hull .....	60
5.2 Discussion of Results .....	66
5.3 Feasibility of Launching a Spar .....	128
6. CONCLUSIONS AND RECOMMENDATIONS .....	130
REFERENCES .....	132
APPENDIX A - BALLASTING PLAN TABLE .....	134
APPENDIX B - VITA .....	140

## LIST OF FIGURES

	Page
Figure 1 Conventional method for spar hull installation.....	2
Figure 2 Launching and self-upending method for spar hull installation .....	3
Figure 3 Drag coefficient versus Reynolds number for a smooth circular cylinder .....	18
Figure 4 Body-fixed coordinate systems.....	19
Figure 5 Spar hull and barge model for bottom launching .....	20
Figure 6 Spar hull and barge model for top launching.....	21
Figure 7 Ballast tank compartments .....	22
Figure 8 Ballasting water ratios on full tank for Case study 1A .....	24
Figure 9 Ballasting water ratios of full tank for Case study 1B & 1C .....	24
Figure 10 Ballasting water ratios on full tank for Case study 2A .....	25
Figure 11 Ballast water ratios on full tank for Case study 2B & 2C.....	25
Figure 12 Free body diagram for spar hull and barge .....	27
Figure 13 Four cases submerged volume .....	34
Figure 14 $H_d$ and $S$ .....	35
Figure 15 Submerged area for the barge volume .....	37
Figure 16 Trimmed model for the WAMIT .....	40
Figure 17 Drag force .....	42
Figure 18 Flow chart .....	55
Figure 19 Added mass of spar hull - Case study 1 .....	64
Figure 20 Added mass of spar hull - Case study 2.....	65
Figure 21 Initial position - Case study 1 .....	69
Figure 22 Initial position - Case study 2 .....	70

Figure 23 Start sliding - Case study 1 .....	71
Figure 24 Start sliding - Case study 2 .....	72
Figure 25 Enter water - Case study 1 .....	73
Figure 26 Enter water - Case study 2 .....	74
Figure 27 Primary rocker arm rotates - Case study 1 .....	75
Figure 28 Rocker arms rotate - Case study 2 .....	76
Figure 29 Secondary rocker arm rotates - Case study 1 .....	77
Figure 30 Spar separates from barge - Case study 1 .....	78
Figure 31 Spar separates from barge - Case study 2 .....	79
Figure 32 Whole launch phase - Case study 1 .....	80
Figure 33 Whole launch phase - Case study 2 .....	81
Figure 34 Oscillation and drift after launch - Case study 1 .....	82
Figure 35 Oscillation and drift after launch - Case study 2 .....	83
Figure 36 Acceleration for spar hull and barge - Case study 1 .....	93
Figure 37 Acceleration of spar hull and barge - Case study 2 .....	94
Figure 38 Velocity for spar hull and barge - Case study 1 .....	97
Figure 39 Velocity for spar hull and barge - Case study 2 .....	98
Figure 40 Displacement for spar hull and barge - Case study 1 .....	100
Figure 41 Displacement for spar hull and barge - Case study 2 .....	101
Figure 42 Angular acceleration for spar hull and barge - Case study 1 .....	103
Figure 43 Angular acceleration for spar hull and barge - Case study 2 .....	104
Figure 44 Pitch angle for spar hull and barge - Case study 1 .....	106
Figure 45 Pitch angle for spar hull and barge - Case study 2 .....	107
Figure 46 Coupling forces - Case study 1 .....	109

Figure 47 Coupling forces - Case study 2 .....	110
Figure 48 Hydrodynamic force for spar hull - Case study 1 .....	112
Figure 49 Hydrodynamic force for spar hull - Case study 2 .....	113
Figure 50 Reynolds number for spar hull upper part- Case study 1 .....	115
Figure 51 Reynolds number for spar hull upper part - Case study 2 .....	116
Figure 52 Reynolds number for spar hull lower part - Case study 1 .....	117
Figure 53 Reynolds number for spar hull lower part - Case study 2 .....	118
Figure 54 Drag coefficient for spar hull upper part - Case study 1 .....	119
Figure 55 Drag coefficient for spar hull upper part - Case study 2 .....	120
Figure 56 Drag coefficient for spar hull lower part - Case study 1 .....	121
Figure 57 Drag coefficient for spar hull lower part - Case study 2 .....	122
Figure 58 Buoyancy of spar hull and barge - Case study 1 .....	124
Figure 59 Buoyancy of spar hull and barge - Case study 2 .....	125
Figure 60 Center of buoyancy of spar hull and barge - Case study 1 .....	126
Figure 61 Center of buoyancy of spar hull and barge - Case study 2 .....	127



## LIST OF TABLES

	Page
Table 1 Spar properties .....	14
Table 2 Barge properties .....	15
Table 3 Design parameters .....	17
Table 4 Initial condition for each scenario .....	22
Table 5 Ballast tank size.....	23
Table 6 Added mass coefficient of spar hull for bottom launch .....	61
Table 7 Added mass coefficient of spar hull for top launch .....	62
Table 8 Summary of results.....	84
Table A 1 Ballast plan for Case 1A.....	134
Table A 2 Ballast plan for Case 1B & 1C .....	135
Table A 3 Ballast plan for Case 2A.....	137
Table A 4 Ballast plan for Case 2B & 2C .....	138

## 1. INTRODUCTION

A spar, floated vertically with a large diameter cylinder, has become increasingly popular as a reliable and economic understructure concept to support the topside of an offshore oil platform in deep water. The spar is typically categorized as either a classic spar, a truss spar or a cell spar. The classic spar, encircled by helical strakes to mitigate the horizontal motions caused by vortex induced vibrations, is selected as a candidate for the barge launching method investigated in this research.

The conventional method to install a spar hull (Figure 1) involves a sequence of operations from transportation to upending of the spar hull. After floating the spar hull on the water, the strakes are assembled offshore and then the ballast water is added. The newly developed method of the barge launching and self-upending of the spar hull, illustrated in Figure 2, enables the elimination of some of the operations relative to the conventional installation method.

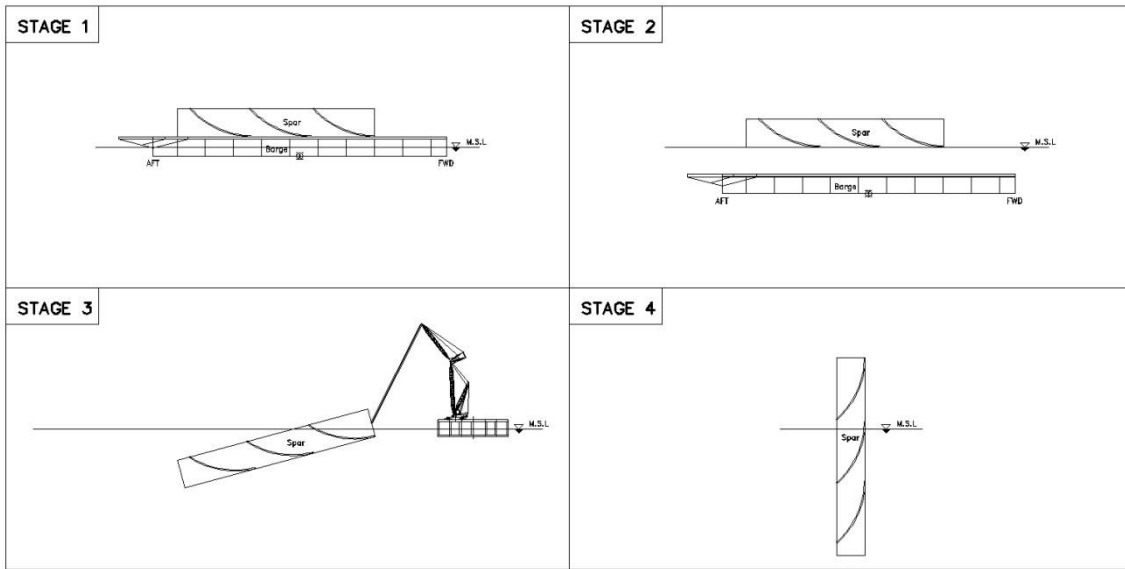


**Figure 1 Conventional method for spar hull installation**

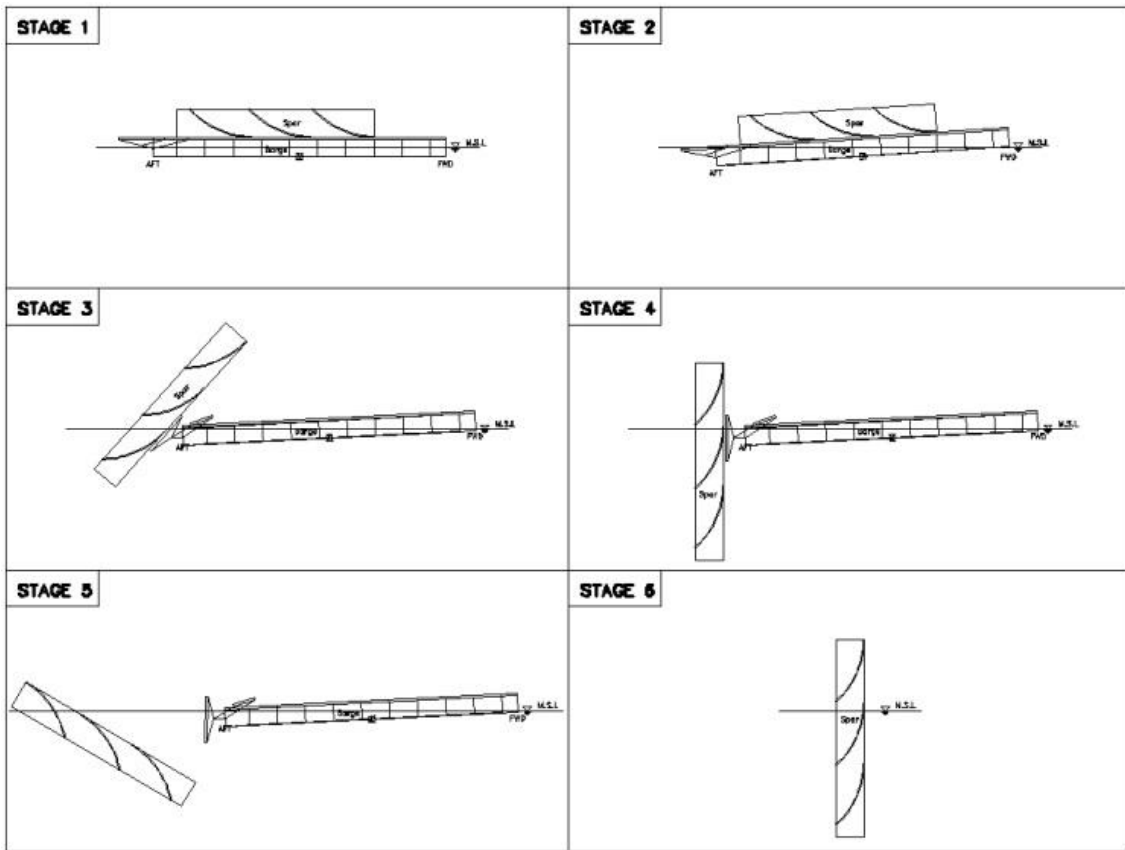


**Figure 2 Launching and self-upending method for spar hull installation**

## 1.1 Motivation and Objectives

This research is intended to investigate the feasibility of the barge launching method for spar installation, through detailed simulation of the associated operations ranging from pre-launch activities to the self-upending of the spar.

With the conventional method, it usually takes several weeks to prepare for the installation of the spar hull by floating the hull and assembling the strakes after wet towing the hull to the offshore field. Lifting the spar for upending and ballasting it with water to lower the center of gravity for stability take additional time.

In contrast to the conventional installation method for the spar hull, the barge launching and self-upending method can remove several operations such as assembling strakes and wet towing using tug boats because the spar hull is transported to the installation field directly on a barge. Furthermore, launching a spar already filled with ballast water rather than ballasting the spar as part of the upending process can reduce expensive offshore installation.

The primary result of this research is the simulation of the trajectories of a spar and barge during all phases of the launching and spar upending process. The ballasting plan for the barge is prepared to define the pre-launching condition and serve as the initial condition. The time domain simulations will compute.

- the relative location of the spar hull and barge
- the relative acceleration and velocity of the spar hull and barge
- the trimmed angle of the barge
- the change of the angle of the spar hull

- the bearing force of the spar hull on the barge deck and the friction force between the spar hull and the skid beam on the barge deck during launching
- the time –dependent change in the total buoyancy and center of buoyancy of the spar and barge
- the water entry force of the spar hull (dependent on the infinite frequency added mass) as it hits the water and penetrates through the surface
- the Reynolds-number dependent drag coefficient and drag force as the spar hull proceeds through the water
- the trajectories for the spar hull and barge during the entire launch sequence from pre-launching through self-upending of the spar hull

Note that this research does not consider any structural strength issues because the aim of this research is simply to investigate the feasibility of installing a spar by this launching method through simulation of global motions.

## **1.2 Literature Survey**

L.Hambro (1982) developed a method for jacket launching simulation involving the differentiation of the coupling constraints. He used the holonomic constraints acting on the jacket-barge system. During launching, constraint forces of equal magnitude and opposite signs act on the jacket and barge respectively. When the jacket has left the barge, he has to differentiate the constraint equations twice with respect to time, giving

additional equations of motion. This method avoids the need to find generalized coordinates such that all constraint forces disappear in the equations of motion. He used the equations of motion of the two systems and solved the programmed system of equations by standard numerical techniques (Runge-Kutta method). He considered also, two-dimensional motion and assumed that both bodies are symmetric.

S.K. Bhattacharyya, V.G. Idichandy and N. R. Joglekar (1985) surveyed the experimental investigation of load-out, launching and upending of offshore steel jackets. Their experimental study on the similitude of scaled models was devised by characteristic equations. They simulated the load-out operation, launching operation and upending operation. They investigated the launching velocities, trajectories and load.

S.K. Chakrabarti (1994) studied the scale effects on a unique launch sequence of a gravity-based structure. He used the support buoyancy can for a cushion of compressed air during launch and load out. By the test, he studied the launching sequence and stability of the rig on the buoyancy can.

C.H. Jo, K.S. Kim and S.H. Lee (2001) studied the effects of parameters on draft and trim angle using numerical simulation. They investigated the loads to the jacket during launching to solve the equation of motion. In this study, the five launch phases were classified; sliding on the barge due to the winch, sliding on the barge due to gravity or self-weight, sliding due to the winch with a tipping of the rocker arm, sliding due to self-gravity weight with a tipping on the rocker arm and separating jacket from barge.

Von Karman (1929) conducted the calculations of the force on a wedge-shaped horizontal cylindrical body as the cylinder hit the water and proceeded through the water.

He said that the effect of the air is negligible compared with the effect of the water in the case of the seaplane float entering the water. And he said that the apparent increase of the mass of the plate is equal to the mass of fluid contained in a circular cylinder of diameter with same width of the plate. Therefore its inertia is considered with the submerged volume for the water entry problem.

J.H.G. Verhagen (1967) investigated the phenomena occurring during the impact of a flat plate on a water surface both theoretically and experimentally. He explained the experimental results by taking into account the influence of the compressible air layer caught between the falling plate and the water surface. He also provided numerical results showing the effects of falling mass, drop velocity, and plate dimensions on the maximum impact pressure. He observed excellent agreement between theory and experiment for a flat bottom body with large mass, slamming into the water. To solve the water entry problem with a heavy body, the theoretical approach can be valid.

M. Greenhow and Li Yanbao (1987) reviewed and applied the added masses for circular cylinders to the water entry problem. They considered, in detail, the high speed entry of a cylinder into initially calm water under the assumption that  $\phi = 0$  on  $\eta = 0$ . They reviewed the Wagner approach mathematically.

O.M. Faltinsen (1990) reviewed the hydrodynamic vertical force when a body enters into the water. And he proposed a model for the water entry force for the cylinder with the high speed downward vertical velocity.

Morison (1950) proposed an equation for the force exerted by surface waves on a slender cylindrical object. His equation considers the total hydrodynamic force on the



object as the sum of the drag force and the inertia force. The Morison equation is applied during oscillation of the spar hull. The hydrodynamic force term of the Morison equation is developed with the hydrodynamic vertical force for the water entry problem.

William H. Press, Saul A. Teukolsky, William T. Vetterling and Brian P.

Flannery (2007) reviewed the Runge-Kutta method and proposed the adaptive step size control for the Runge-Kutta method. To achieve predetermined accuracy with minimum computational effort, the adaptive step size control is used. And many small time steps were applied for some distinct phases sensitive to the time step due to the high speed launching.

### **1.3 Approach**

In order to perform the simulations of barge launching and self-upending of a spar described above, a mathematical model for the coupled dynamics of the spar and barge during all phases of the launch sequence was first formulated. A numerical solution procedure was then developed and implemented as Matlab code. The code was exercised to produce the simulation results presented and discussed herein. The solution procedure also involves use of WAMIT (2013) to obtain infinite frequency added mass values needed to calculate the water entry force. WAMIT is a commercial program for linear analysis of the surface wave interactions with floating structures.

In essence, a two dimensional model for a spar and barge is used for this analysis because the vessels are assumed to be symmetric template structures about the plane of

the launching operation. Out-of-plane forces, moments and responses such as rolling effects are neglected in this symmetric model.

Two basic scenarios are investigated. The first scenario is to launch the spar from the bottom of the spar; that is the bottom of the spar is in the path of launching as the spar slides off the deck of the launching barge. The second scenario is to launch the spar from the top of the spar; that is, the top of the spar is in the path of launching as the spar slides off the deck of the launching barge. For both of these launch scenarios, three cases involving different trim angles and kinetic friction coefficients are investigated.

The detailed scenarios and descriptions are provided in Sections 2.1, 2.5 and 2.6.

#### **1.4 Overview of Thesis**

This thesis consists of six chapters and an appendix.

Chapter 1 explains the motivation and objectives of this research. The scenarios are briefly introduced and the literature survey is presented in this chapter.

Chapter 2 explains the parameters and coordinates associated with the numerical simulation. In this chapter, the ballasting plan for the pre-launching condition is set and a hydraulic jack load is defined to overcome the static friction and initiate the launch. Also the distinct stages for the launching procedure are defined.

Chapter 3 develops the formulation for the simulation model and defines the equation of motions. This chapter explains the logical assumptions for the applied loads using the free body diagrams and fundamental formulas.

Chapter 4 presents the numerical solution procedure with the aid of a flow chart. In this chapter, the ODE solver and the Runge-Kutta method are explained for the numerical analysis method.

Chapter 5 provides and discusses the simulation results from the six case studies.

Conclusion and recommendations based on the analysis results are presented in Chapter 6, as well as suggestions for future studies.

The detailed ballasting plan table for each of the case studies is included in the Appendix.

## 2. OVERVIEW OF SPAR LAUNCHING PROCEDURE

### 2.1 Launch Trajectory Analysis Procedure

This research addresses the feasibility of installing a spar hull using the barge launching method after transportation. The distinct stages of the launch sequence are defined by the distinct systems of forces that are applicable.

The pre-launching phase is for initiation of spar sliding at the designed draft and pitch trim angle of the barge. This is achieved by ballasting compartments in the barge as needed, assuming calm water. In this phase, the static equilibrium of the spar resting on the barge deck with its self-weight should be satisfied.

The first phase is to start sliding the spar on the skid beams. At the initial time, 6 hydraulic jacks with 500-ton capacity are used to assist in sliding the spar hull to provide an initial velocity and to avoid unfortunate accident with a safe working condition. The total hydraulic force includes a 10% contingency factor on the required force to start sliding the spar smoothly by pushing the spar. When the kinetic friction coefficient is applied after the spar starts sliding, the hydraulic jacks will no longer be in use. As the spar slides on the deck, the trim angle of the barge changes since the bearing reaction force on the skid rails changes with the position of the spar. This phase ends once the spar touches down through the water surface.

During the second phase the spar starts to enter the water and become partially submerged. Once the spar hull begins to enter the sea, the buoyancy and center of buoyancy of the spar (generated by the submerged volume), the water entry force and

the drag forces on the spar must be considered in the dynamic equilibrium. The water entry force is proportional to the infinite frequency added mass, which is dependent on the instantaneous position of the spar. This phase will continue until the spar's center of gravity reaches a point directly above the primary tilting beam hinge pin.

In the third phase, the primary tilting beam separates from the barge and the primary rocker arm rotates with the spar as the CoG of the spar hull moves aft of the pivot point on the primary rocker arm. This occurs if the righting moment from the buoyancy of the spar is insufficient to overcome the tilting moment from the weight of the spar, or more precisely, if the tilting moment on the rocker arm determined by the dynamic moment equilibrium is positive. If a positive tilting moment is not generated, then the primary tilting beam does not separate, the primary rocker does not rotate and the spar exerts a righting moment on the barge. The change of the spar buoyancy and the center of buoyancy for the spar are the sensitive factors influencing the behavior of the barge and spar. Assuming the primary rocker arm does rotate then this phase will continue until the pitch angle limit of the rocker arm (15 degrees relative to the barge) is reached.

In the fourth phase, the secondary tilting beam separates from the primary tilting beam and the secondary rocker arm rotates with the spar as its center of gravity moves aft of the secondary rocker arm pivot point. Again, the tilting of the secondary rocker arm is determined by the dynamic moment equilibrium of the coupled spar and barge. If a positive tilting moment is not generated, then the secondary tilting beam does not separate and the secondary rocker does not rotate. The result from the spar equilibrium

has a direct influence on the barge equilibrium. Assuming the secondary rocker arm does rotate then this phase will continue until the spar completely separates from the barge and the two vessels start to move independently from each other.

The fifth phase is the final stage where the spar and barge move independently. After the spar separates from the barge, the bearing force and the relative friction force on the barge are zero and the barge moves forward continuously under its remaining momentum. As time progresses the drag force applied to the barge will slow its drift velocity while the barge achieves a stable trim angle determined by the static equilibrium resulting from the ballasted compartments and without the weight of the spar.

Meanwhile, the spar will oscillate in heave and pitch as it drifts away from the barge. As time progresses the drag force applied to the spar will dampen the oscillations and slow the drift velocity. The spar will reach static equilibrium in a stable upright position determined by its ballasted compartments. This means that, prior to initiating the launch sequence, the spar must be ballasted on the barge so that it will adopt the desired stable equilibrium position after the launch is complete.

## **2.2 Description of Structures**

The spar hull modeled in this research is a cylindrical structure of 25 m diameter and 175 m length in the longitudinal direction. The dry weight of the spar hull is assumed to be 13,000 metric tons, and the transportation weight, assumed and selected to realize the behavior of a spar to fulfill the objectives of this research, is 54,000 metric tons.

The barge assumed in this research is a rectangular template structure of 260 m length, 63 m breadth and 15 m depth. The lightship weight, assumed to be representative of a real barge in the field, is 48,560 metric tons including the rocker arms, skid beams and the non-modeled structures for the actual transportation and launching condition in the field.

The primary rocker arm, secondary rocker arm, tilting beam and skid beam, designed considering the strake height and actual behavior of the spar at each launch phase, are modeled on the barge.

Further details of the spar are summarized in Table 1.

**Table 1 Spar properties**

Length (m)	175
Diameter (m)	25
Dry weight (Mton)	13,000
Transportation weight including ballast water weight (Mton)	54,000
XCG from center (m)	0
YCG form center (m)	0
ZCG from keel (m)	51.69
Ryy, Pitch radius of gyration (m)	41.352

The barge is equipped with double rocker arms and the barge is modeled to account for its buoyancy. Details of the barge are provided in Table 2.

**Table 2 Barge properties**

Length between perpendiculars, LBP (m)	260
Breadth at midship center (m)	63
Breadth at bow (m)	42
Depth (m)	15
Lightship weight (Mton)	48,560
Xcg from bow (m)	136.76
Ycg form center (m)	0
Zcg from keel (m)	7.5
Ryy, Pitch radius of gyration (m)	75.2
Total ballast tanks	45
Skid beam length (m)	220
Skid beam height (m)	4
Primary rocker arm	
Pin location, x (m) from bow	260
Pin location, y (m) from center	+/- 6
Pin, location, z (m) from keel	7.1
Primary tilt beam length forward of pin (m)	30.625
Primary tilt beam length aft of pin (m)	15.313
Maximum rotation (deg)	15
Secondary rocker arm	
Pin location, x (m) from bow	275.313



**Table 2 Continued**

Pin location, y (m) from center	+/- 6
Pin location, z (m) from keel	11.05
Secondary tilt beam length forward of pin (m)	15.313
Secondary tilt beam length aft of pin (m)	15.312
Skid beam length on the rocker arm #1 & 2 (m)	61.25

### 2.3 Design Parameters

The assumed values of various design parameters, coefficients and initial condition are provided in Table 3.

**Table 3 Design parameters**

Drag coefficient for flow normal to plate	2.0
Drag coefficient for inclined rectangular barge	1.6
Coefficient of static friction between spar and launch rails	0.1
Coefficient of kinetic friction between spar and launch rails	0.05 or 0.06*
Hydraulic jack force to initiate spar sliding (Mton)	2,964
Sea water density (kg/m <sup>3</sup> )	1,025
Pre-launch barge trim angle (radian)	0.05 or 0.06*
Barge draft at midship for initial condition launching from bottom (m)	8
Barge draft at midship for initial condition launching from top (m)	9.5

\* The trim angle and kinetic friction coefficient are set equal to either 0.05 or 0.06 for the individual launching scenarios (See Section 2.5).

The local drag force on an element of the spar is modeled with a drag coefficient that is dependent on the instantaneous Reynolds number for the smooth cylinder. Figure 3 is the assumed curve of drag coefficient versus Reynolds number.

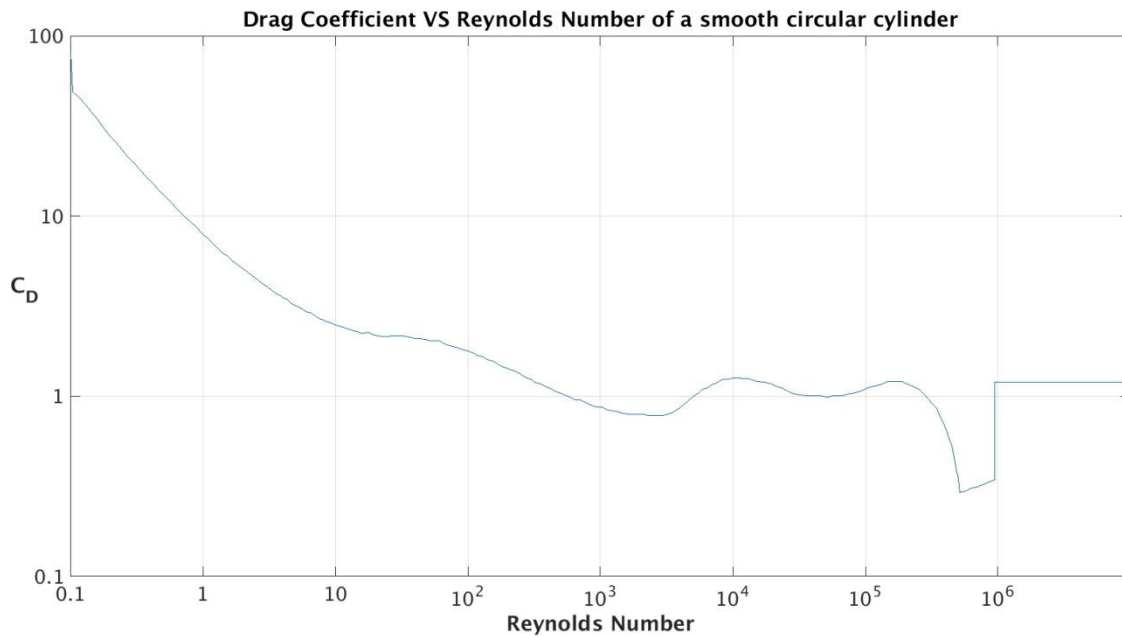


**Figure 3 Drag coefficient versus Reynolds number for a smooth circular cylinder**

## 2.4 Coordinate Systems

The two dimensional time domain analysis of the launch sequence is performed with body-fixed X axis, Z axis and  $\theta$  as generalized coordinates for the spar and launch barge. The barge and spar are each assumed to be symmetric to the port and starboard in all aspects. For the initial at rest condition, the parallel body-fixed X axes for the barge and spar are positive toward the bow of the barge and the parallel Z axes point vertically upward.

The origin of the body-fixed coordinate system for the barge is located at its center of gravity for the barge at the initial condition. This is also the assigned origin of the global coordinate system. The draft of the barge is measured at the origin of its body-fixed coordinate system.

Similarly, the origin of the body-fixed coordinate system for the spar is located at its center of gravity. When the pitch angles for the spar and barge are both zero, the X axes of the body-fixed systems are parallel to, and the Z axes of the body-fixed systems are perpendicular to, the X axis of the global system. Figure 4 is a sketch of the body-fixed coordinate systems at an arbitrary point in time during the launch sequence. The behavior of the spar and barge at each instant of time is described with reference to the positions and orientations of the two body-fixed coordinate systems relative to the global coordinate system.

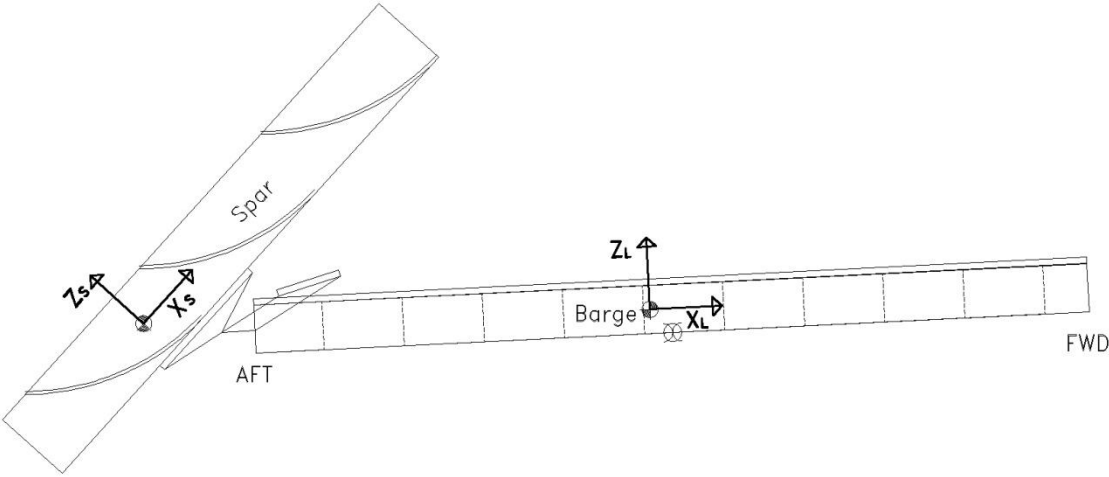


**Figure 4 Body-fixed coordinate systems**

## 2.5 Scenarios and Initial Conditions

This research investigates two primary case studies. The first case study is launching a spar hull from the bottom of the spar. In this case, the bottom of the spar is located in the path of launching, and the bottom of the spar touches down on the water surface first. The second case study is launching a spar from the top of the spar. In this case, the top of the spar is located in the path of launching and the top of the spar approaches to the water surface first.

For the first case study, illustrated in Figure 5, the center of gravity of the spar (corresponding to the origin of the spar body-fixed coordinate system) is positioned 50 meters aft of the origin of the body-fixed coordinate system for the barge (which is located at its center of gravity) and the spar centerline is aligned on the barge centerline. The elevation of the spar origin relative to the barge origin is in part determined by the deck plate and skid beam height. In this initial resting condition, the pitch angle is zero, which means that the barge compartments have not yet been ballasted according to the ballasting plan for the pre-launching phase.

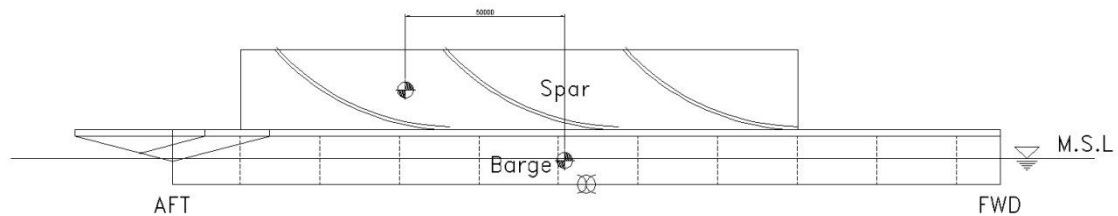


**Figure 5 Spar hull and barge model for bottom launching**

For the second case study, illustrated in Figure 6, the center of gravity of the spar (corresponding to the origin of the spar-fixed coordinate system) is positioned 8 meters forward of the barge center of gravity (corresponding to the origin of the barge-fixed coordinate system) and 0 meter port of the barge centerline. Again, the elevation of the spar origin relative to the barge origin is in part determined by the deck plate and skid beam height.

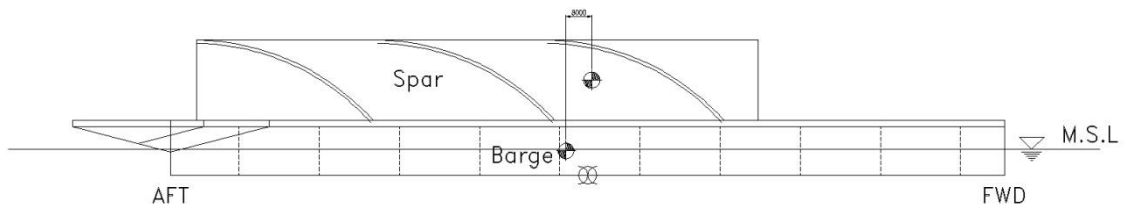


**Figure 6 Spar hull and barge model for top launching**

These two launching cases are each carried out with three scenarios for the initial trim angle and the assigned kinetic coefficient of friction. Table 4 provides the initial conditions for the six scenarios.

**Table 4 Initial condition for each scenario**

Case Study	Trim Angle (radian)	Kinetic Friction Coefficient	Initial Spar Location Aft of Barge Origin (m)	Initial Draft at Midship
1A	0.05	0.05	50	8
1B	0.06	0.06	50	8
1C	0.06	0.05	50	8
2A	0.05	0.05	-8	9.5
2B	0.06	0.06	-7	10
2C	0.06	0.05	-7	10

## 2.6 Ballasting Plan

The assumed compartmentation for the launch barge is based on publicly available information for the Heerema H851S launch barge provided by Bentley (<http://bentley.ultramarine.com/hdesk/tools/vessels/lbarges/h851.htm>). The assumed compartmentation is shown in Figure 7.

PSW 11	PSW 10	PSW 9	PSW 8	PSW 7	PSW 6	PSW 5	PSW 4	PSW 3	PSW 2	
PSC 11	PSC 10	PSC 9	PSC 8	PSC 7	PSC 6	PSC 5	PSC 4	PSC 3	PSC 2	PSC 1
C 11	SBC 10	SBC 9	SBC 8	SBC 7	PSO 6	SBC 5	SBC 4	SBC 3	SBC 2	SBC 1
					SBC 6					
SBC 11					SBC 6					
SBW 11	SBW 10	SBW 9	SBW 8	SBW 7	SBW 6	SBW 5	SBW 4	SBW 3	SBW 2	

**Figure 7 Ballast tank compartments**

The ballast tank dimensions are provided in Table 5 below.

**Table 5 Ballast tank size**

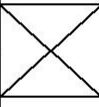
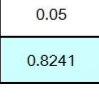
Tank No.	L (m)	B (m)	D (m)
PSC & SBC #1	13.75	21	15
PSC & SBC #2, #6, #7	25	10.75	15
PSC & SBC #3 ~ #5, #8~ #10	25	21	15
PSC & SBC #11	21.25	10.75	15
C #11	21.25	21	15
PSO & SBO #6	25	10.75	15
PSW & SBW #2 ~ #10	25	10.75	15
PSC & SBC #11	21.25	10.75	15

In order to prepare the spar for launching, the barge is trimmed to a specified pitch angle by ballasting selected tanks. At the pre-launching phase, the spar remains at rest on the barge deck under its self-weight.

To incline the barge with the pitch trim, the ballasting water is filled in the designated ballast tanks. Considering the remaining water in each ballast tank after prior transportation phases, the minimum ballast water ratio for each individual tank is assumed to be 5 % of the full tank.

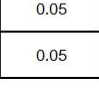
For the Case study 1A scenario, the barge system is placed at an initial midships draft of 8 m with a trim angle 0.05 radian. The ballast plan to achieve this initial condition is provided in Figure 8 and in Table A1 of the Appendix.



0.05	0.05	0.4306	0.05	0.8241	0.05	0.05	0.05	0.05	0.05	
0.05	0.7	0.05	0.05	0.05	0.05	0.05	0.05	0.05	0.05	0.05
0.05		0.05	0.05		0.05				0.05	
0.05	0.7	0.05	0.05	0.05	0.05	0.05	0.05	0.05	0.05	0.05
0.05		0.05	0.05		0.05				0.05	
0.05	0.05	0.4306	0.05	0.8241	0.05	0.05	0.05	0.05	0.05	

**Figure 8 Ballasting water ratios on full tank for Case study 1A**

For the Case studies 1B and 1C, the barge system is placed at an initial midships draft of 8 m with a trim angle 0.06 radian. The ballast plan to achieve this initial condition is provided in Figure 9 and in Table A2 of the Appendix.

0.7377	0.2093	0.05	0.05	0.05	0.05	0.05	0.05	0.05	0.05	
0.6	0.4	0.05	0.05	0.05	0.05	0.05	0.05	0.05	0.05	0.05
0.7		0.05	0.05		0.05				0.05	
0.6	0.4	0.05	0.05	0.05	0.05	0.05	0.05	0.05	0.05	0.05
0.7377		0.05	0.05		0.05				0.05	

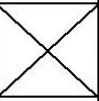
**Figure 9 Ballasting water ratios of full tank for Case study 1B & 1C**

For the Case study 2A, the barge system is placed at an initial midships draft of 9.5 m with a trim angle 0.05 radian. The ballast plan to achieve this initial condition is provided in Figure 10 and in Table A3 of the Appendix.

0.92	0.5032	0.9421	0.05	0.05	0.05	0.05	0.05	0.05	0.05	
0.92	0.98	0.05	0.05		0.05	0.05	0.05	0.05	0.05	0.05
0.94					0.05				0.05	
0.92	0.98	0.05	0.05		0.05	0.05	0.05	0.05	0.05	0.05
0.91	0.5032	0.9421	0.05	0.05	0.05	0.05	0.05	0.05	0.05	

**Figure 10 Ballasting water ratios on full tank for Case study 2A**

For the Case studies 2B and 2C, the barge system is placed at an initial midships draft of 10 m with a trim angle 0.06 radian. The ballast plan to achieve this initial condition is provided in Figure 11 and in Table A4 of the Appendix.

0.9223	0.9439	0.8188	0.05	0.05	0.05	0.05	0.05	0.05	0.05	
0.9223	0.9834	0.2	0.05		0.05	0.05	0.05	0.05	0.05	0.05
0.9421					0.05				0.05	
0.9223	0.9834	0.2	0.05		0.05	0.05	0.05	0.05	0.05	0.05
0.9223	0.9439	0.8188	0.05	0.05	0.05	0.05	0.05	0.05	0.05	

**Figure 11 Ballast water ratios on full tank for Case study 2B & 2C**

### 3. MODEL FORMULATION

#### 3.1 Equations of Motion

The coupled equations of motion for the spar and barge are integrated in time starting from the barge inclined position. During the launch sequence, the barge and spar will move relative to each other. The simulation is treated as a two-dimensional problem formulated in the plane of rotation of the barge, with phenomena such as hydrodynamic lift forces that generate out-of-plane forces and moments neglected. Consequently, the spar and barge are each modeled with 3 degrees of freedom, denoted as  $X_S, Z_S, X_L, Z_L, \theta_S, \theta_L$ .

The matrix system of equations is written as

$$([M_{ij}]) \cdot \ddot{\xi}_j = F_i + C_i \quad (3.1)$$

where  $M$  is the body mass and  $\xi$  is a position coordinate or angle. The external force vector  $F_i$  includes hydrostatic buoyancy and hydrodynamic forces. The hydrodynamic forces include the water entry force, inertia force and drag force. The coupling force vector  $C_i$  includes friction and normal reaction force contributions associated with the sliding contact between the spar and the barge.

During the launch of the spar, the viscous damping effect is neglected in comparison to the water entry force. After the complete separation of the spar hull from the barge, the viscous drag force and inertia force exerted on the spar reduce its oscillation and drift.

### 3.2 Free Body Diagram and Equations of Motion

To formulate the coupled second order ordinary differential equations for the launching simulation, the free body diagram is shown in Figure 12. The body-fixed coordinate systems  $(X_S, Z_S)$  and  $(X_L, Z_L)$  on the free body diagram were defined in Section 2.4.

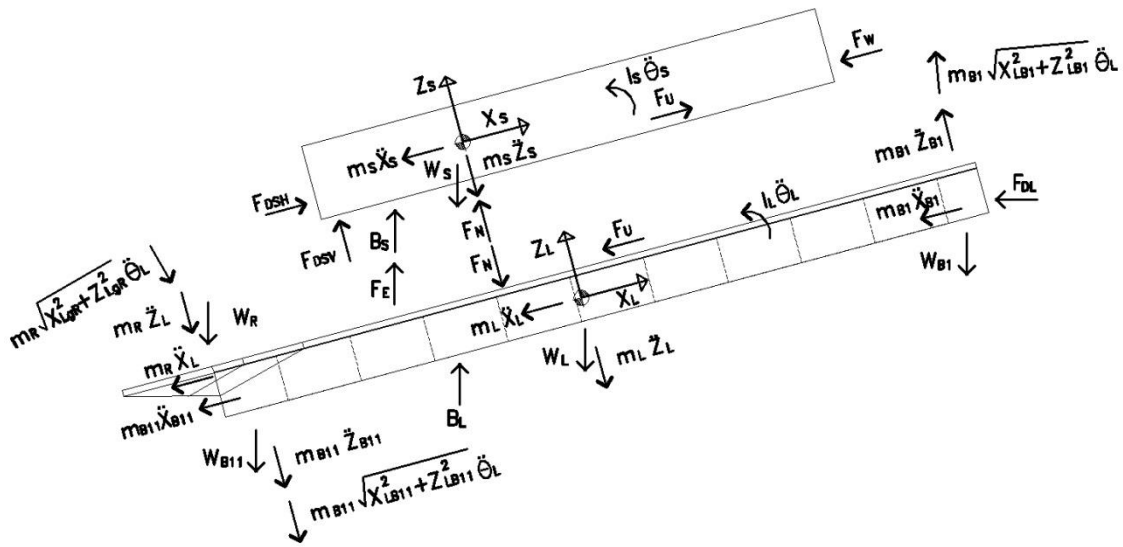


Figure 12 Free body diagram for spar hull and barge

For clarity, in Figure 12 the forces associated with ballast water tanks No. 2 through No. 10 are omitted.

In the free body diagram:

- $m_S$ ,  $m_L$  and  $m_R$  are the mass of the spar, barge and rocker arm, respectively;
- $m_{B1} \sim m_{B11}$  are each filled ballast water mass from No. 1 ballast water tank to No. 11 ballast water tank;

- $W_S$ ,  $W_L$  and  $W_R$  are the weight of the spar, barge and rocker arm, respectively;
- $W_{B1} \sim W_{B11}$  are each filled ballast water weight from No. 1 ballast water tank to No. 11 ballast water tank;
- $F_N$  is the normal bearing force and  $F_U$  is the friction force resulting from the coupling between the spar hull and barge;
- $X_{LgR}$  and  $Z_{LgR}$  are the X-direction and Z-direction distance, respectively, at the local origin of the barge for the rocker arm moment;
- $X_{LB1} \sim X_{LB11}$  and  $Z_{LB1} \sim Z_{LB11}$  are the X-direction and Z-direction distance, respectively, at the local origin of the barge for the moment arm for each ballast water tank;
- $\ddot{X}_S$ ,  $\ddot{Z}_S$ ,  $\ddot{\theta}_S$ ,  $\ddot{X}_L$ ,  $\ddot{X}_L$  and  $\ddot{\theta}_L$  are the X-direction, Z-direction and angular acceleration variables, respectively, at each body-fixed origin for the spar and barge;
- $\ddot{X}_{B1} \sim \ddot{X}_{B11}$  and  $\ddot{Z}_{B1} \sim \ddot{Z}_{B11}$  are the X-direction and Z-direction acceleration for the inertia forces of the filled ballast water from No. 1 ballast water tank to No. 11 ballast water tank, respectively;
- $I_S$  and  $I_L$  are the moment of inertia for the spar and barge, respectively;
- $B_S$  and  $B_L$  are the buoyancy of the spar and barge, respectively;
- $F_{DL}$  is the drag force for the projected area of the barge;
- $F_W$  is the hydraulic jack force which is applied at the start to overcome the static friction;

- $F_{DSH}$ ,  $F_{DSV}$  are the horizontal and vertical drag forces for the spar;
- $F_E$  is the water entry force which acts vertically upward in the global frame of reference.

The drag forces for the spar hull are added during launching and oscillation. The water entry force is applied during launching up to the point in time where the spar vertical velocity becomes zero and it starts to oscillate.

The equilibrium equations for the coupled system with 6 degrees of freedom,  $X_S, Z_S, \theta_S, X_L, Z_L$  and  $\theta_L$  are written as

$$\begin{aligned}
\sum F_{XS}; \quad & -m_S \cdot \ddot{X}_S + W_S \cdot \sin \theta_S + F_U + F_{DSH} - F_W - B_S \cdot \sin \theta_S - F_E \cdot \sin \theta_S = 0 \\
\sum F_{ZS}; \quad & -m_S \cdot \ddot{Z}_S - W_S \cdot \cos \theta_S + F_N + F_{DSV} + B_S \cdot \cos \theta_S + F_E \cdot \cos \theta_S = 0 \\
\sum M_{YS}; \quad & -I_S \cdot \ddot{\theta}_S + F_U \cdot Z_{SU} - F_W \cdot Z_{SW} + F_{DSH} \cdot Z_{DS} - F_{DSV} \cdot X_{DS} - (B_S \cdot X_{SBL} \\
& + F_E \cdot X_{ES}) \cdot \cos \theta_S = 0
\end{aligned} \tag{3.2}$$

$$\begin{aligned}
\sum F_{XL}; \quad & -(m_L + m_R + m_{B1} + m_{B2} + \dots + m_{B10} + m_{B11}) \cdot \ddot{X}_L \\
& - (m_R \cdot Z_{LGR} + m_{B1} \cdot Z_{LB1} + m_{B2} \cdot Z_{LB2} + \dots + m_{B9} \cdot Z_{LB9} + m_{B10} \\
& \cdot Z_{LB10} + m_{B11} \cdot Z_{LB11}) \cdot \ddot{\theta}_L \\
& + (W_L + W_R - B_L + W_{B1} + W_{B2} + \dots + W_{B10} + W_{B11}) \cdot \sin \theta_L - F_U \\
& - F_{DL} \cdot \cos \theta_L = 0
\end{aligned}$$

$$\begin{aligned}
\sum F_{ZL}; & \quad -(m_L + m_R + m_{B1} + m_{B2} + \dots + m_{B10} + m_{B11}) \cdot \ddot{Z}_L \\
& \quad + (m_R \cdot X_{LgR} + m_{B1} \cdot X_{LB1} + m_{B2} \cdot X_{LB2} + \dots + m_{B10} \cdot X_{LB10} + m_{B11} \\
& \quad \cdot X_{LB11}) \cdot \ddot{\theta}_L - (W_L + W_R - B_L + W_{B1} + W_{B2} + \dots + W_{B10} + W_{B11}) \\
& \quad \cdot \text{Cos}\theta_L - F_N + F_{DL} \cdot \text{Sin}\theta_L = 0 \\
\sum M_{YL}; & \quad -I_L \cdot \ddot{\theta}_L \\
& \quad - (m_R \cdot [X_{LgR}^2 + Z_{LgR}^2] + m_{B1} \cdot [X_{LB1}^2 + Z_{LB1}^2] + m_{B2} \cdot [X_{LB2}^2 + Z_{LB2}^2] \\
& \quad + \dots + m_{B10} \cdot [X_{LB10}^2 + Z_{LB10}^2] + m_{B11} \cdot [X_{LB11}^2 + Z_{LB11}^2]) \cdot \ddot{\theta}_L \\
& \quad - (m_R \cdot Z_{LgR} + m_{B1} \cdot Z_{LB1} + m_{B2} \cdot Z_{LB2} + \dots + m_{B10} \cdot Z_{LB10} + m_{B11} \\
& \quad \cdot Z_{LB11}) \cdot \ddot{X}_L + (m_R \cdot X_{LgR} + m_{B1} \cdot X_{LB1} + m_{B2} \cdot X_{LB2} + \dots + m_{B10} \\
& \quad \cdot X_{LB10} + m_{B11} \cdot X_{LB11}) \cdot \ddot{Z}_L + (W_R \cdot X_{LgR} - B_L \cdot X_{LBL} + W_{B1} \cdot X_{LB1} \\
& \quad + W_{B2} \cdot X_{LB2} + \dots + W_{B10} \cdot X_{LB10} + W_{B11} \cdot X_{LB11}) \cdot \text{Cos}\theta_L - F_U \cdot Z_{LU} \\
& \quad + F_N \cdot X_{LN} = 0 \tag{3.3}
\end{aligned}$$

where:

- $Z_{SU}$ ,  $Z_{SW}$  and  $Z_{DS}$  are the spar-fixed  $Z_S$ -coordinates of the line of action of the friction force, hydraulic jack force, and horizontal component of the drag and inertia forces, respectively;
- $X_{SBL}$  and  $X_{ES}$  are the spar-fixed  $X_S$ -coordinates of the spar buoyancy force and water entry force, respectively;
- $X_{LgR}$  and  $Z_{LgR}$  are the barge-fixed  $X_L$ - and  $Z_L$ -coordinates of the rocker arm pivot point;
- $X_{LB1} \sim X_{LB11}$  are the barge-fixed  $X_L$ -coordinates of the ballast tanks;

- $Z_{LB1} \sim Z_{LB11}$  are the barge-fixed  $Z_L$ -coordinates of the ballast tanks;
- $Z_{LU}$  is the barge-fixed  $Z_L$ -coordinate of the friction force;
- $X_{LN}$  is the barge-fixed  $X_L$ -coordinate of the normal (bearing) force.

$W_S$  is applied at the origin of the spar-fixed coordinate system and therefore does not have an associated moment. Similarly,  $W_L$  is applied at the origin of the barge-fixed coordinate system and does not have an associated moment. The vertical drag force on the barge has been neglected for the barge equilibrium system because the vertical velocity of the barge is very small.

For the initial pre-launch static equilibrium configuration with the ballast tanks filled with water as needed to achieve the desired trim angle, the net moment on the barge should be zero, in which case

$$\sum M_{YL}; \quad +(W_R \cdot X_{LgR} - B_L \cdot X_{LbL} + W_{B1} \cdot X_{LB1} + W_{B2} \cdot X_{LB2} + \dots + W_{B10} \cdot X_{LB10} + W_{B11} \cdot X_{LB11}) \cdot \cos\theta_L - F_U \cdot Z_{LU} + F_N \cdot X_{LN} = 0 \quad (3.4)$$

To overcome the static friction of the initial pre-launch condition, the hydraulic jack forces are added to initiate the sliding motion of the spar on the launch rails.



### 3.3 Bearing Force and Friction Force

During launching of the spar hull on the deck of the barge, the trim angle of the barge varies in time along with the inertia of the spar and the location of its center of gravity relative to the barge. Tangential (frictional) and normal (bearing) reaction forces are exerted on the launch rails by the spar. It is necessary to track the center of effort of the bearing reaction relative to the barge, not only as it affects the coupled dynamics of the system but also as it induces rotation of the rocker arm when acting aft of the rocker arm pivot point.

The friction force is defined as

$$F_U = C_f \cdot F_N \quad (3.5)$$

where  $C_f$  is the friction coefficient (with separate values for the static and dynamic condition) and  $F_N$  is the normal reaction force which is also known as the bearing force.

The static friction coefficient was set to 0.1 and the kinetic friction coefficient was set to 0.05 or 0.06 depending on the assumed initial trim angle. According to L. Hambro (1982), the kinetic friction coefficient should be set equal to the barge trim (in radians).

The coupling forces, which are the bearing force and friction force, with equal magnitude but opposite signs on the spar and barge, act together to couple the equations of motions for the spar with the equations of motion for the barge.

When the spar moves past the pivot point of the rocker arm, the coupling forces are applied to the rocker arm as it rotates as long as there is a net bearing force. When

the bearing force becomes zero the spar hull detaches from the barge, and from then on the spar hull and barge move independently from each other.

### 3.4 Hydrostatic Buoyancy

The spar is modeled as a simple circular cylinder without a moon pool. The launch barge is modeled as a simple compound rectangular box (a rectangular box-shaped bow section appended to a rectangular box-shaped stern section). As the launching simulation proceeds, the total buoyancy and the center of buoyancy of the spar hull and barge are individually updated at each time step using exact analytic functions.

The hydrostatic buoyancy is presented as

$$F_{\text{Static}} = \rho \cdot g \cdot \nabla \quad (3.6)$$

where  $\rho$  is the sea water density,  $g$  is the gravitational acceleration and  $\nabla$  is the submerged volume for the body.

Ken Edwards (2014) calculated the volume of liquid in a partially full cylindrical container which is tilted for the 4 cases of liquid volume in the inclined cylinder shown in Figure 13.

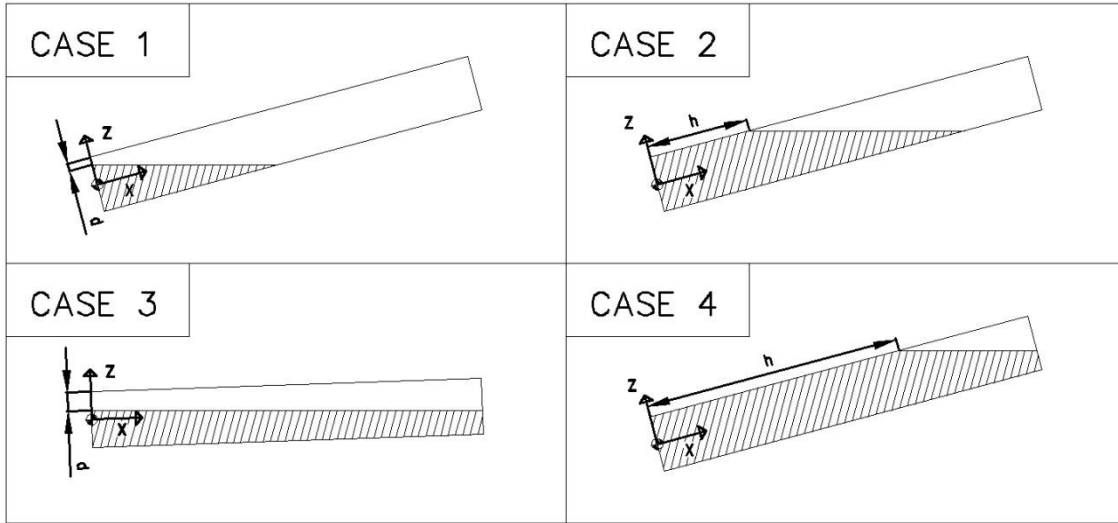


**Figure 13 Four cases submerged volume**

According to Edwards (2014), the equations for the liquid volume of Figure 13 are

$$\text{Case1: } \mathcal{V} = \int_{-G \cdot \tan \theta}^r \int_{-\sqrt{r^2-y^2}}^{\sqrt{r^2-y^2}} \int_0^{\frac{y}{\tan \theta} + G} dz dx dy \quad (3.7)$$

$$\text{Case2: } \mathcal{V} = \int_{-r}^r \int_{-\sqrt{r^2-y^2}}^{\sqrt{r^2-y^2}} \int_0^{\frac{y}{\tan \theta} + G} dz dx dy$$

$$\text{Case3: } \mathcal{V} = \int_{-G \cdot \tan \theta}^{(L-G) \cdot \tan \theta} \int_{-\sqrt{r^2-y^2}}^{\sqrt{r^2-y^2}} \int_0^{\frac{y}{\tan \theta} + G} dz dx dy + \int_{(L-G) \cdot \tan \theta}^r \int_{-\sqrt{r^2-y^2}}^{\sqrt{r^2-y^2}} \int_0^L dz dx dy$$

$$\text{Case4: } \mathcal{V} = \int_{-r}^{(L-G) \cdot \tan \theta} \int_{-\sqrt{r^2-y^2}}^{\sqrt{r^2-y^2}} \int_0^{\frac{y}{\tan \theta} + G} dz dx dy + \int_{(L-G) \cdot \tan \theta}^r \int_{-\sqrt{r^2-y^2}}^{\sqrt{r^2-y^2}} \int_0^L dz dx dy$$

where,  $G = S + (r - H_d) / \tan \theta$ ,  $L$  is the length of the cylinder,  $r$  is the radius of the cylinder bottom and  $\theta$  is the trimmed angle of the cylinder.  $S$  and  $H_d$  are shown in Figure 14.

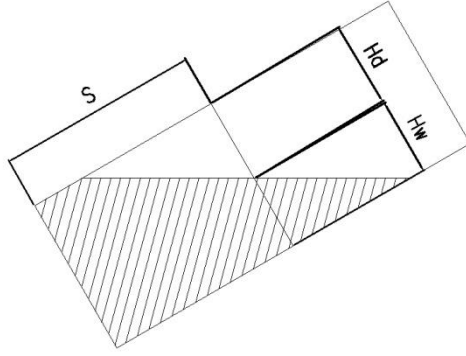


**Figure 14**  $H_d$  and  $S$

For the submerged volume of the spar hull, Equation (3.7) can be developed as

$$\text{Case1: } \forall = \int_{d-r}^r \int_{-R}^R \int_0^{\frac{y+r-d}{\tan \theta}} 1 \, dz \, dx \, dy \quad (3.8)$$

$$\text{Case2: } \forall = \int_{-r}^r \int_{-R}^R \int_0^{\frac{y+r-d}{\tan \theta} + h} 1 \, dz \, dx \, dy$$

$$\text{Case3: } \forall = \left( \int_{d-r}^{L \cdot \tan \theta - r + d} \int_{-R}^R \int_0^{\frac{y+r-d}{\tan \theta}} 1 + \int_{L \cdot \tan \theta - r + d}^r \int_{-R}^R \int_0^L 1 \right) dz \, dx \, dy$$

$$\text{Case4: } \forall = \left( \int_{-r}^{(L-h) \cdot \tan \theta - r + d} \int_{-R}^R \int_0^{\frac{y+r-d}{\tan \theta} + h} 1 + \int_{(L-h) \cdot \tan \theta - r + d}^r \int_{-R}^R \int_0^L 1 \right) dz \, dx \, dy$$

where,  $R = \sqrt{r^2 - y^2}$ .

The equations for the center of buoyancy of the spar hull can be written as

Case 1;

$$XCoB = \frac{\int_{d-r}^r \int_{-R}^R \int_0^{\frac{y+r-d}{\tan \theta}} X dz dx dy}{\forall} \quad (3.9)$$

$$ZCoB = \frac{\int_{d-r}^r \int_{-R}^R \int_0^{\frac{y+r-d}{\tan \theta}} Z dz dx dy}{\forall}$$

Case 2;

$$XCoB = \frac{\int_{-r}^r \int_{-R}^R \int_0^{\frac{y+r-d}{\tan \theta}+h} X dz dx dy}{\forall}$$

$$ZCoB = \frac{\int_{-r}^r \int_{-R}^R \int_0^{\frac{y+r-d}{\tan \theta}+h} Z dz dx dy}{\forall}$$

Case 3;

$$XCoB = \frac{\left( \int_{d-r}^{L \cdot \tan \theta - r + d} \int_{-R}^R \int_0^{\frac{y+r-d}{\tan \theta}} X + \int_{L \cdot \tan \theta - r + d}^r \int_{-R}^R \int_0^L X \right) dz dx dy}{\forall}$$

$$ZCoB = \frac{\left( \int_{d-r}^{L \cdot \tan \theta - r + d} \int_{-R}^R \int_0^{\frac{y+r-d}{\tan \theta}} Z + \int_{L \cdot \tan \theta - r + d}^r \int_{-R}^R \int_0^L Z \right) dz dx dy}{\forall}$$

Case 4;

$$XCoB = \frac{\left( \int_{-r}^{(L-h) \cdot \tan \theta - r + d} \int_{-R}^R \int_0^{\frac{y+r-d}{\tan \theta}+h} X + \int_{(L-h) \cdot \tan \theta - r + d}^r \int_{-R}^R \int_0^L X \right) dz dx dy}{\forall}$$

$$ZCoB = \frac{\left( \int_{-r}^{(L-h) \cdot \tan \theta - r + d} \int_{-R}^R \int_0^{\frac{y+r-d}{\tan \theta}+h} Z + \int_{(L-h) \cdot \tan \theta - r + d}^r \int_{-R}^R \int_0^L Z \right) dz dx dy}{\forall}$$

The buoyancy and center of buoyancy are calculated by Matlab using Equation (3.8) and (3.9), i.e. by symbolic integration.

The barge is modeled as two rectangular boxes as shown in Figure 15.

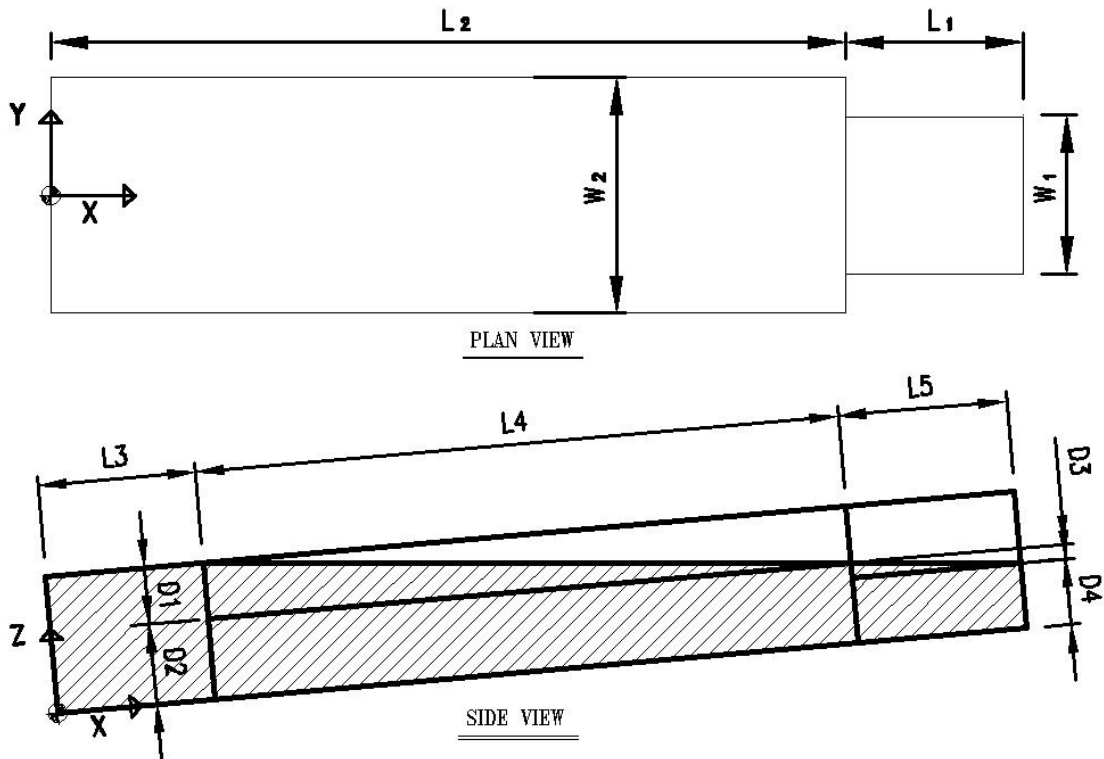


**Figure 15 Submerged area for the barge volume**

For the submerged volume of the rectangular barge, the basic geometry is expressed as

$$V = A1 \cdot W2 + A2 \cdot W2 + A3 \cdot W2 + A4 \cdot W1 + A5 \cdot W1 \quad (3.10)$$

$$A1 = L3 \cdot (D1 + D2)$$

$$A2 = L4 \cdot \frac{D1}{2}$$

$$A3 = L4 \cdot D2$$

$$A4 = L5 \cdot \frac{D3}{2}$$

$$A5 = L5 \cdot D4$$

The center of buoyancy for the barge can be calculated as

XCoG

$$= \frac{A1 \cdot \frac{L3}{2} + A2 \cdot \left(\frac{L4}{3} + L3\right) + A3 \cdot \left(\frac{L4}{2} + L3\right) + A4 \cdot \left(\frac{L5}{3} + L2\right) + A5 \cdot \left(\frac{L5}{2} + L2\right)}{\sum_{n=1}^5 A_n}$$

ZCoG

$$= \frac{A1 \cdot \frac{D1 + D2}{2} + A2 \cdot \left(\frac{D1}{3} + D2\right) + A3 \cdot \frac{D2}{2} + A4 \cdot \left(\frac{D3}{3} + D4\right) + A5 \cdot \frac{D4}{2}}{\sum_{n=1}^5 A_n} \quad (3.11)$$

where  $L1=L5$ ,  $L2=L3+L4$ .

### 3.5 Hydrodynamic Forces

The hydrodynamic force for the spar hull launching sequence includes the inertia force, the drag force and the water entry force. For oscillations of the spar hull, the hydrodynamic force includes the drag force and inertia force. And the hydrodynamic force for the barge includes the drag force and the inertia force.

#### 3.5.1 Water entry problem

For the high speed vertical water entry of a body, the hydrodynamic (including hydrostatic) vertical force on the body as it penetrates into the water with downward velocity  $V$  can be written as

$$F_3 = \frac{d}{dt}(A_{33} \cdot V) + \rho \cdot g \cdot \nabla \quad (3.12)$$

where  $\nabla$  is the submerged volume and  $A_{33}$  is the infinite-frequency added mass in heave for the body (Faltinsen, 1990).

The first term of the right hand side of equation (3.3) can be written as

$$\frac{d}{dt}(A_{33} \cdot V) = A_{33} \cdot \frac{d}{dt}(V) + V \frac{d}{dt}(A_{33}) \quad (3.13)$$

For the velocities and accelerations associated with the spar launching scenarios considered herein, the second term in equation (3.13) is about one order of magnitude smaller than the first term, consequently it will be neglected. The vertical water entry force will therefore be modeled as

$$F_3 = A_{33} \cdot \frac{d}{dt}(V) \quad (3.14)$$

The infinite frequency added mass as a function of the submerged spar position (draft and trim angle) is calculated using WAMIT as described below.

### 3.5.2 Added mass

In the two dimensional analysis with X-axis and Z-axis, the heave added mass  $A_{33}$  for the water entry force is calculated using WAMIT. The added masses yielded by WAMIT are applied on the body-fixed X-axis and Z-axis, however for the calculation of the heave added mass the body-fixed coordinate system is rotated so that the Z-axis is vertically upward, as shown in Figure 16.

After the first trial simulation using nominal values of the added mass coefficients, the approximate trajectory of the spar is extracted. Then, given the



approximate trajectory, the submerged volume of the spar in the inclined position is discretized using the Rhino 3D modeling program for preparation of the geometric definition file for WAMIT. Infinite frequency heave added mass values are calculated for a representative set of submerged positions of the spar. See Section 4.4 for the flow chart.

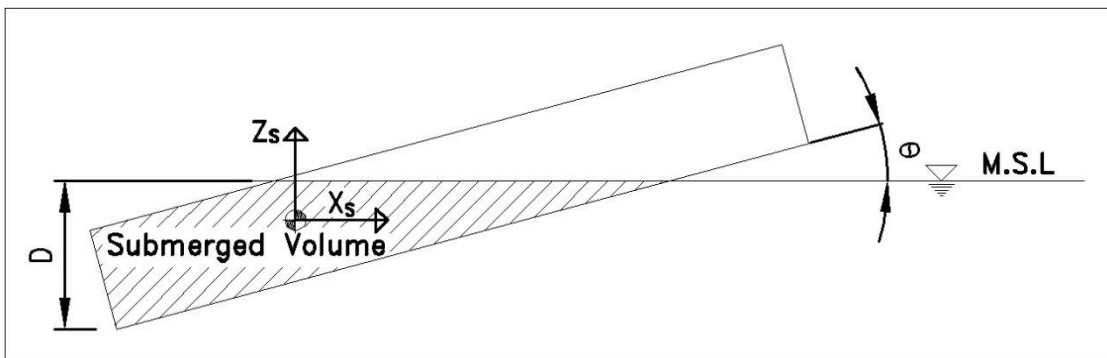


**Figure 16 Trimmed model for the WAMIT**

The water entry force continues to be applied after the spar hull separates from the barge until it has reached its maximum depth of submergence and begins to oscillate.

When the spar hull starts to oscillate, the water entry force is replaced with the Morison inertia force and the added mass coefficient 1.0 is applied from then onward. The hydrodynamic inertia force for the barge is also modeled using Morison's model, and the added mass coefficient for the barge is set equal to 1.0 during the entire launching sequence.

### 3.5.3 The drag force and inertia force

Morison proposed an equation for the force exerted by surface waves on a slender cylindrical object (1950).

When the spar hull slides down the deck of the launching barge and enters the water, the drag force of Morison's equation and the water entry force are used to evaluate the hydrodynamic force on the spar hull. During this phase, the hydrodynamic force considering the water entry problem and the drag force for the spar hull can be written as

$$F_{DS} = A_{33} \cdot \frac{d}{dt}(V) + \frac{1}{2} \rho \cdot C_d \cdot A_w (u - v) |u - v| \quad (3.15)$$

where  $C_d$  is the Reynolds number-dependent drag coefficient,  $u$  is a current velocity (assumed as zero in the calm water),  $v$  is the body velocity and  $A_w$  is the submerged area normal to the velocity of the body.

Once the spar hull and barge are set to move in an oscillating mode, the Morison's equation is represented as

$$F_D = \rho \cdot C_a \cdot \nabla(\dot{u} - \dot{v}) + \frac{1}{2} \rho \cdot C_d \cdot A_w (u - v) |u - v| \quad (3.16)$$

where  $C_a$  is the added mass coefficient. The first term of the right hand side of equation (3.16) is the inertia force term and the second term accounts for the drag force effect. In calculating the inertia force an added mass coefficient of 1.0 is applied for the spar and the barge.

When the spar rotates, the drag moment is calculated considering the rotational velocity at the rotational pivot point. The hull is divided into a number of elements and

for each element the local velocity and the associated Reynolds number is calculated. Each element is then assigned a drag coefficient based on the plot of drag coefficient versus Reynolds number for a smooth cylinder shown in Figure 2. The net drag forces and moments are obtained by vector summation of the elemental drag forces, as illustrated in Figure 17. A similar procedure is used to calculate the net inertia force and moment on the spar.

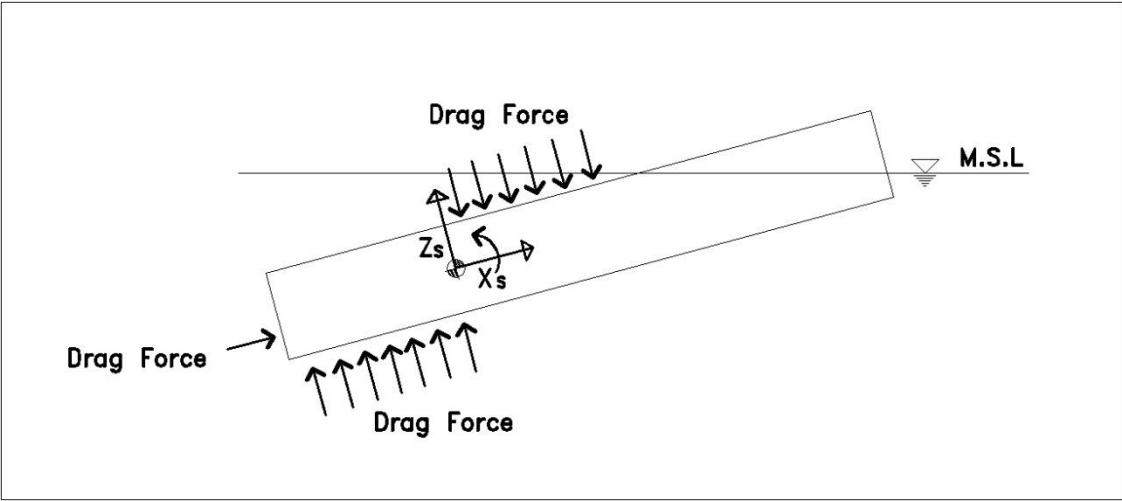


**Figure 17 Drag force**

## 4. NUMERICAL SOLUTION PROCEDURE

### 4.1 Matlab ODE Solver

The numerical time integration of the matrix system of equations is performed using the Matlab ODE (Ordinary Differential Equation) solver based on fourth and fifth order Runge-Kutta formulas.

Given an initial position and an unbalanced set of forces, the Matlab ODE solver computes the future accelerations, velocities and positions, which then represent a system in dynamic equilibrium at each instant of time. The ODE solver will integrate the equations of motion over a defined time period using a time step which may either be specified on input or allowed to be set and under the control of the ODE algorithm.

For use by the ODE solver, the ordinary differential equations are cast in the following form.

For the spar motion,

$$\frac{d\dot{x}_S}{dt} = f_{xS}(F_{Si}, C_i, \theta_S)$$

$$\frac{dx_S}{dt} = \dot{x}_S$$

$$\frac{d\dot{z}_S}{dt} = f_{zS}(F_{Si}, C_i, \theta_S)$$

$$\frac{dz_S}{dt} = \dot{z}_S$$

$$\frac{d\dot{\theta}_S}{dt} = f_{\theta S}(F_{Si}, C_i, \theta_S)$$

$$\frac{d\theta_S}{dt} = \dot{\theta}_S \quad (4.1)$$

and for the barge motion,

$$\frac{d\dot{x}_L}{dt} = f_{xL}(F_{Li}, C_i, \ddot{\theta}_L, \theta_L)$$

$$\frac{dx_L}{dt} = \dot{x}_L$$

$$\frac{d\dot{z}_L}{dt} = f_{zL}(F_{Li}, C_i, \ddot{\theta}_L, \theta_L)$$

$$\frac{dz_L}{dt} = \dot{z}_L$$

$$\frac{d\dot{\theta}_L}{dt} = f_{\theta L}(F_{Li}, C_i, \dot{x}_L, \dot{z}_L, \theta_L)$$

$$\frac{d\theta_L}{dt} = \dot{\theta}_L \quad (4.2)$$

The equations (4.1) and (4.2) represent a coupled second order system of ordinary differential equations for the spar hull and barge respectively. We see that as long as the coupling forces  $C_i$  are nonzero (implying contact between the barge and spar) then the equations of motion for the spar are coupled to those for the barge.

The variables  $x_S, z_S, \theta_S$  and  $x_L, z_L, \theta_L$  are the position coordinate or angle of the spar hull and barge respectively.  $F_{Si}, F_{Li}$  includes hydrostatic buoyancy and hydrodynamic contributions for the spar hull and the barge, respectively.  $C_i$  represents the coupling forces that are dependent variables calculated outside of the ODE solver at each time step with the following key parameters updated accordingly.

- Center of buoyancy of the barge
- Total buoyancy of the barge

- Center of buoyancy of the spar
- Total buoyancy of the spar
- Infinite frequency added mass of the spar.
- Reynolds number dependent drag coefficients and local drag forces on the spar
- Normal (bearing) and tangential (frictional) forces between the spar and barge

When the spar hull is initially positioned on the deck of the barge, the trim angle of the spar hull and the barge is the same and the magnitudes of the coupling forces are equal with opposite signs. When the hydraulic jack forces are applied to overcome the static friction of the pre-launching condition, the spar hull starts sliding. As the spar slides down the launch rails, the inclination of the barge and spar remain identical until the center of gravity of the spar is directly above the pivot point on the rocker arm.

Once the spar center of gravity passes the pivot point, the moment induced on the rocker arm by the weight of the spar, if it exceeds the counter moment from the hydrostatic and hydrodynamic force on the spar, will cause it to rotate, in which case the trim angle of the spar becomes different than that of the barge. When the rocker arm starts to rotate the trim angle of the spar hull is calculated independently to the trim angle of the barge. From this point onward the trim angle of the spar hull becomes an additional degree of freedom in the coupled system of equations, in which case the spar hull and the rocker arm rotate together with the same trim angle. The inertia of the rocker arm is incorporated in the coupled system of equations for the spar hull. The coupling forces continue to be calculated outside of the ODE solver at each time step

and once the coupling forces become zero, the spar hull is separated from the barge and the system of equations for the spar hull and barge are independent from each other.

After the spar hull separates completely from the barge, the coupling forces  $C_i$  become zero and the ODE solver will compute derivatives for the spar (equation (4.1)) separately from those for the barge (equation (4.2)).

To achieve the predetermined accuracy in the solution, the coupling forces are calculated outside of the ODE solver at each time step during the launching sequence. The time step for each call to the ODE solver is set manually after monitoring the results from initial trial simulations at each distinct stage. If the input time step is too long to maintain the accuracy of the solution, the ODE solver will automatically refine it under internal iteration on the basis of the designated time step. When the coupling forces become zero after separating the spar hull from the barge, the time step is calculated in the ODE solver automatically during oscillation of the spar hull since there is no need to update coupling forces outside of the ODE solver. The adjusted time step size contributes to the accuracy of the ODE solution.

## 4.2 Matrix System of Equations

From Section 3, the matrix system of the equivalent second order coupled equations for the launching analysis is represented as

$$([M_{ij} + A_{ij}]) \cdot \ddot{\xi}_j = F_i + C_i \quad (4.3)$$

The mass matrix is

$$[M_{ij}] = \begin{bmatrix} m_S & 0 & 0 & 0 & 0 & 0 \\ 0 & m_S & 0 & 0 & 0 & 0 \\ 0 & 0 & I_S & 0 & 0 & 0 \\ 0 & 0 & 0 & A & 0 & B \\ 0 & 0 & 0 & 0 & A & C \\ 0 & 0 & 0 & B & C & D \end{bmatrix} \quad (4.4)$$

where

$$A = m_L + m_R + m_{B1} + m_{B2} + \dots + m_{B10} + m_{B11}$$

$$B = m_R \cdot Z_{LgR} + m_{B1} \cdot Z_{LB1} + m_{B2} \cdot Z_{LB2} + \dots + m_{B10} \cdot Z_{LB10} + m_{B11} \cdot Z_{LB11}$$

$$C = -(m_R \cdot X_{LgR} + m_{B1} \cdot X_{LB1} + m_{B2} \cdot X_{LB2} + \dots + m_{B10} \cdot X_{LB10} + m_{B11} \cdot X_{LB11})$$

$$D = m_R \cdot [X_{LgR}^2 + Z_{LgR}^2] + m_{B1} \cdot [X_{LB1}^2 + Z_{LB1}^2] + m_{B2} \cdot [X_{LB2}^2 + Z_{LB2}^2] + \dots + m_{B10} \cdot [X_{LB10}^2 + Z_{LB10}^2] + m_{B11} \cdot [X_{LB11}^2 + Z_{LB11}^2] + I_L$$

The added mass matrix is

$$[a_{ij}] = \begin{bmatrix} A_{11}^S & 0 & 0 & 0 & 0 & 0 \\ 0 & A_{33}^S & 0 & 0 & 0 & 0 \\ 0 & 0 & A_{55}^S & 0 & 0 & 0 \\ 0 & 0 & 0 & A_{11}^L & 0 & 0 \\ 0 & 0 & 0 & 0 & A_{33}^L & 0 \\ 0 & 0 & 0 & 0 & 0 & A_{55}^L \end{bmatrix} \quad (4.5)$$

The acceleration vector is

$$\ddot{\xi}_j = \begin{bmatrix} \ddot{X}_S \\ \ddot{Z}_S \\ \ddot{\theta}_S \\ \ddot{X}_L \\ \ddot{Z}_L \\ \ddot{\theta}_L \end{bmatrix} \quad (4.6)$$



The vector of hydrodynamic and hydrostatic forces is

$$F_i = \begin{bmatrix} -W_S \cdot \sin \theta_S + F_{DSH} - B_S \cdot \sin \theta_S - F_E \cdot \sin \theta_S \\ -W_S \cdot \cos \theta_S + F_{DSV} + B_S \cdot \cos \theta_S + F_E \cdot \cos \theta_S \\ F_{DSH} \cdot Z_{DS} - F_{DSV} \cdot X_{DS} - (B_S \cdot X_{SBL} + F_E \cdot X_{ES}) \cdot \cos \theta_S \\ (W_L + W_R - B_L + W_{B1} + \dots + W_{B11}) \cdot \sin \theta_L \\ -(W_L + W_R - B_L + W_{B1} + \dots + W_{B1}) \cdot \cos \theta_L \\ (W_R \cdot X_{LGR} - B_L \cdot X_{LBL} + W_{B1} \cdot X_{LB1} + \dots) \cdot \cos \theta_L \end{bmatrix} \quad (4.7)$$

The vector of coupling forces is

$$C_i = \begin{bmatrix} F_U - F_W \\ F_N \\ F_U \cdot X_{SU} + F_W \cdot X_{SW} \\ -F_U - F_{DL} \cdot \cos \theta_L \\ -F_N - F_{DL} \cdot \sin \theta_L \\ -F_U \cdot Z_{LU} + F_N \cdot X_{LN} \end{bmatrix} \quad (4.8)$$

### 4.3 Runge-Kutta Method

To trace the future trajectories of the rigid bodies, the fourth-order Runge-Kutta method is applied. The Runge-Kutta method is one of the most popular methods for the numerical solution of ordinary differential equations. The fourth-order Runge-Kutta method yields a fourth-order approximation of the corresponding time interval.

Considering,

$$\frac{dy}{dx} = f(x, y) \quad (4.9)$$

the fourth-order Runge-Kutta formulas are written as

$$K_1 = h \cdot f(X_n, Y_n)$$

$$K_2 = h \cdot f\left(X_n + \frac{1}{2}h, Y_n + \frac{1}{2}K_1\right)$$

$$\begin{aligned}
K_3 &= h \cdot f\left(X_n + \frac{1}{2}h, Y_n + \frac{1}{2}K_2\right) \\
K_4 &= h \cdot f(X_n + h, Y_n + K_3) \\
Y_{n+1} &= Y_n + (K_1 + 2K_2 + 2K_3 + K_4)/6
\end{aligned} \tag{4.10}$$

where  $h$  is the time step, and  $X_{n+1} = X_n + h$ . The fourth-order Runge-Kutta integration algorithm approximates the next approach variable with increment and midpoints calculated at each initial point using the fourth derivative.

In the two dimensional analysis with two bodies associated with coupling forces for the launching analysis, the fourth-order Runge-Kutta method is developed for the coupled ordinary differential equations as

$$\frac{dx_S}{dt} = f_1(t, x_S, z_S, \theta_S)$$

$$\frac{dz_S}{dt} = f_2(t, x_S, z_S, \theta_S)$$

$$\frac{d\theta_S}{dt} = f_3(t, x_S, z_S, \theta_S)$$

$$k_{1,xS} = f_1(t_j, x_{j,S}, z_{j,S}, \theta_{j,S})$$

$$k_{1,zS} = f_2(t_j, x_{j,S}, z_{j,S}, \theta_{j,S})$$

$$k_{1,\theta S} = f_3(t_j, x_{j,S}, z_{j,S}, \theta_{j,S})$$

$$k_{2,xS} = f_1\left(t_j + \frac{h}{2}, x_{j,S} + \frac{h}{2}k_{1,xS}, z_{j,S} + \frac{h}{2}k_{1,zS}, \theta_{j,S} + \frac{h}{2}k_{1,\theta S}\right)$$

$$k_{2,ZS} = f_2\left(t_j + \frac{h}{2}, x_{j,S} + \frac{h}{2}k_{1,XS}, z_{j,S} + \frac{h}{2}k_{1,ZS}, \theta_{j,S} + \frac{h}{2}k_{1,\theta S}\right)$$

$$k_{2,\theta S} = f_3\left(t_j + \frac{h}{2}, x_{j,S} + \frac{h}{2}k_{1,XS}, z_{j,S} + \frac{h}{2}k_{1,ZS}, \theta_{j,S} + \frac{h}{2}k_{1,\theta S}\right)$$

$$k_{3,XS} = f_1\left(t_j + \frac{h}{2}, x_{j,S} + \frac{h}{2}k_{2,XS}, z_{j,S} + \frac{h}{2}k_{2,ZS}, \theta_{j,S} + \frac{h}{2}k_{2,\theta S}\right)$$

$$k_{3,ZS} = f_2\left(t_j + \frac{h}{2}, x_{j,S} + \frac{h}{2}k_{2,XS}, z_{j,S} + \frac{h}{2}k_{2,ZS}, \theta_{j,S} + \frac{h}{2}k_{2,\theta S}\right)$$

$$k_{3,\theta S} = f_3\left(t_j + \frac{h}{2}, x_{j,S} + \frac{h}{2}k_{2,XS}, z_{j,S} + \frac{h}{2}k_{2,ZS}, \theta_{j,S} + \frac{h}{2}k_{2,\theta S}\right)$$

$$k_{4,XS} = f_1\left(t_j + h, x_{j,S} + h \cdot k_{3,XS}, z_{j,S} + h \cdot k_{3,ZS}, \theta_{j,S} + h \cdot k_{3,\theta S}\right)$$

$$k_{4,ZS} = f_2\left(t_j + h, x_{j,S} + h \cdot k_{3,XS}, z_{j,S} + h \cdot k_{3,ZS}, \theta_{j,S} + h \cdot k_{3,\theta S}\right)$$

$$k_{4,\theta S} = f_3\left(t_j + \frac{h}{2}, x_{j,S} + h \cdot k_{3,XS}, z_{j,S} + h \cdot k_{3,ZS}, \theta_{j,S} + h \cdot k_{3,\theta S}\right)$$

$$x_{j+1,S} = x_{j,S} + h \left( \frac{k_{1,XS}}{6} + \frac{k_{2,XS}}{3} + \frac{k_{3,XS}}{3} + \frac{k_{4,XS}}{6} \right)$$

$$z_{j+1,S} = z_{j,S} + h \left( \frac{k_{1,ZS}}{6} + \frac{k_{2,ZS}}{3} + \frac{k_{3,ZS}}{3} + \frac{k_{4,ZS}}{6} \right)$$

$$\theta_{j+1,S} = \theta_{j,S} + h \left( \frac{k_{1,\theta S}}{6} + \frac{k_{2,\theta S}}{3} + \frac{k_{3,\theta S}}{3} + \frac{k_{4,\theta S}}{6} \right) \quad (4.11)$$

$$\frac{dx_L}{dt} = f_1(t, x_L, z_L, \theta_L)$$

$$\frac{dz_L}{dt} = f_2(t, x_L, z_L, \theta_L)$$

$$\frac{d\theta_L}{dt} = f_3(t, x_L, z_L, \theta_L)$$

$$k_{1,XL} = f_1(t_j, x_{j,L}, z_{j,L}, \theta_{j,L})$$

$$k_{1,ZL} = f_2(t_j, x_{j,L}, z_{j,L}, \theta_{j,L})$$

$$k_{1,\theta L} = f_3(t_j, x_{j,L}, z_{j,L}, \theta_{j,L})$$

$$k_{2,XL} = f_1\left(t_j + \frac{h}{2}, x_{j,L} + \frac{h}{2}k_{1,XL}, z_{j,L} + \frac{h}{2}k_{1,ZL}, \theta_{j,L} + \frac{h}{2}k_{1,\theta L}\right)$$

$$k_{2,ZL} = f_2\left(t_j + \frac{h}{2}, x_{j,L} + \frac{h}{2}k_{1,XL}, z_{j,L} + \frac{h}{2}k_{1,ZL}, \theta_{j,L} + \frac{h}{2}k_{1,\theta L}\right)$$

$$k_{2,\theta L} = f_3\left(t_j + \frac{h}{2}, x_{j,L} + \frac{h}{2}k_{1,XL}, z_{j,L} + \frac{h}{2}k_{1,ZL}, \theta_{j,L} + \frac{h}{2}k_{1,\theta L}\right)$$

$$k_{3,XL} = f_1\left(t_j + \frac{h}{2}, x_{j,L} + \frac{h}{2}k_{2,XL}, z_{j,L} + \frac{h}{2}k_{2,ZL}, \theta_{j,L} + \frac{h}{2}k_{2,\theta L}\right)$$

$$k_{3,ZL} = f_2\left(t_j + \frac{h}{2}, x_{j,L} + \frac{h}{2}k_{2,XL}, z_{j,L} + \frac{h}{2}k_{2,ZL}, \theta_{j,L} + \frac{h}{2}k_{2,\theta L}\right)$$

$$k_{3,\theta L} = f_3\left(t_j + \frac{h}{2}, x_{j,L} + \frac{h}{2}k_{2,XL}, z_{j,L} + \frac{h}{2}k_{2,ZL}, \theta_{j,L} + \frac{h}{2}k_{2,\theta L}\right)$$

$$k_{4,XL} = f_1(t_j + h, x_{j,L} + h \cdot k_{3,XL}, z_{j,L} + h \cdot k_{3,ZL}, \theta_{j,L} + h \cdot k_{3,\theta L})$$

$$k_{4,ZL} = f_2(t_j + h, x_{j,L} + h \cdot k_{3,XL}, z_{j,L} + h \cdot k_{3,ZL}, \theta_{j,L} + h \cdot k_{3,\theta L})$$

$$k_{4,\theta L} = f_3\left(t_j + \frac{h}{2}, x_{j,L} + h \cdot k_{3,XL}, z_{j,L} + h \cdot k_{3,ZL}, \theta_{j,L} + h \cdot k_{3,\theta L}\right)$$

$$x_{j+1,L} = x_{j,L} + h \left( \frac{k_{1,XL}}{6} + \frac{k_{2,XL}}{3} + \frac{k_{3,XL}}{3} + \frac{k_{4,XL}}{6} \right)$$

$$z_{j+1,L} = z_{j,L} + h \left( \frac{k_{1,ZL}}{6} + \frac{k_{2,ZL}}{3} + \frac{k_{3,ZL}}{3} + \frac{k_{4,ZL}}{6} \right)$$

$$\theta_{j+1,L} = \theta_{j,L} + h \left( \frac{k_{1,\theta L}}{6} + \frac{k_{2,\theta L}}{3} + \frac{k_{3,\theta L}}{3} + \frac{k_{4,\theta L}}{6} \right) \quad (4.12)$$

The equations (4.11) and (4.12) are the coupled ordinary differential equations with the fourth-order Runge-Kutta method for the spar hull and barge during the launching sequence, respectively.

#### 4.4 Simulation Flow Chart

Figure 18 is the flow chart for the simulation procedure. Each computational time step involves an entry into the ODE solver with an unbalanced system of forces and moments, which the ODE solver uses to calculate updated accelerations to achieve dynamic equilibrium, followed by an exit from the ODE solver to update the right-hand side forces and moments in equations (4.1) and (4.2). After attaining the computational solutions using the ODE solver and exiting, the geometry model of the spar hull and barge relative to the water line (i.e. the global coordinate system) is updated with the output positions from the ODE solver, along with the next position of the center of gravity of the spar hull and barge. The updated positions, velocities and accelerations of

the spar and barge then give rise to a new unbalanced system of right hand side forces and moments, ready for re-entry into the ODE solver with the time incremented using the time step output by the previous ODE solution.

The first trial simulation is performed using nominal values of the added mass coefficients instead of the values computed by WAMIT. This trial simulation is performed to determine the approximate trajectories of the bodies during the launch sequence. This then allows the WAMIT computations to be performed for a limited range of trimmed positions that correspond to the expected spar trajectory. After the initial simulation, the launching analysis is repeated with the added masses obtained from WAMIT to achieve more accuracy in predicting the behavior of the spar hull and barge.

As depicted in Figure 18, the launch simulation proceeds through the following stages:

- Pre-launch static configuration with barge trimmed
- Initiation of sliding
- Sliding before water entry of spar
- Water entry of spar
  - Prior to rotation of primary rocker arm
  - During rotation of primary rocker arm (Case 1)
  - During rotation of secondary rocker arm (Case 2)
  - Following separation of spar from barge (Case 3)
- Spar damped free oscillations

The iteration analysis is performed both inside and outside of the ODE solver.  
When the end of each stage is detected, the computational analysis proceeds to the next stage.

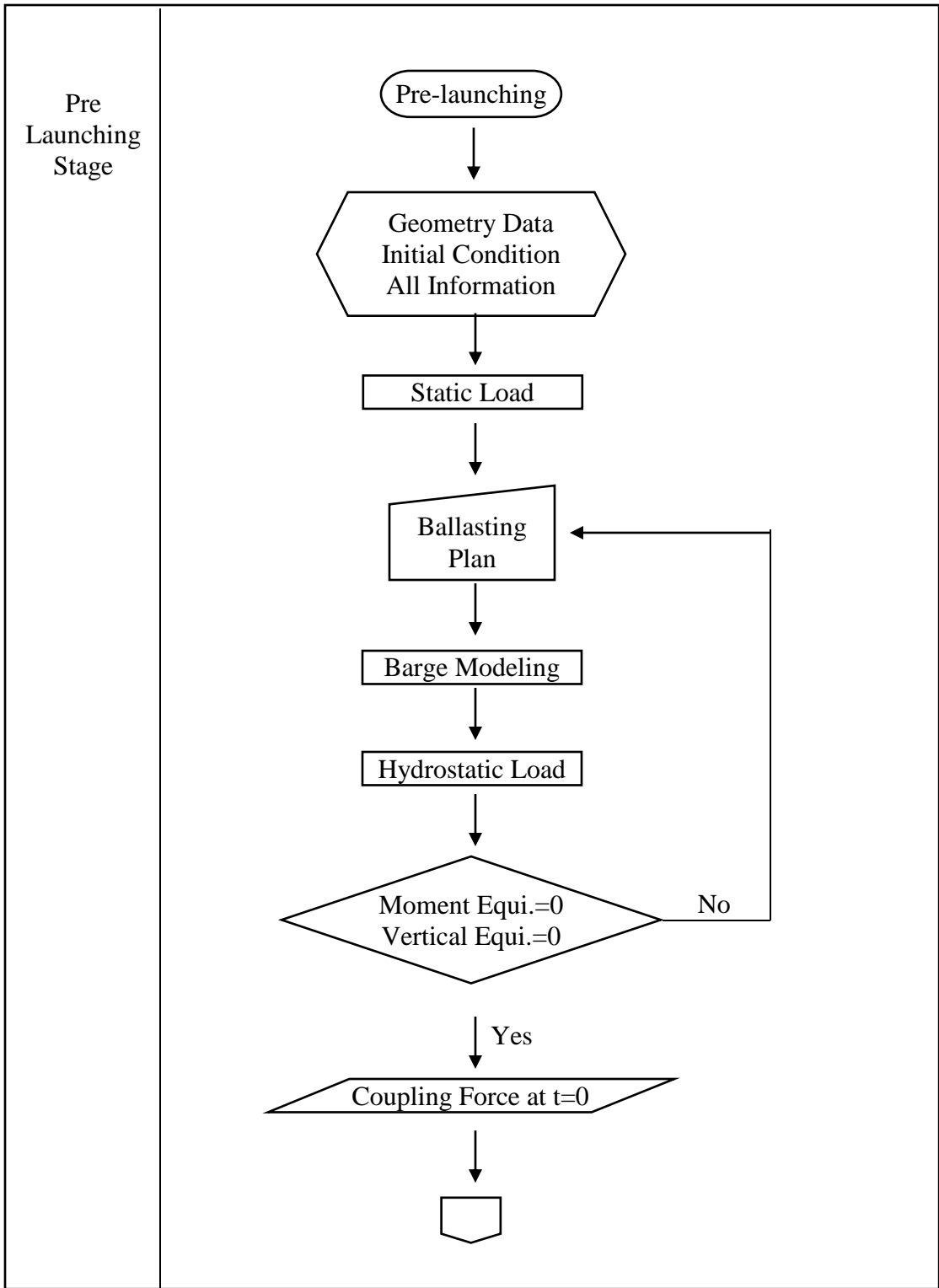


Figure 18 Flow chart



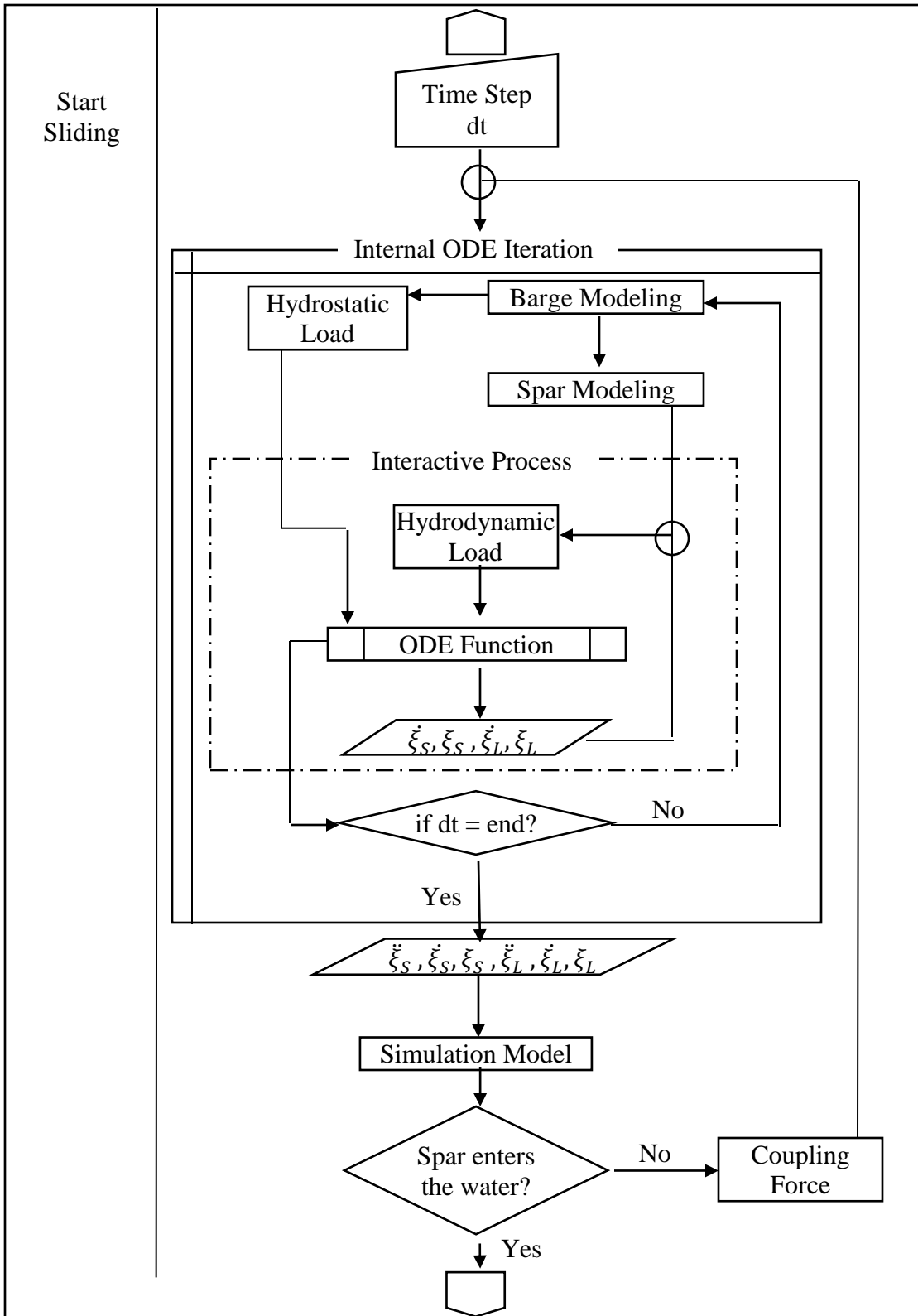


Figure 18 Continued

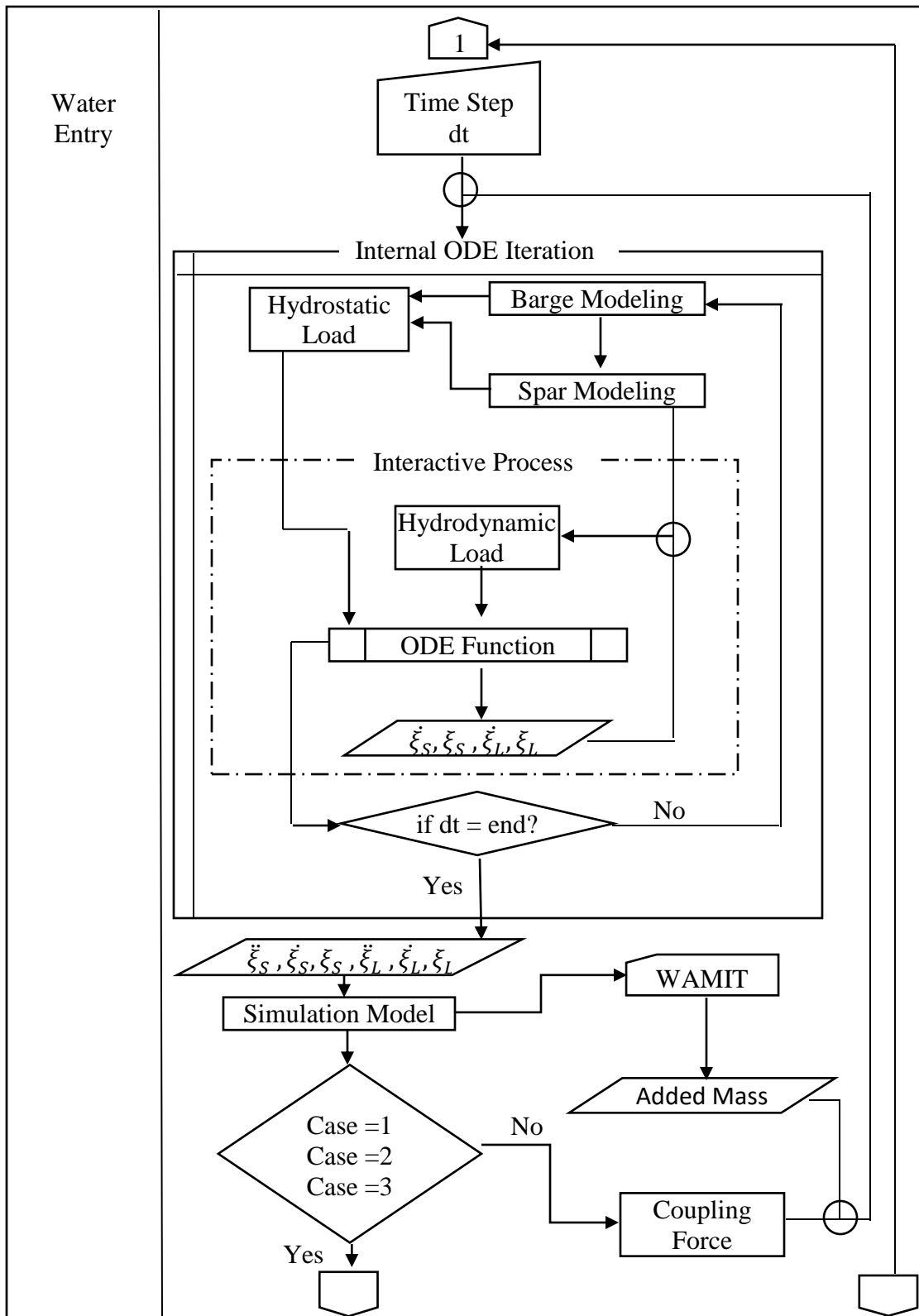


Figure 18 Continued

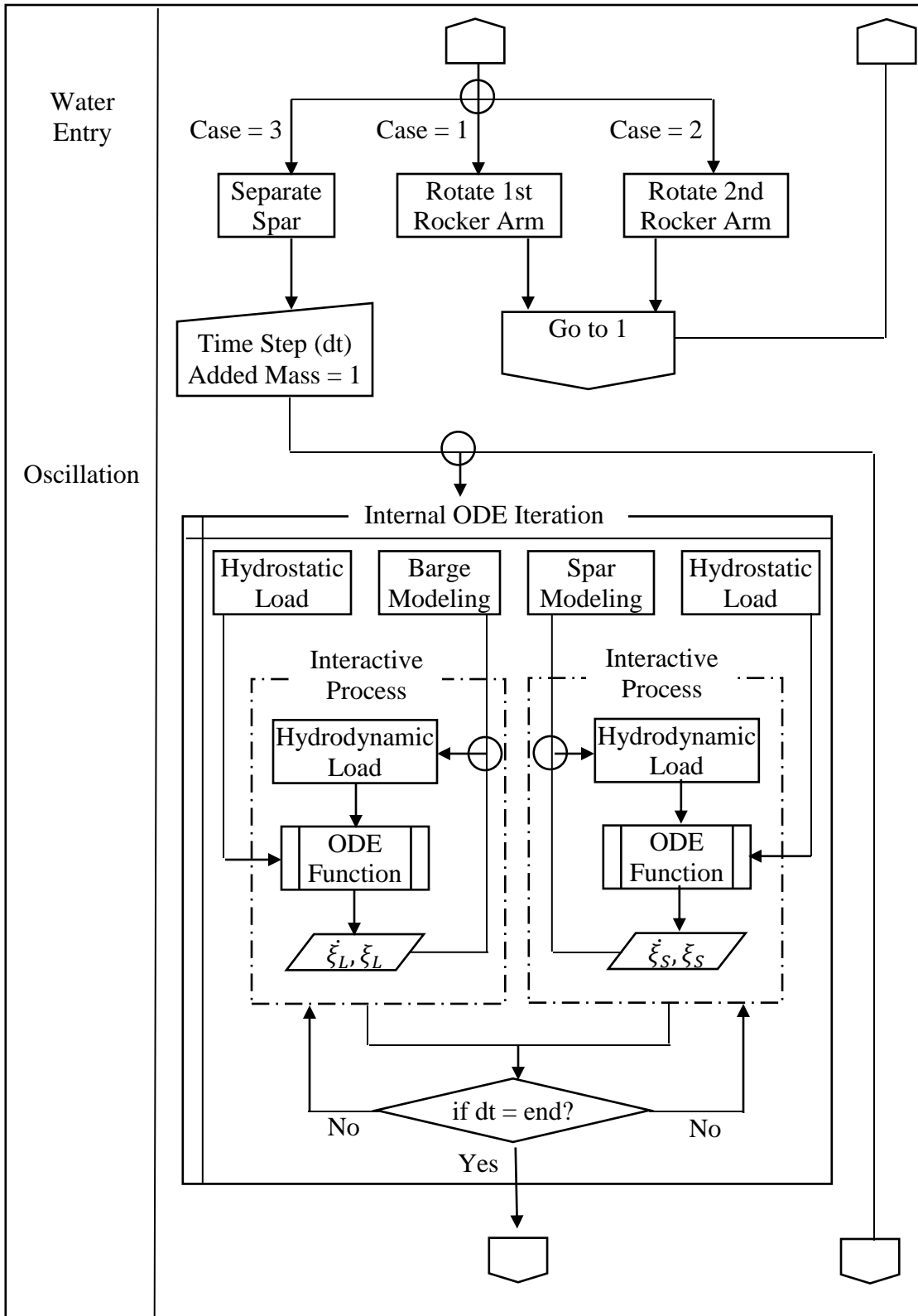


Figure 18 Continued

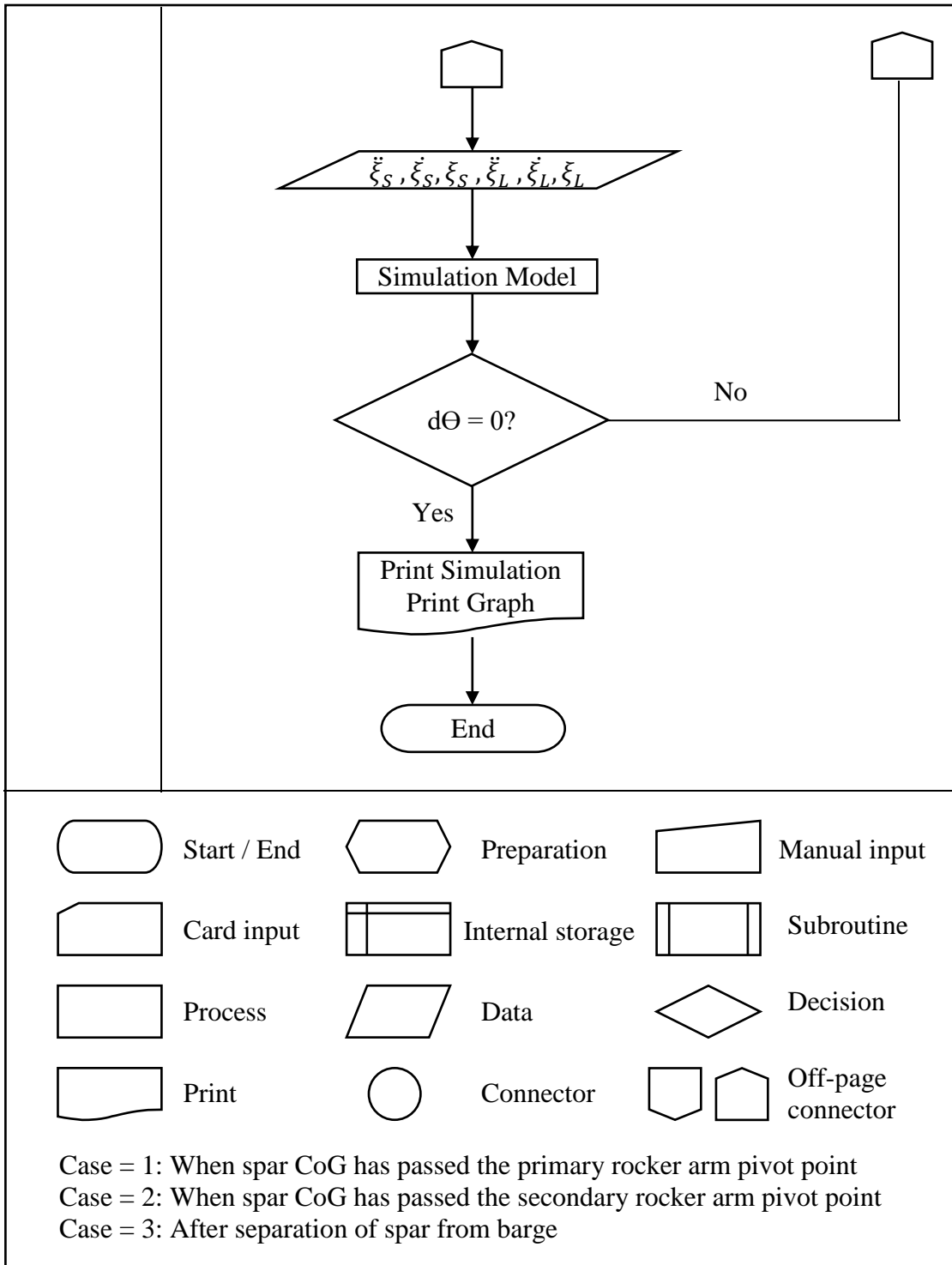


Figure 18 Continued

## 5. LAUNCHING AND UPENDING SIMULATION RESULTS

### 5.1 Added Mass for Spar Hull

$A_{11}$ ,  $A_{33}$  and  $A_{55}$  are the infinite frequency added mass yielded by WAMIT for the surge, heave and pitch motion during water entry, respectively.  $C_{a11}$ ,  $C_{a33}$ ,  $C_{a55}$  are the ratio comparing with the spar mass.

$$C_{a11} = \frac{A_{11}}{m_S}, C_{a33} = \frac{A_{33}}{m_S}, C_{a55} = \frac{A_{55}}{m_S} \quad (5.1)$$

For purposes of the simulation, the added mass ratios are defined as functions of the trim angle and the submerged depth from the water surface to the end of the spar hull,  $D$ , as shown in Figure 16.

Initial simulations with nominal values of the added mass coefficients were run to determine the approximate trajectory of the spar for each of the two methods of launching. Based on the approximate trajectories, a sequence of discrete spar positions was identified and a WAMIT calculation of the infinite frequency added mass values was performed for each position.

Table 6 provides the discrete ranges of spar position and the associated added mass value for the bottom launch scenario. In the case of the bottom launch scenario the trim angle was monitored as the basis for assigning the associated values of added mass in the simulation.

**Table 6 Added mass coefficient of spar hull for bottom launch**

No.	Trim angle (degree)	D (m)	Description	Ca <sub>11</sub>	Ca <sub>33</sub>	Ca <sub>55</sub>
1	$2.5 \leq \theta \leq 5.28$	$D \leq 4.33$	Start entering water	0	0.05	0.01
2	$5.28 < \theta \leq 7.23$	$4.33 < D \leq 11.33$	Entering water	0.05	0.2	0
3	$7.23 < \theta \leq 10.14$	$11.33 < D \leq 14.99$	Rotating primary rocker arm	0.07	0.22	0
4	$10.14 < \theta \leq 18.9$	$14.99 < D \leq 27.38$	Rotating 2nd rocker arm	0.2	0.28	0.01
5	$18.9 < \theta \leq 32.14$	$27.38 < D \leq 46.31$	Rotating 2nd rocker arm	0.39	0.33	0.1
6	$32.14 < \theta \leq 41.84$	$46.31 < D \leq 59.73$	Rotating 2nd rocker arm	0.48	0.32	0.24
7	$41.84 < \theta \leq 48.22$	$59.73 < D \leq 68.13$	Rotating 2nd rocker arm	0.53	0.29	0.37
8	$48.22 < \theta \leq 60.14$	$68.13 < D \leq 80.21$	Rotating 2nd rocker arm	0.59	0.21	0.64
9	$60.14 < \theta \leq 72.51$	$80.21 < D \leq 89.96$	Rotating 2nd rocker arm	0.64	0.13	0.92
10	$72.51 < \theta \leq 90$	$89.96 < D \leq 94.34$	Rotating 2nd rocker arm	0.67	0.07	1.15
11	$90 < \theta \leq 100$	$94.34 < D \leq 97.74$	Separating spar & high speed water entry	0.71	0.08	1.32
12	$100 < \theta \leq 121$	$94.85 < D \leq 97.74$	Separating spar & high speed water entry	0.77	0.27	1.24
13	$121 < \theta \leq 131$	$87.7 < D \leq 94.85$	Separating spar & high speed water entry	0.81	0.37	1.21
14	$131 < \theta \leq 143$	$77.6 < D \leq 87.7$	Separating spar & high speed water entry	0.94	0.65	1.13
15	$143 < \theta \leq 155$	$D \leq 77.6$	Separating spar & high speed water entry	1.1	0.96	1
16			Oscillation	1	1	1

Table 7 provides the corresponding information for the top launching scenario. In the case of the top launch scenario the depth of submergence was monitored as the basis for assigning the associated values of added mass before the spar separated from the barge. After the spar separated from the barge and while it was rotating into the vertical position, the trim angle was monitored as the basis for assigning the associated value of added mass in the simulation.

**Table 7 Added mass coefficient of spar hull for top launch**

No.	Trim angle (degree)	D (m)	Description	Ca <sub>11</sub>	Ca <sub>33</sub>	Ca <sub>55</sub>
1	$\theta \leq 5.05$	$D \leq 1.88$	Start entering water	0	0.05	0.01
2	$\theta \leq 5.05$	$1.88 < D \leq 3.67$	Entering water	0	0.1	0.06
3	$5.05 < \theta \leq 6.43$	$3.67 < D \leq 7.2$	Entering water	0.01	0.17	0.16
4	$6.43 < \theta \leq 6.89$	$7.2 < D \leq 10.49$	Entering water	0.02	0.27	0.38
5	$6.89 < \theta \leq 8.05$	$10.49 < D \leq 15.82$	Entering water	0.04	0.4	0.86
6	$6.2 < \theta \leq 8.05$	$15.82 < D \leq 16.11$	Rotating primary rocker arm	0.04	0.54	2.03
7	$6.2 < \theta \leq 6.66$	$16.11 < D \leq 21$	Rotating 2nd rocker arm	0.06	0.68	3.23
8	$2 < \theta \leq 4.22$	$15.56 < D \leq 16.11$	Rotating 2nd rocker arm	0.2	0.59	0
9	$0 < \theta \leq 2$	$11.8 < D \leq 15.56$	Rotating 2nd rocker arm	0.18	0.62	0
10	$-6 < \theta \leq 0$	$D \leq 16.4$	Separating spar & high speed water entry	0.2	0.57	0
11	$-15 < \theta \leq -6$	$16.4 < D \leq 27.62$	Separating spar & high speed water entry	0.35	0.52	0.02

**Table 7 Continued**

No.	Trim angle (degree)	D (m)	Description	Ca <sub>11</sub>	Ca <sub>33</sub>	Ca <sub>55</sub>
12	$-27 < \theta \leq -15$	$27.62 < D \leq 48.34$	Separating spar & high speed water entry	0.64	0.65	0.18
13	$-45 < \theta \leq -27$	$48.34 < D \leq 75.24$	Separating spar & high speed water entry	0.81	0.61	0.69
14	$-80 < \theta \leq -45$	$75.24 < D \leq 99.25$	Separating spar & high speed water entry	0.77	0.23	1.3
15	$-90 < \theta \leq -80$	$99.25 < D \leq 109.75$	Separating spar & high speed water entry	0.81	0.1	1.8
16			Oscillation	1	1	1

The time series of added mass applied in each of the three bottom launch and top launch case studies are presented in Figure 19 and Figure 20.



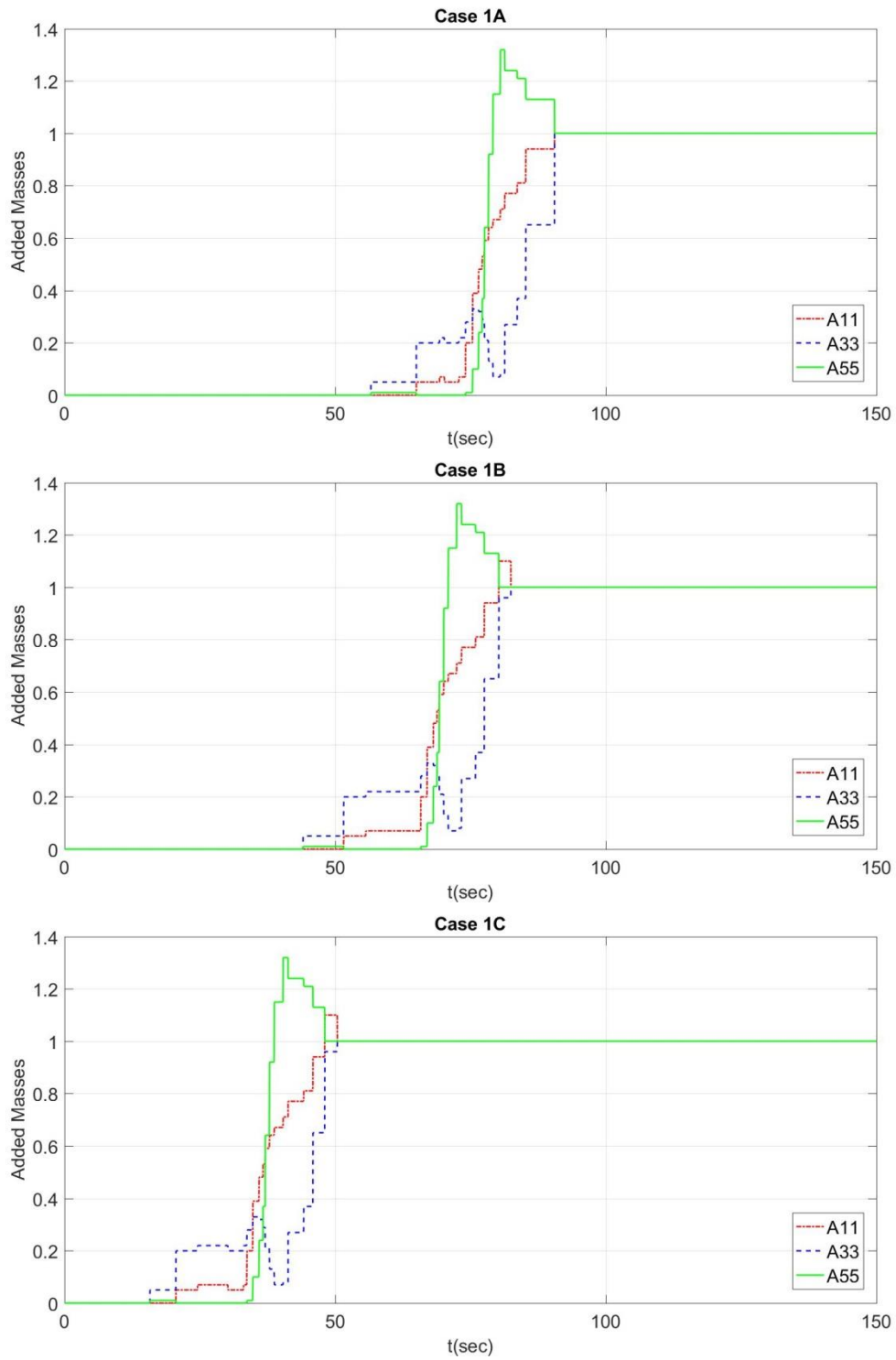


**Figure 19 Added mass of spar hull - Case study 1**

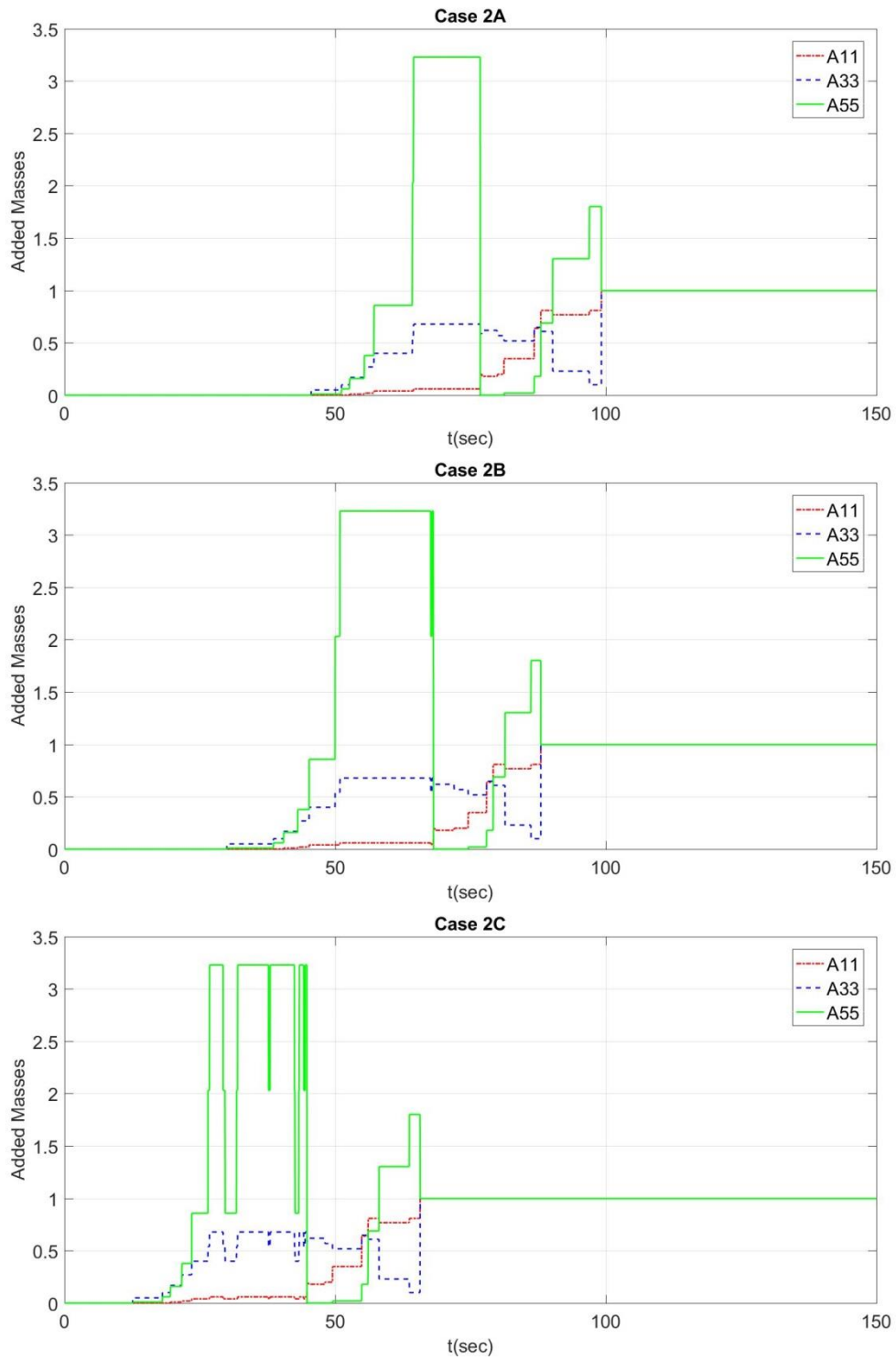


**Figure 20 Added mass of spar hull - Case study 2**

## 5.2 Discussion of Results

This section provides the following simulation results.

- Launching trajectories
  - Pre-launching
  - Sliding
  - Water entry
  - Rotating rocker arm
  - Separating the spar hull
- Acceleration of the spar hull and the barge
- Velocity of the spar hull and the barge
- Displacement of the spar hull and the barge
- Angular acceleration of the spar hull and the barge
- Pitch trim angle of the spar hull and the barge
- Bearing force and friction force
- Hydrodynamic force of the spar hull
- Reynolds number of the spar hull
- Drag coefficient of the spar hull
- Buoyancy of the spar hull and the barge
- Center of buoyancy of the spar hull and the barge

Figures are provided illustrating the time-evolution of the above quantities during the launching sequence on the barge for detailed investigation of critical phases.

Figures 21 to 35 show the distinct stages of the launch trajectories for the six case studies. The launch trajectories are plotted in the global (X, Z) frame of reference. The Z-axis is the vertical direction (positive upward) and the X-axis is the horizontal direction (positive toward the right). The origin of the global coordinate system is the barge center of gravity at the start of the launching sequence.

Figure 21 and Figure 22 show the model for the initial condition as described in Section 2.5. Figure 23 and Figure 24 illustrate the spar sliding phase. This phase finishes when the spar hull touches down on the water surface. Figure 25 and Figure 26 show the simulation of water entry of the spar hull. This phase finishes when the primary rocker arm starts to rotate after the CoG of the spar hull moves past the pivot point of the primary rocker arm.

Figure 27 and Figure 29 simulate the rotating primary rocker arm and secondary rocker arm, respectively, for Case study 1. The primary rocker arm and the secondary rocker arm rotate with the spar hull.

Figure 28 simulates the rotating primary rocker arm for Case study 2. In this case, the primary rocker arm rotates counterclockwise while the spar hull rotates clockwise as the end of the spar hull moves past the pivot point of the primary rocker arm. The clockwise rotation of the spar hull relative to the rocker arm is due to the large countermoment developed by the increasing buoyancy of the spar. The secondary rocker arm will rotate when the end of the spar hull moves past the pivot point of the secondary rocker arm.

Figure 30 shows the spar hull separating from the barge for Case study 1. The forward momentum of the spar hull causes it to rotate by a large amount as it begins to undergo free oscillations.

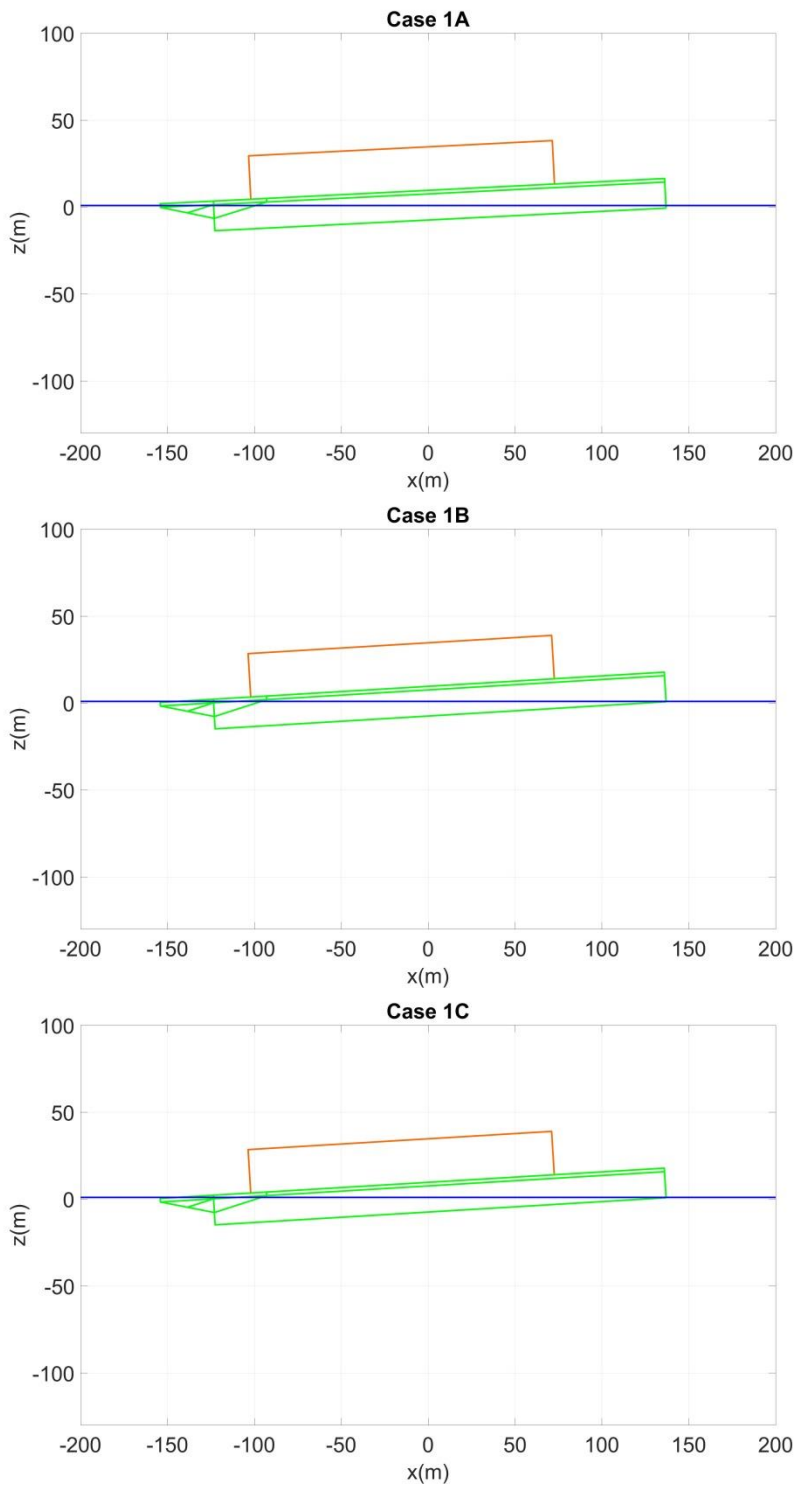
Figure 31 shows the spar hull separation for Case study 2. This phase is noteworthy compared with the Case study 1. The spar hull upends by rotating in the reverse direction compared to Case study 1.

Figure 32 and Figure 33 show the complete launching simulation for Case study 1 and Case study 2, respectively. Figure 34 and Figure 35 show the entire simulation from launching to oscillation of the spar hull.

The main results from the six case studies are summarized in Table 8 to facilitate comparison.

The bottom launching and top launching are investigated with three scenarios according to the initial condition, respectively. The trends in the results for Cases 1A, 1B and 1C are similar. The trends in the results for Cases 2A, 2B and 2C are similar to each other, but distinctly different than those for the Case 1 simulations. In all cases the timing of the individual stages is different in a manner that is consistent with the initial conditions.

In Case study 1, the rate of increase of the linear and angular velocity of the spar during the launching phase is significantly higher than in Case study 2, due to the larger buoyancy moment that is quickly developed in the latter case. In both cases the linear and angular velocity decrease dramatically following separation and during upending of the spar hull.



**Figure 21 Initial position - Case study 1**

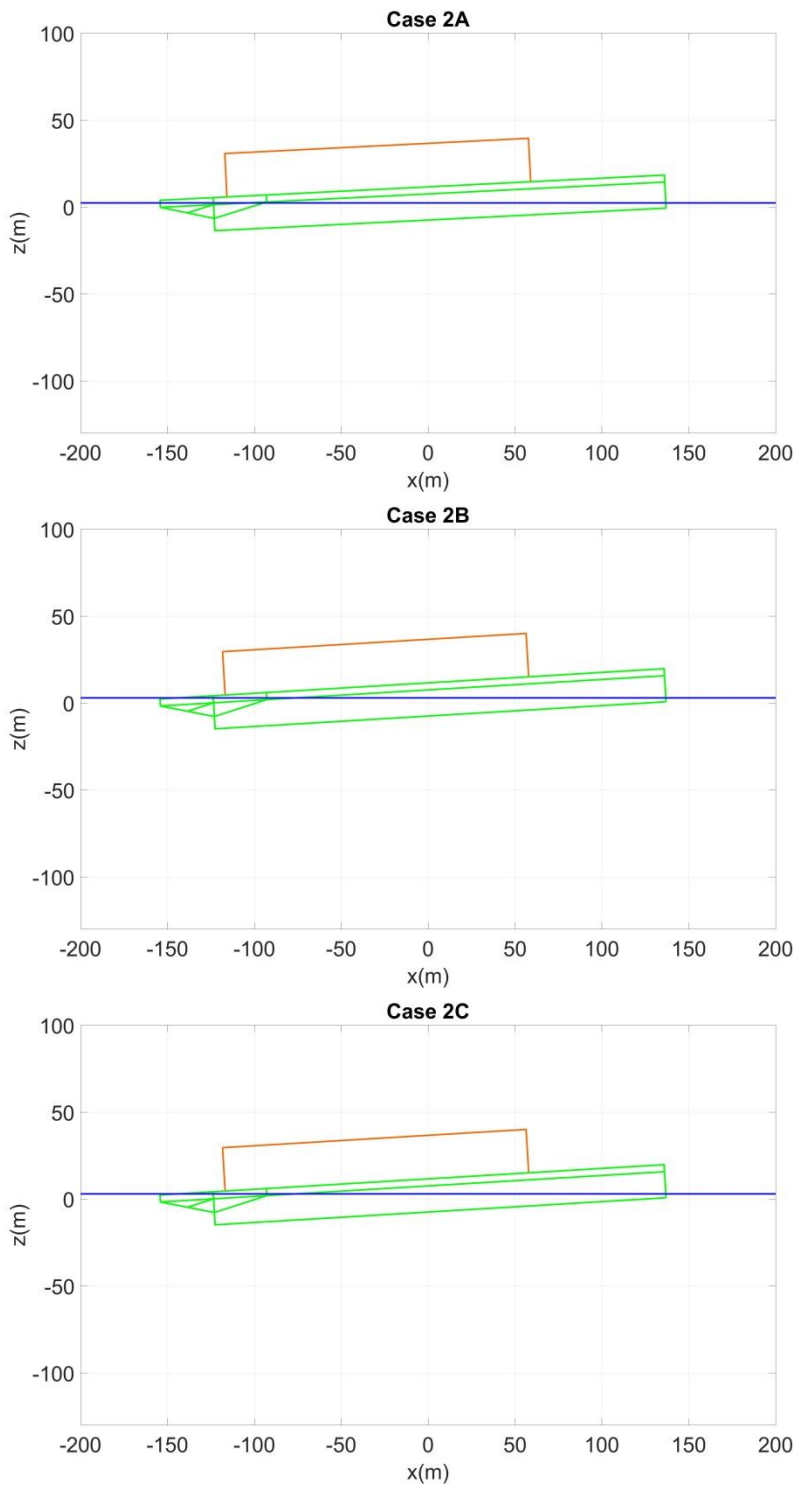


**Figure 22 Initial position - Case study 2**

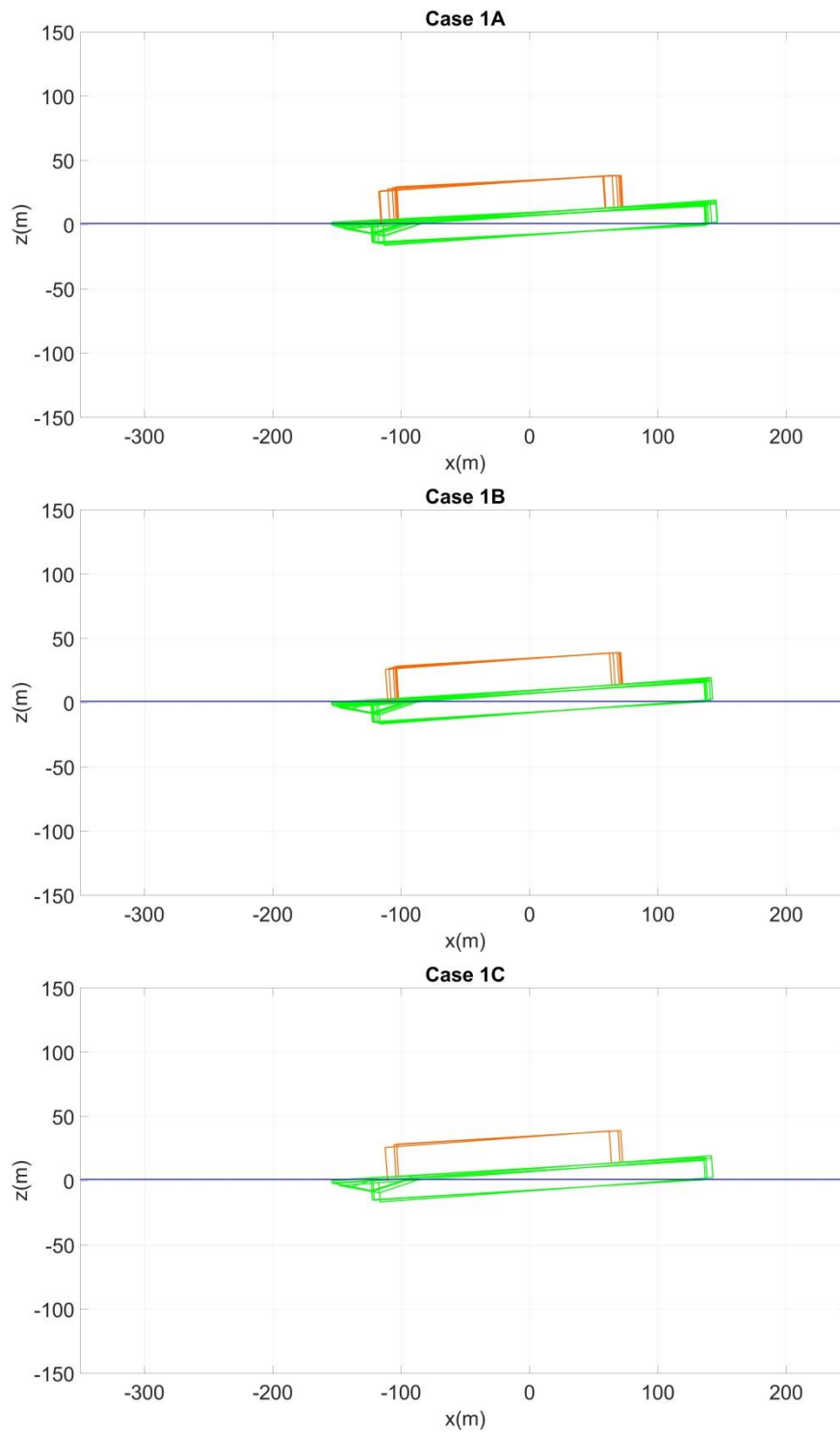


**Figure 23 Start sliding - Case study 1**



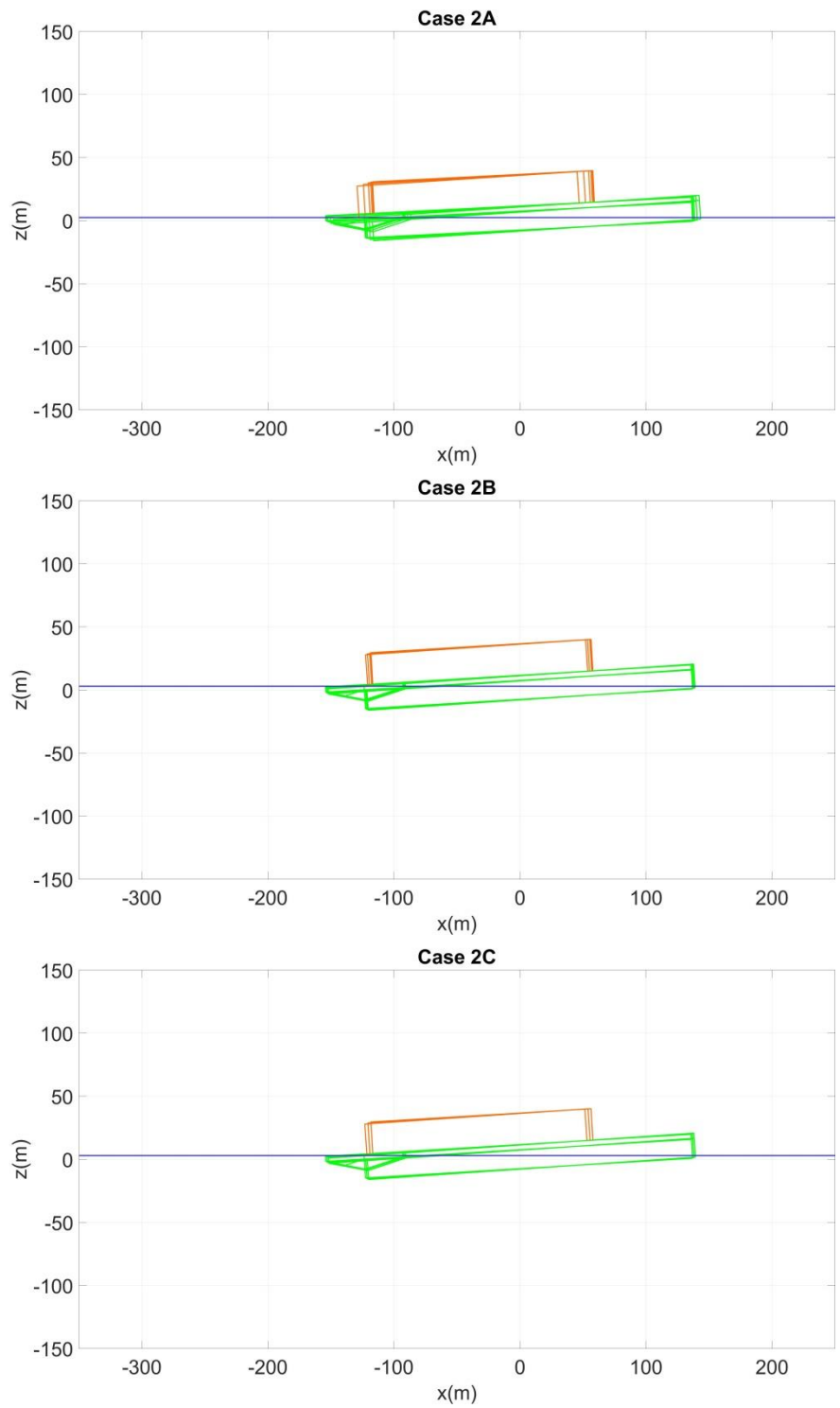


**Figure 24 Start sliding - Case study 2**

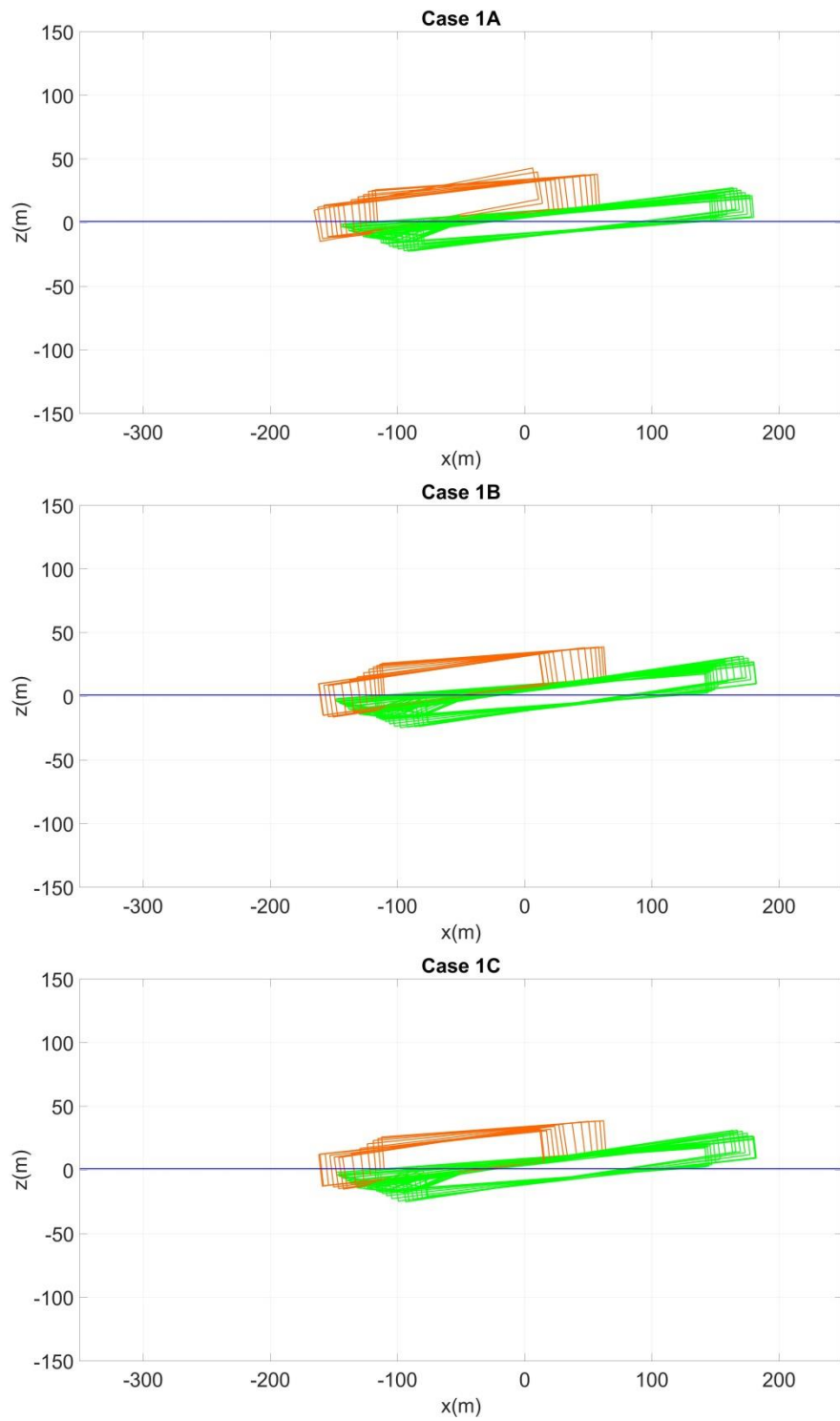


**Figure 25 Enter water - Case study 1**

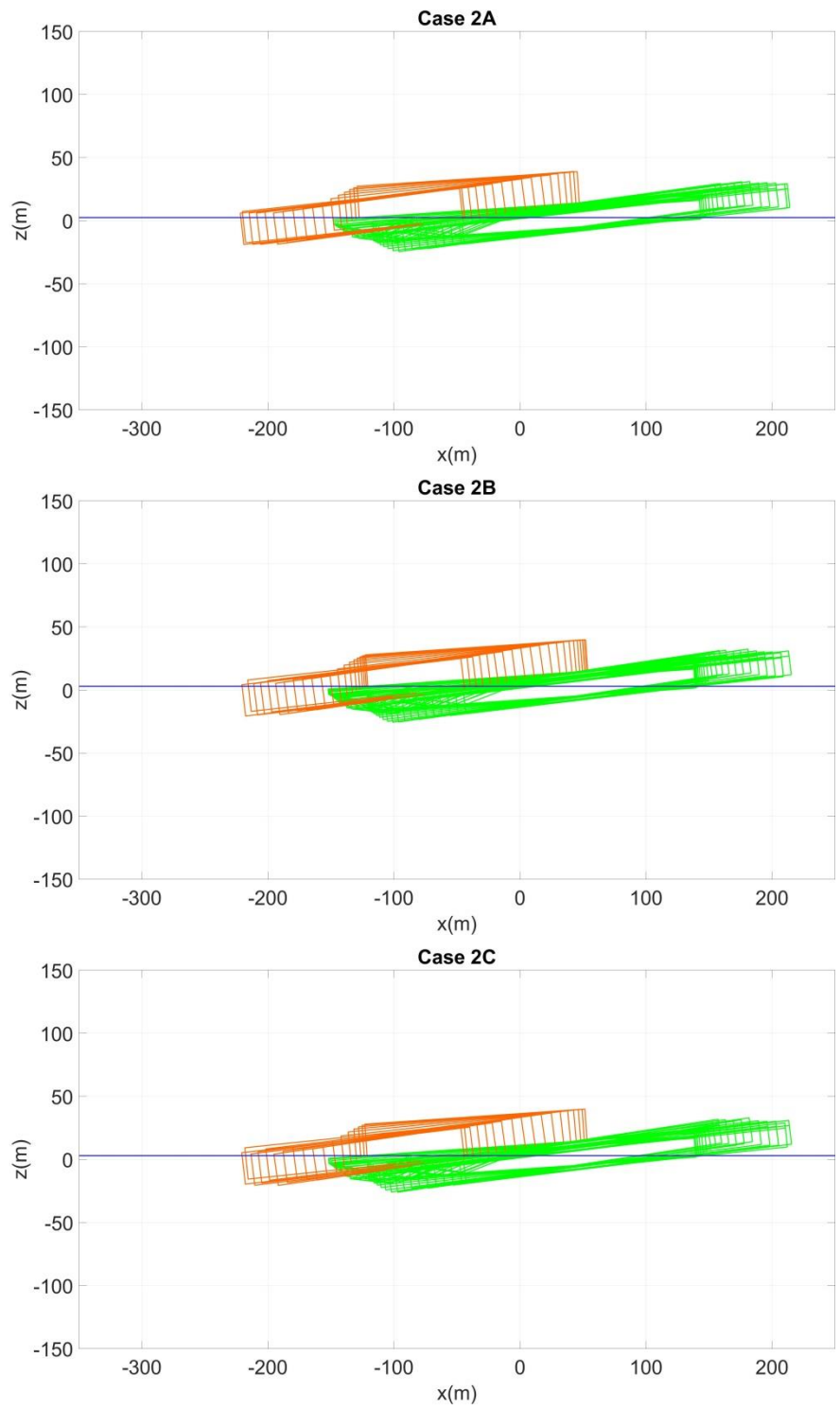


**Figure 26 Enter water - Case study 2**

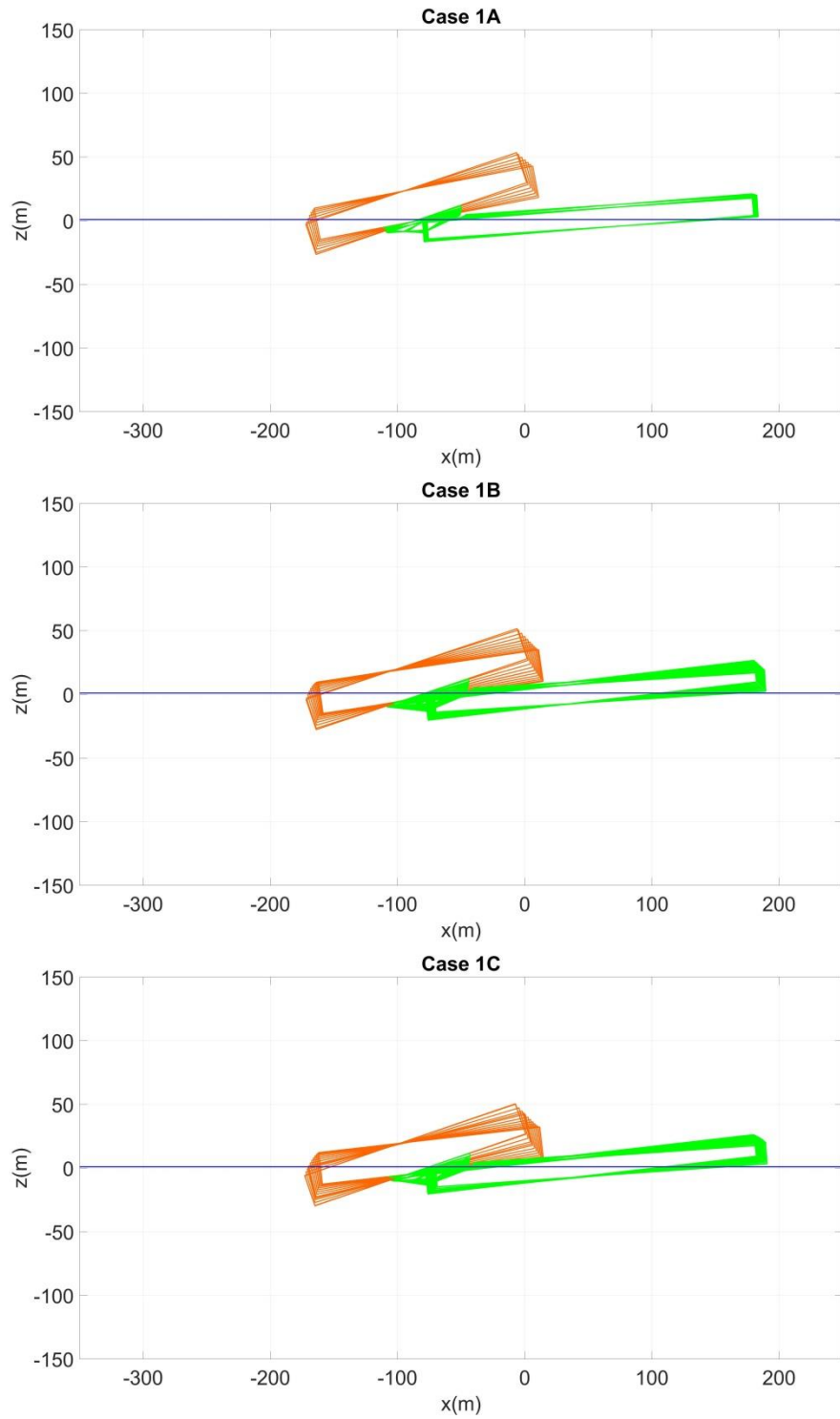


**Figure 27 Primary rocker arm rotates - Case study 1**

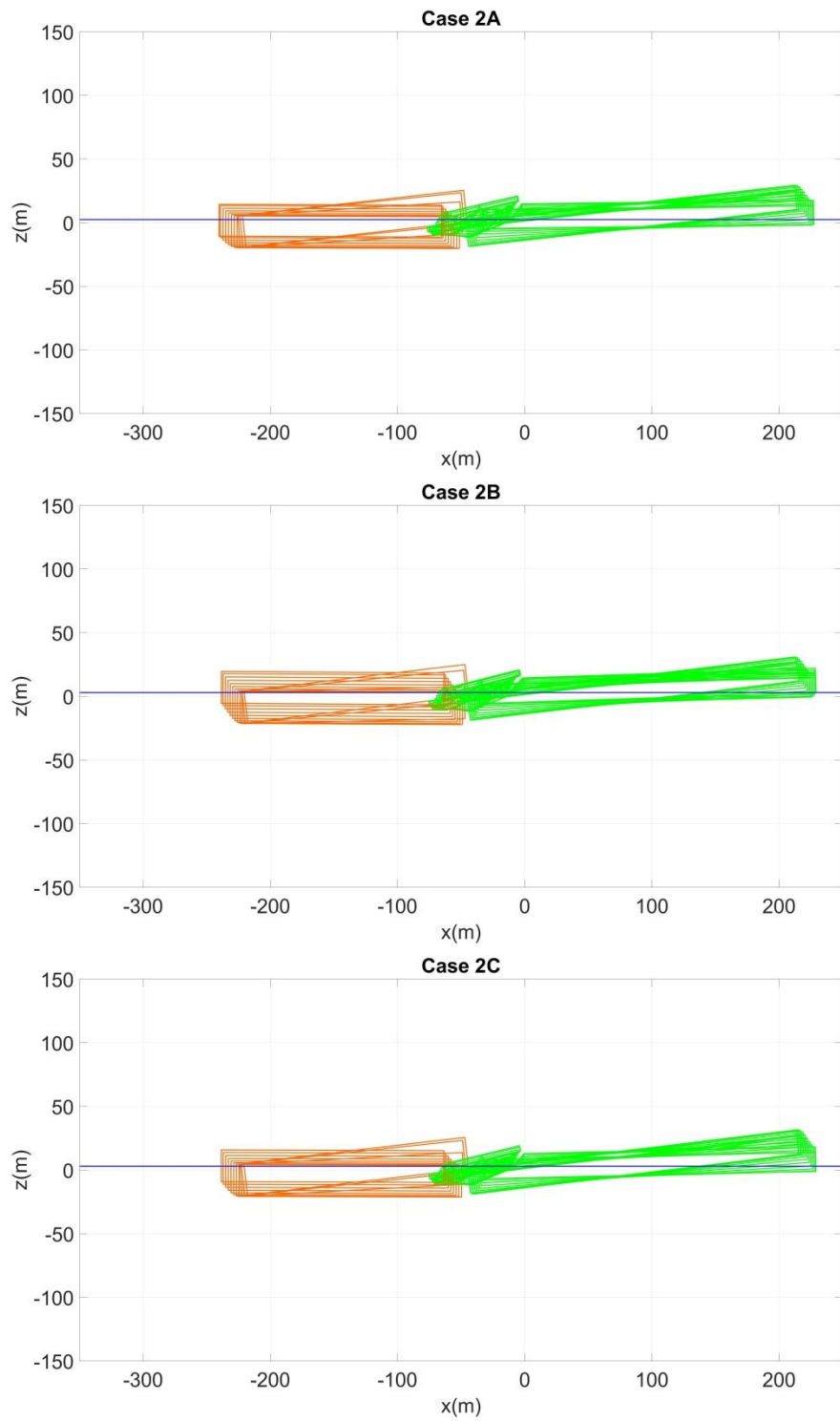


**Figure 28 Rocker arms rotate - Case study 2**

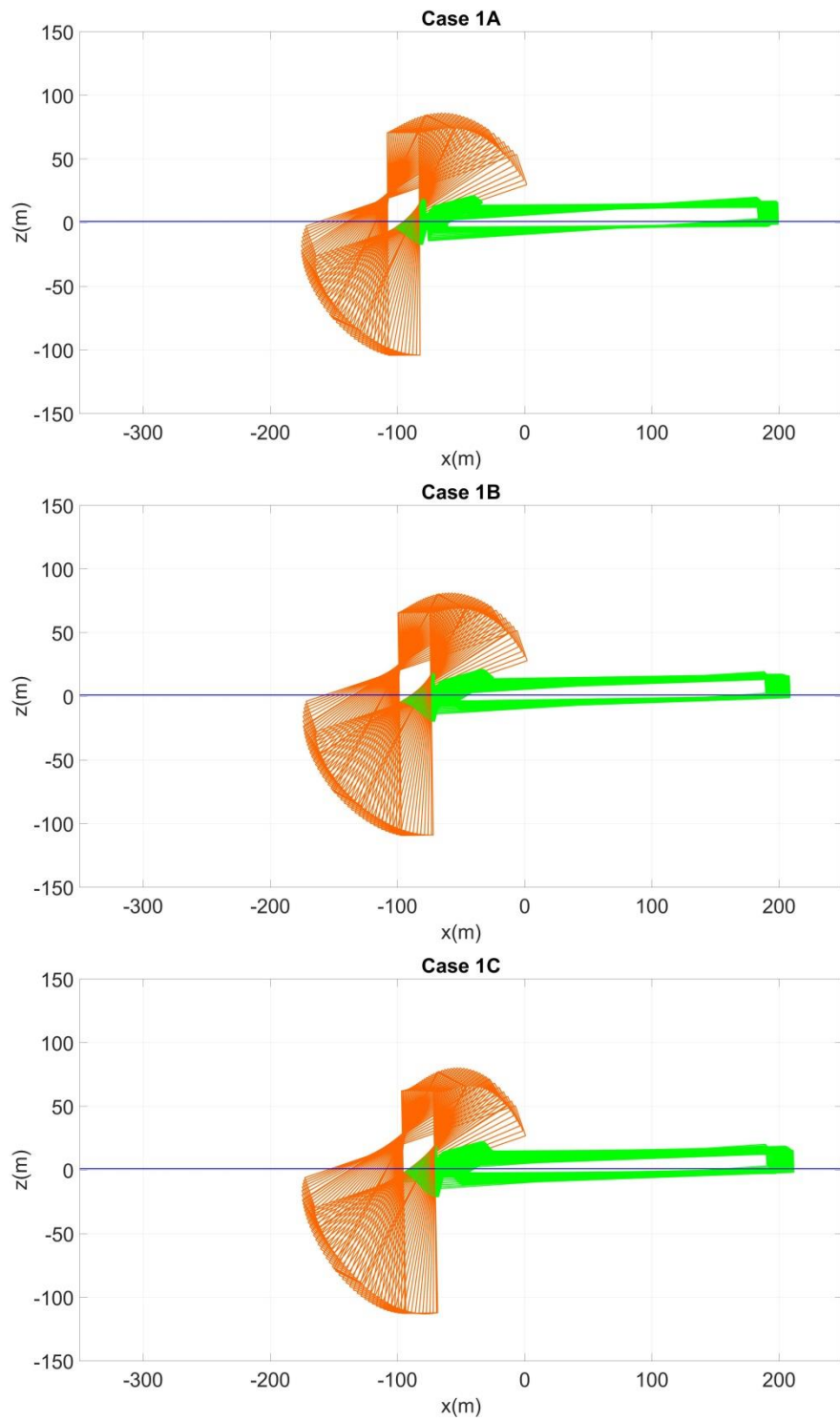


**Figure 29 Secondary rocker arm rotates - Case study 1**

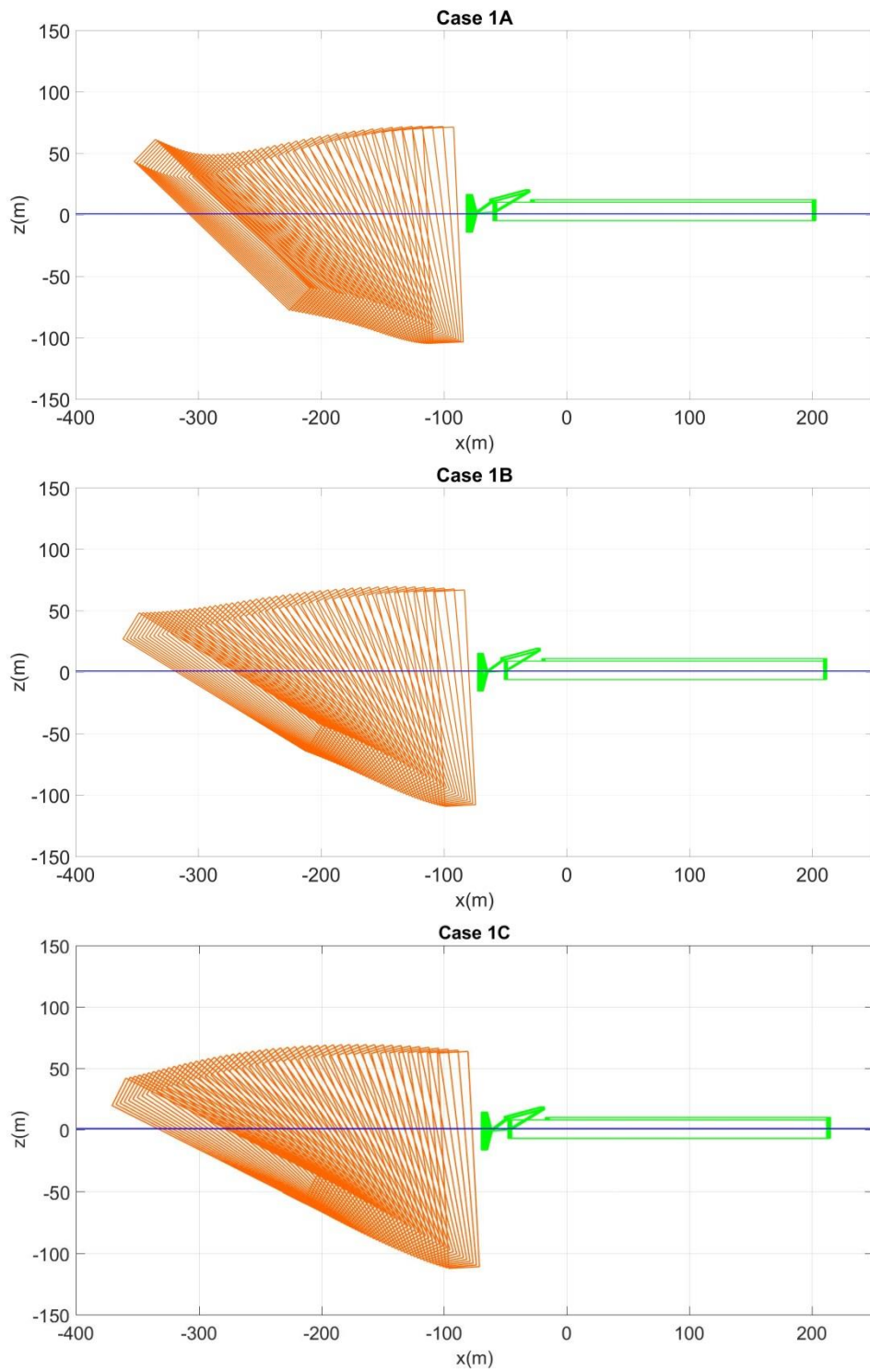


**Figure 30 Spar separates from barge - Case study 1**

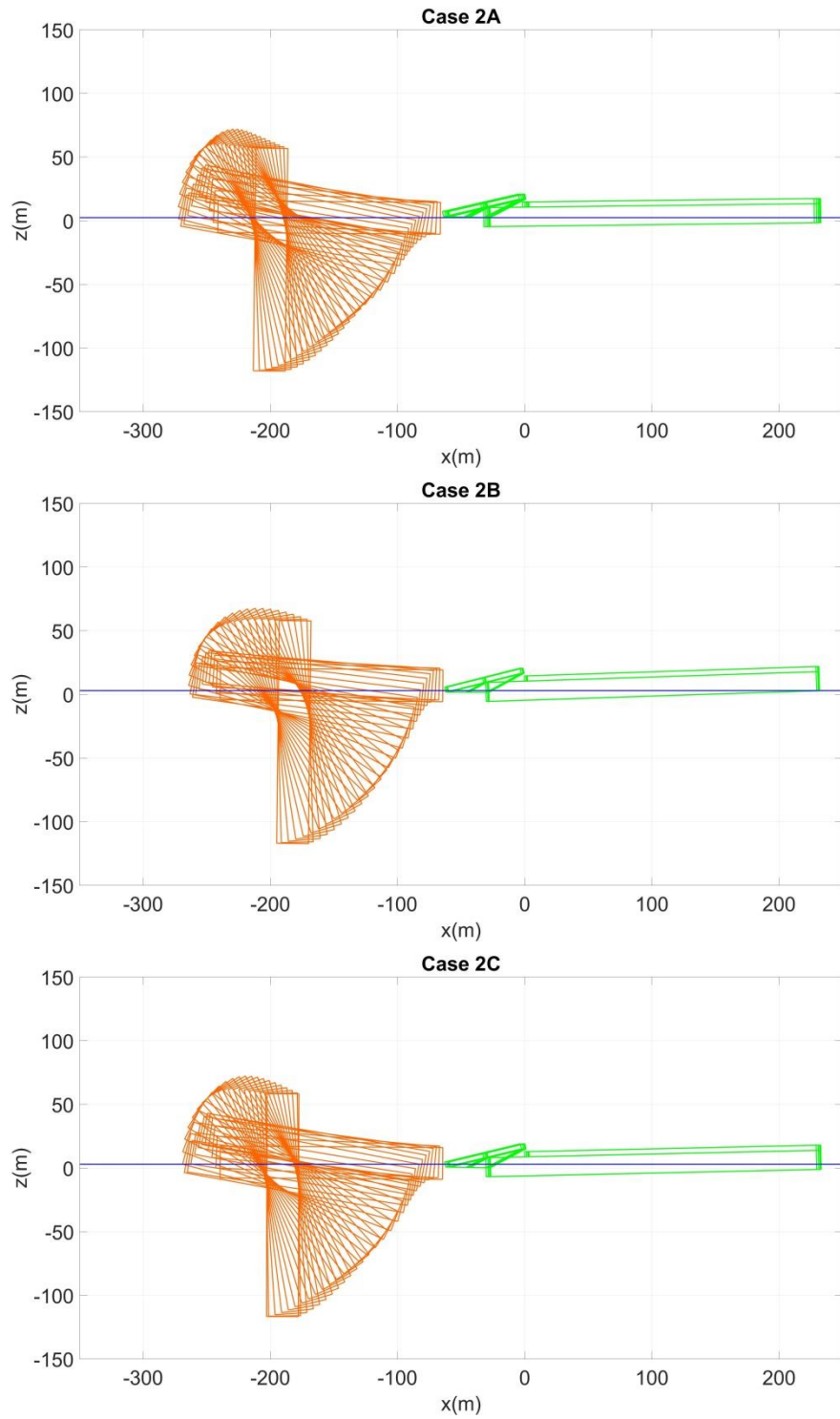


**Figure 31 Spar separates from barge - Case study 2**



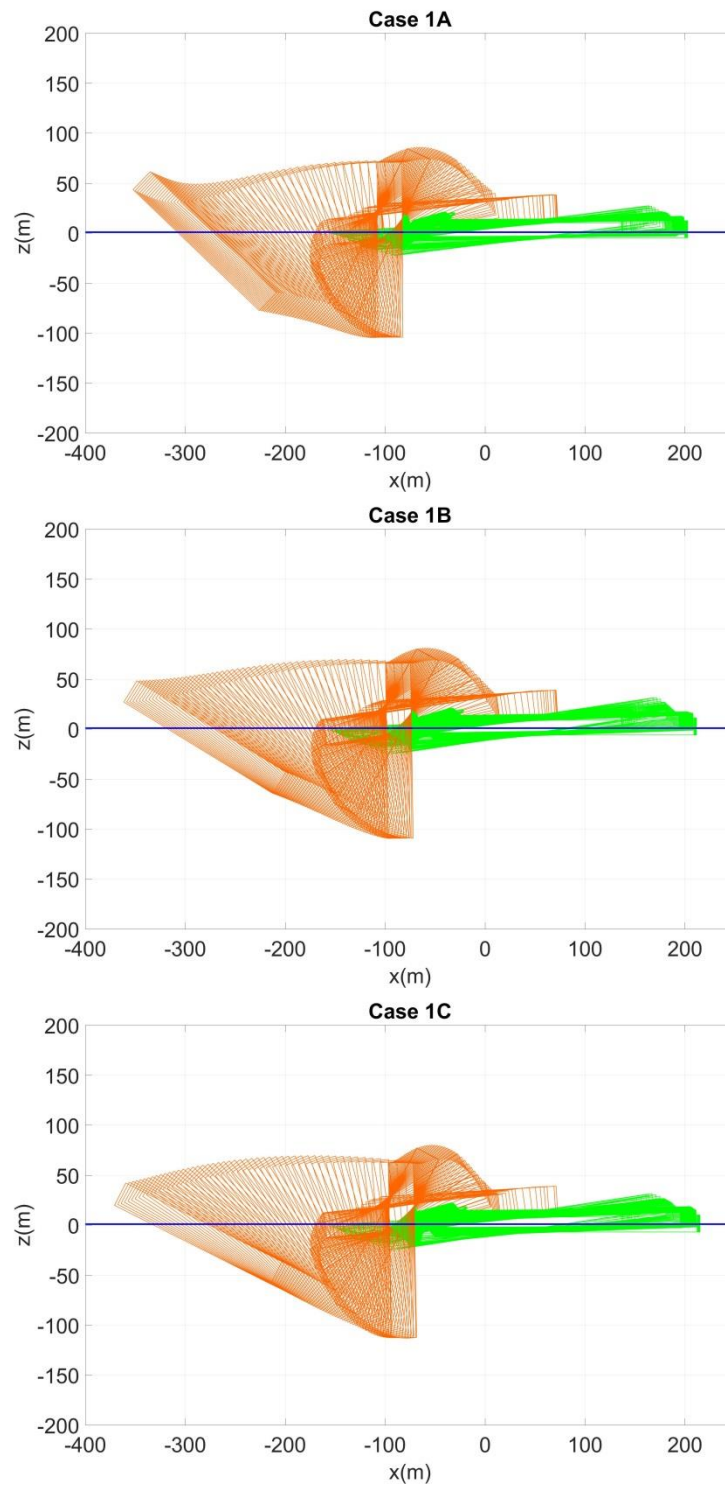


**Figure 32 Whole launch phase - Case study 1**

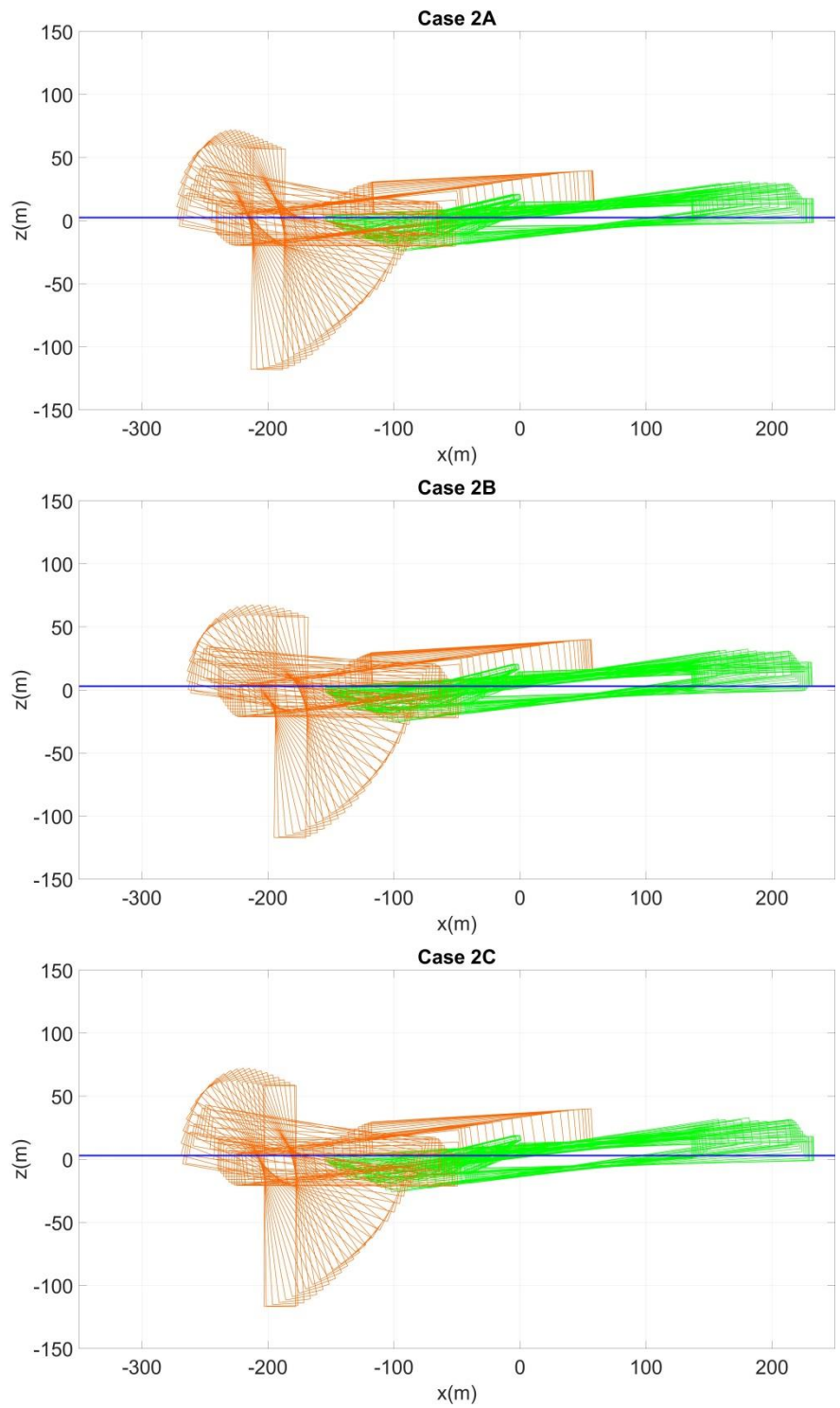


**Figure 33 Whole launch phase - Case study 2**

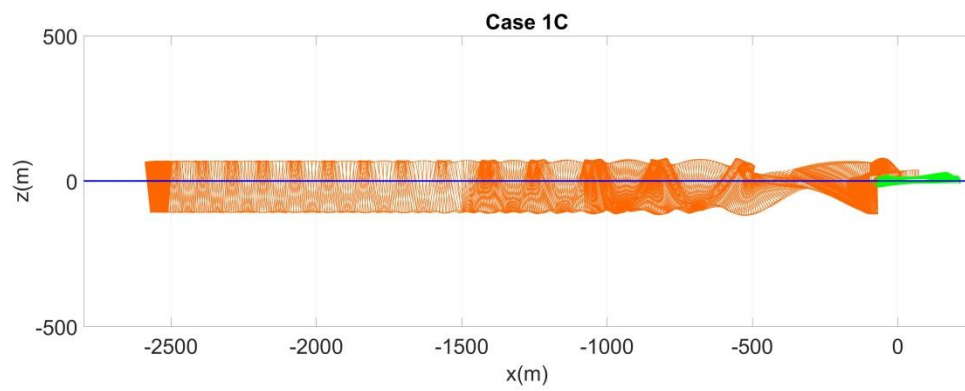
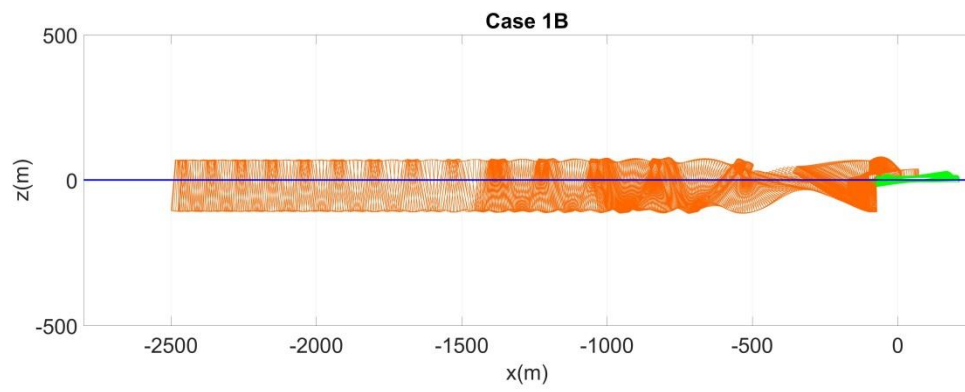
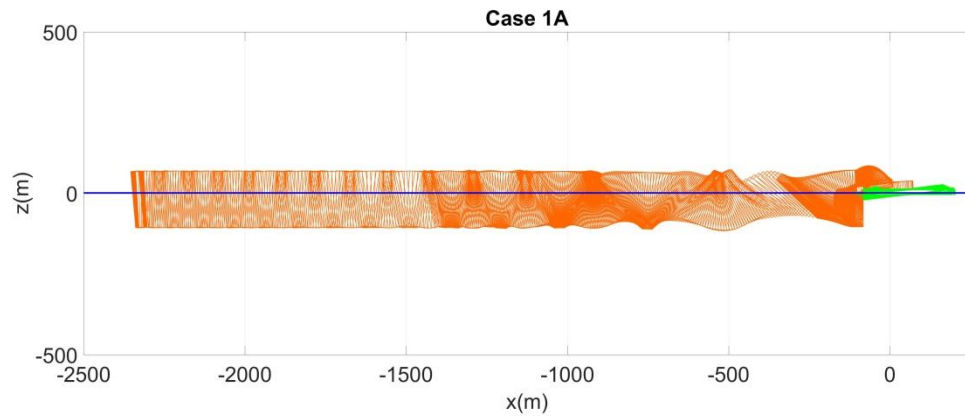


**Figure 34 Oscillation and drift after launch - Case study 1**

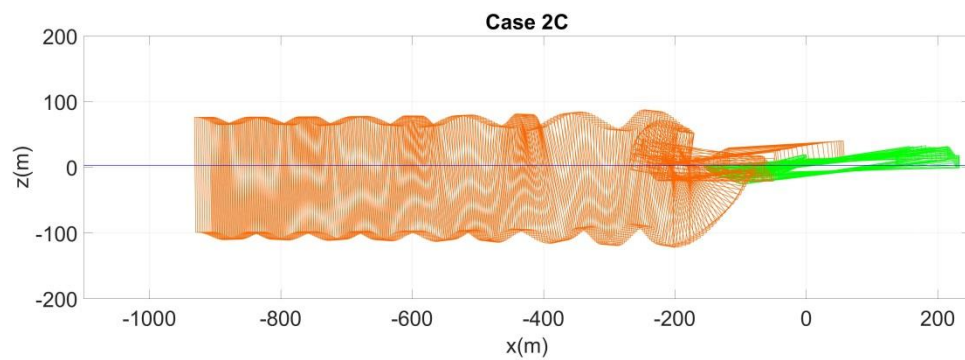
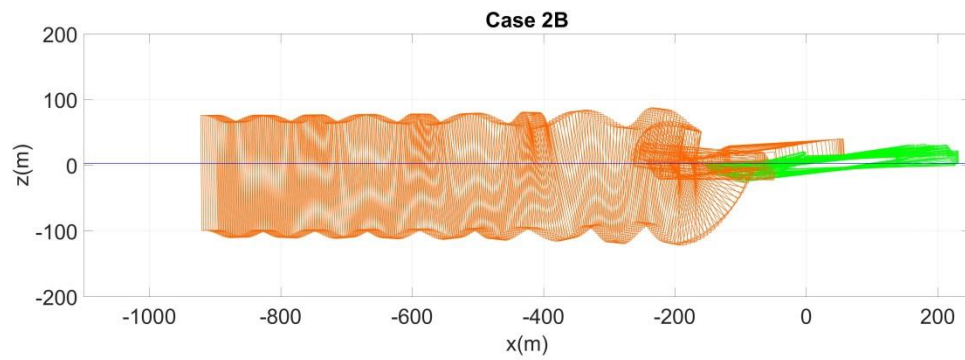
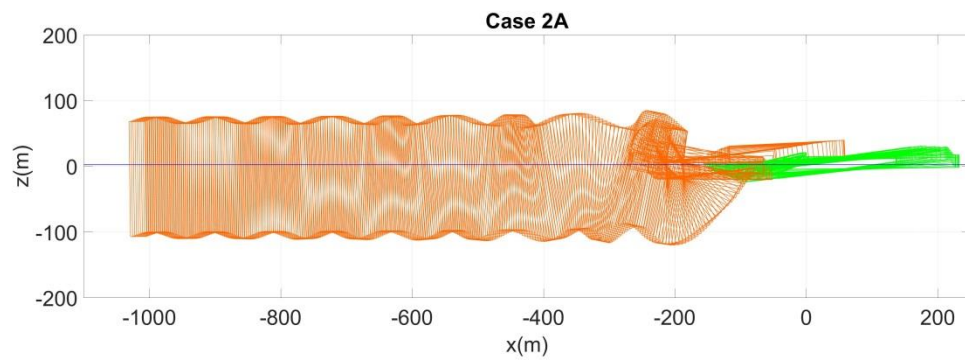


**Figure 35 Oscillation and drift after launch - Case study 2**

**Table 8 Summary of results**

	<b>Case 1A</b>	<b>Case 1B</b>	<b>Case 1C</b>	<b>Case 2A</b>	<b>Case 2B</b>	<b>Case 2C</b>
Draft midships (m)	8.0	8.0	8.0	9.5	10.0	10.0
Trim angle (radians)	0.05	0.06	0.06	0.05	0.06	0.06
Kinetic friction coefficient	0.05	0.06	0.05	0.05	0.06	0.05
Beginning of simulation (sec)	0	0	0	0	0	0
End of simulation (sec)	1252	1234.47	1241.41	357.2	339	316.72
<b>Pre-launching</b>						
Time (sec)	0	0	0	0	0	0
Spar						
weight (M-tons)	54,000	54,000	54,000	54,000	54,000	54,000
CG from center, keel (m)	(0, 51.69)	(0, 51.69)	(0, 51.69)	(0, 51.69)	(0, 51.69)	(0, 51.69)
Barge						
weight (M-tons)	48,560	48,560	48,560	48,560	48,560	48,560
CG from center, keel (m)	(136.8, 7.5)	(136.8, 7.5)	(136.8, 7.5)	(136.8, 7.5)	(136.8, 7.5)	(136.8, 7.5)
buoyancy (M-tons)	133,936	134,009	134,009	158,039	163,123	163,123
CB from CG (m)	(-28.9, -4.05)	(-32.3, -4.37)	(-32.3, -4.37)	(-23.3, -3.19)	(-25.5, -3.25)	(-25.5, -3.25)
Total ballast water						
weight (M-tons)	31,377	31,450	31,450	55,480	60,565	60,565
CG from center, keel (m)	(-38.6, 3.68)	(-65.7, 3.10)	(-65.7, 3.10)	(-74.8, 5.79)	(-82.4, 6.36)	(-82.4, 6.36)
Jack force at start (M-tons)	2,964	2,367	2,367	2,964	2,367	2,367
Bearing load on deck (M-tons)	53,933	53,903	53,903	53,933	53,903	53,903
Trim angle	2.863°	3.438°	3.438°	2.863°	3.438°	3.438°

**Table 8 Continued**

	<b>Case 1A</b>	<b>Case 1B</b>	<b>Case 1C</b>	<b>Case 2A</b>	<b>Case 2B</b>	<b>Case 2C</b>
<b>Spar slides on barge</b>						
Start time (sec)	0	0	0	0	0	0
End time (sec)	56.70	44.17	15.9	45.51	27.7	11.2
Barge						
buoyancy at end (M-tons)	131,732	132,957	133,443	159,468	164,099	162,335
CB from CG at end (m)	(-40.8, -4.83)	(-41.8, -4.94)	(-41.4, -4.90)	(-28.5, -3.55)	(-27.3, -3.43)	(-28.1, -3.51)
Spar						
X-velocity (m/s)	-1.884	-1.336	-2.167	-1.743	-0.722	-1.408
Z-velocity (m/s)	-0.469	-0.290	-0.457	-0.273	-0.071	-0.257
Angular velocity (deg/sec)	0.392	0.017	0.151	0.195	0.092	0.839
Bearing load (M-tons)	53,932	53,903	53,902	53,932	53,903	53,903
Trim angle	4.028°	4.224°	4.205°	3.762°	3.898°	3.925 °
<b>Spar enters into water</b>						
Start time (sec)	56.70	44.17	15.9	45.51	27.7	11.2
End time (sec)	69.95	62.51	28.23	76.2	67.7	44.2
Barge						
buoyancy (M-tons)	121,792	113,809	119,213	117,440	117,160	114,589
CB from CG (m)	(-55.2, -8.24)	(-60.1, -10.1)	(-57.6, -9.73)	(-55.9, -7.64)	(-56.8, -8.11)	(-57.8, -8.12)
Spar						
X-velocity (m/s)	-6.282	-7.182	-7.175	-5.966	-5.245	-5.685
Z-velocity (m/s)	-0.255	-0.087	0.030	-2.376	-1.698	-4.239
Angular velocity (deg/sec)	-0.099	-0.028	0.005	-0.081	-0.117	0.839
buoyancy at end (M-tons)	11,118	18,642	15,623	40,691	47,172	43,939
CB from CG (m)	(-21.0, -9.97)	(-16.3, -8.11)	(-19.1, -9.00)	(-65.1, -11.3)	(-62.5, -10.8)	(-64.1, -11.2)

**Table 8 Continued**

	<b>Case 1A</b>	<b>Case 1B</b>	<b>Case 1C</b>	<b>Case 2A</b>	<b>Case 2B</b>	<b>Case 2C</b>
Bearing load (M-tons)	43,299	35,856	38,765	12,939	6,349	9,602
Trim angle	7.285°	8.51°	8.604°	6.377°	6.831°	6.676 °
<b>Primary rocker arm rotates</b>						
Start time (sec)	69.95	62.51	28.23	76.2	67.7	44.2
End time (sec)	75.41	66.99	34.83	77.327	68.602	45.25
Barge						
buoyancy at end (M-tons)	112,103	115,363	115,503	118,465	120,258	115,742
CB from CG at end (m)	(-46.7, -5.55)	(-43.2, -5.23)	(-46.6, -5.49)	(-54.6, -7.17)	(-54.2 -7.23)	(-57.5, -8.23)
trim angle	3.87°	3.63°	3.96°	5.969°	6.157°	6.860 °
Rocker arm						
load at start (M-tons)	43,299	35,856	38,764	12,939	6,348	9,602
load at end (M-tons)	21,579	17,445	12,446	0	0	0
Spar						
X-velocity (m/s)	-8.618	-8.364	-8.630	-5.727	-5.061	-5.459
Z-velocity (m/s)	-3.527	-2.858	-1.626	-31.508	-34.795	-34.098
Angular velocity (deg/sec)	-9.945	9.819	9.903	-18.158	-15.971	-15.509
buoyancy (M-tons)	24,248	26,603	29,403	83,344	87,910	86,791
CB from CG (m)	(-22.0, -10.0)	(-20.1, -9.07)	(-17.9, -8.22)	(-35.6, -0.50)	(-35.7,0.16)	(-35.7,-0.07)
trim angle	18.87°	18.63°	18.96°	0°	0°	0 °

**Table 8 Continued**

	<b>Case 1A</b>	<b>Case 1B</b>	<b>Case 1C</b>	<b>Case 2A</b>	<b>Case 2B</b>	<b>Case 2C</b>
<b>Second rocker arm rotates</b>						
Start time (sec)	75.41	66.99	34.83			
End time (sec)	80.529	72.388	40.295			
Barge						
buoyancy (M-tons)	88,518	108,907	126,089			
CB from CG (m)	(-20.8, -5.02)	(-23.6, -4.53)	(-22.5, -4.02)			
trim angle	1.432°	1.971°	2.175°			
Rocker arm						
load at start (M-tons)	21,579	17,445	12,446			
load at end (M-tons)	0	0	0			
Spar						
X-velocity (m/s)	-19.119	-19.561	-20.553			
Z-velocity (m/s)	-2.402	0.548	5.262			
Angular velocity (deg/sec)	11.676	10.672	9.936			
buoyancy (M-tons)	52,810	55,315	57,179			
CB from CG (m)	(0, 0.79)	(0, 3.28)	(0, 5.13)			
trim angle	90°	90°	90°			
<b>Spar separates from barge</b>						
Start time (sec)	80.53	72.34	40.295	77.327	68.602	45.25
End time(sec)	90.55	82.47	50.41	99.225	88.075	65.895
Barge						
buoyancy (M-tons)	91,429	113,236	129,880	92,014	72,852	115,606
CB from CG (m)	(4.55, -4.73)	(4.55, -4.07)	(4.55, -3.56)	(-6.95, -4.73)	(-35.2, -5.79)	(-12.7, -4.09)
trim angle	1.424°	2.01°	2.14°	0.677°	1.85°	1.276 °



**Table 8 Continued**

	<b>Case 1A</b>	<b>Case 1B</b>	<b>Case 1C</b>	<b>Case 2A</b>	<b>Case 2B</b>	<b>Case 2C</b>
<b>Spar</b>						
X-velocity (m/s)	-12.390	-12.675	-13.212	-3.986	-4.022	-3.875
Z-velocity (m/s)	5.696	5.976	5.481	-1.242	-2.188	-2.323
Angular velocity (deg/sec)	-0.996	2.064	3.549	0.963	-5.358	-4.466
buoyancy (M-tons)	50,496	52,653	54,519	61,035	61,284	61,096
CB from CG (m)	(1.22, -1.19)	(-0.65, 0.07)	(-2.53, 0.80)	(0.56, 8.95)	(0.67, 9.19)	(0.52, 9.01)
max dive depth (m)	84.21	78.16	76.0	-117.91	116.947	116.694
trim angle	136.232°	148.48°	153.248°	-90°	-90°	-90°
<b>Maxima</b>						
<b>Barge for launching</b>						
buoyancy (M-tons)	138,457	136,105	134,263	159,732	164,231	163,329
X-velocity (m/s)	3.266	3.802	4.105	3.454	3.224	3.450
Z-velocity (m/s)	1.259	2.085	2.227	0.380	0.512	0.625
pitch angular velocity (deg/s)	0.929	0.525	1.336	0.548	0.461	0.875
pitch angle	7.285°	8.51°	8.604°	7.771°	8.356°	8.620°
<b>Spar for launching</b>						
buoyancy (M-tons)	52,810	55,315	57,215	83,344	87,910	86,791
X-velocity (m/s)	-0.001	-0.001	-0.001	-0.001	-0.001	-0.001
Z-velocity (m/s)	1.524	1.911	5.262	0.062	4.386	1.156
pitch angular velocity (deg/s)	15.776	15.004	15.125	0.548	0.461	0.875
pitch angle	90°	90°	90°	7.771°	8.356°	8.620°
<b>Spar for oscillation</b>						
pitch angle	150.405°	167.426°	171.911°	-79.902°	-76.987°	-77.454°
dive depth at bottom (m)	115.66	113.2	116.8	119.157	120.557	120.744

**Table 8 Continued**

	<b>Case 1A</b>	<b>Case 1B</b>	<b>Case 1C</b>	<b>Case 2A</b>	<b>Case 2B</b>	<b>Case 2C</b>
<b>Minima</b>						
Barge for launching						
buoyancy (M-tons)	59,281	46,781	40,652	117,437	116.355	114,458
X-velocity (m/s)	0.001	0.001	0.001	0.001	0.001	0.001
Z-velocity (m/s)	-1.610	-2.291	-2.994	-0.288	-0.480	-0.391
pitch angular velocity (deg/s)	-2.049	-2.089	-2.945	-1.851	-2.220	-0.866
pitch angle	0.132°	0.782°	0.016°	2.865°	3.438°	3.438 °
Spar for launching						
X-velocity (m/s)	-19.119	-19.561	-20.553	-7.063	-6.592	-7.126
Z-velocity (m/s)	-16.048	-14.923	-18.469	-31.508	-34.795	-34.098
pitch angular velocity (deg/s)	-0.492	-0.238	-1.243	-18.158	-16.313	-15.509
pitch angle for launching	2.863°	3.438°	3.438°	0°	0 °	0 °
Spar for oscillation						
pitch angle	44.745°	49.548°	51.277°	-106.320°	-102.449 °	-101.3 °

Figure 36 and Figure 37 show the acceleration of the spar hull and barge. *Spar AX* and *Spar AZ* are the X-directional acceleration and Z-directional acceleration of the spar hull, respectively. *Barge AX* and *Barge AZ* are the X-directional acceleration and Z-directional acceleration of the barge, respectively.

In Case study 1:

The spar hull enters into the water with its relatively stagnant X-directional acceleration between 56.7 seconds and 69.95 seconds for Case 1A, between 44.17 seconds and 62.51 seconds for Case 1B, and between 15.9 seconds and 28.23 seconds for Case 1C, respectively.

The primary rocker arm and the secondary rocker arm are rotated with the spar experiencing its second largest negative Z-directional acceleration between 69.95 seconds to 80.529 seconds for Case 1A, between 62.51 seconds to 72.388 seconds for Case 1B, and between 28.23 seconds to 40.295 seconds for Case 1C, respectively.

The spar hull separates from the barge with its largest negative X-directional acceleration between 80.53 seconds and 90.53 seconds for Case 1A, between 72.34 seconds and 82.47 seconds for Case 1B, and between 40.295 seconds and 50.41 seconds for Case 1C, respectively.

The barge is restored to its peak Z-directional acceleration between 80.53 seconds and 90.53 seconds for Case 1A, between 72.34 seconds and 82.47 seconds for Case 1B, between 40.295 seconds and 50.41 seconds for Case 1C, respectively, after drifting away from the spar hull.

The oscillatory motion of the spar hull following separating from the barge is reflected in the Z-directional acceleration variation.

In Case study 2:

The spar hull enters into the water with its relatively stagnant X-directional acceleration between 45.51 seconds and 76.2 seconds for Case 2A, between 27.7 seconds and 67.7 seconds for Case 2B, and between 11.2 seconds and 44.2 seconds for Case 2C, respectively.

The primary rocker arm is rotated with the spar experiencing its peak Z-directional acceleration between 76.2 seconds and 77.327 seconds for Case 2A, between 67.7 seconds and 68.602 seconds for Case 2B, and between 44.2 seconds and 45.25 seconds for Case 2C, respectively.

The spar hull separates from the barge at the largest negative X-directional acceleration of the spar hull between 77.327 seconds and 99.225 seconds for Case 2A, between 68.602 seconds and 88.075 seconds for Case 2B, and between 45.25 seconds and 65.895 seconds for Case 2C, respectively.

The barge is restored to its peak Z-directional acceleration between 77.327 seconds and 99.225 seconds for Case 2A, between 68.602 seconds and 88.075 seconds for Case 2B, and between 45.25 seconds and 65.895 seconds for Case 2C, respectively, after drifting away from the spar hull.

The oscillatory motion of the spar hull following separation from the barge is reflected in the Z-directional acceleration variation.

The timing of the individual stages in the launch sequence is observed to be consistent with the initial conditions. That is to say, the higher the initial pitch trim angle and the lower the kinetic friction coefficient, the sooner each stage of launching occurs.

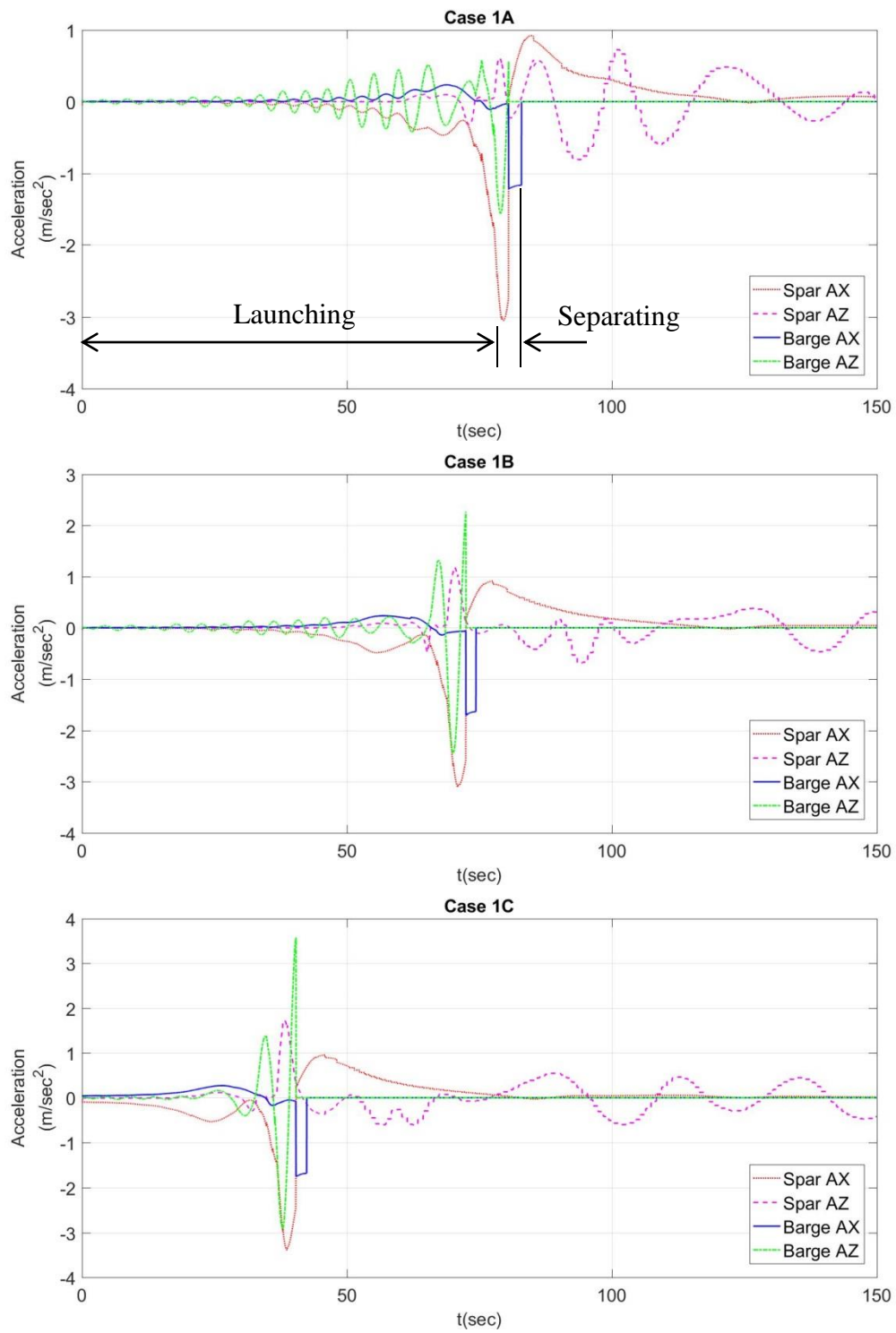


**Figure 36 Acceleration for spar hull and barge - Case study 1**

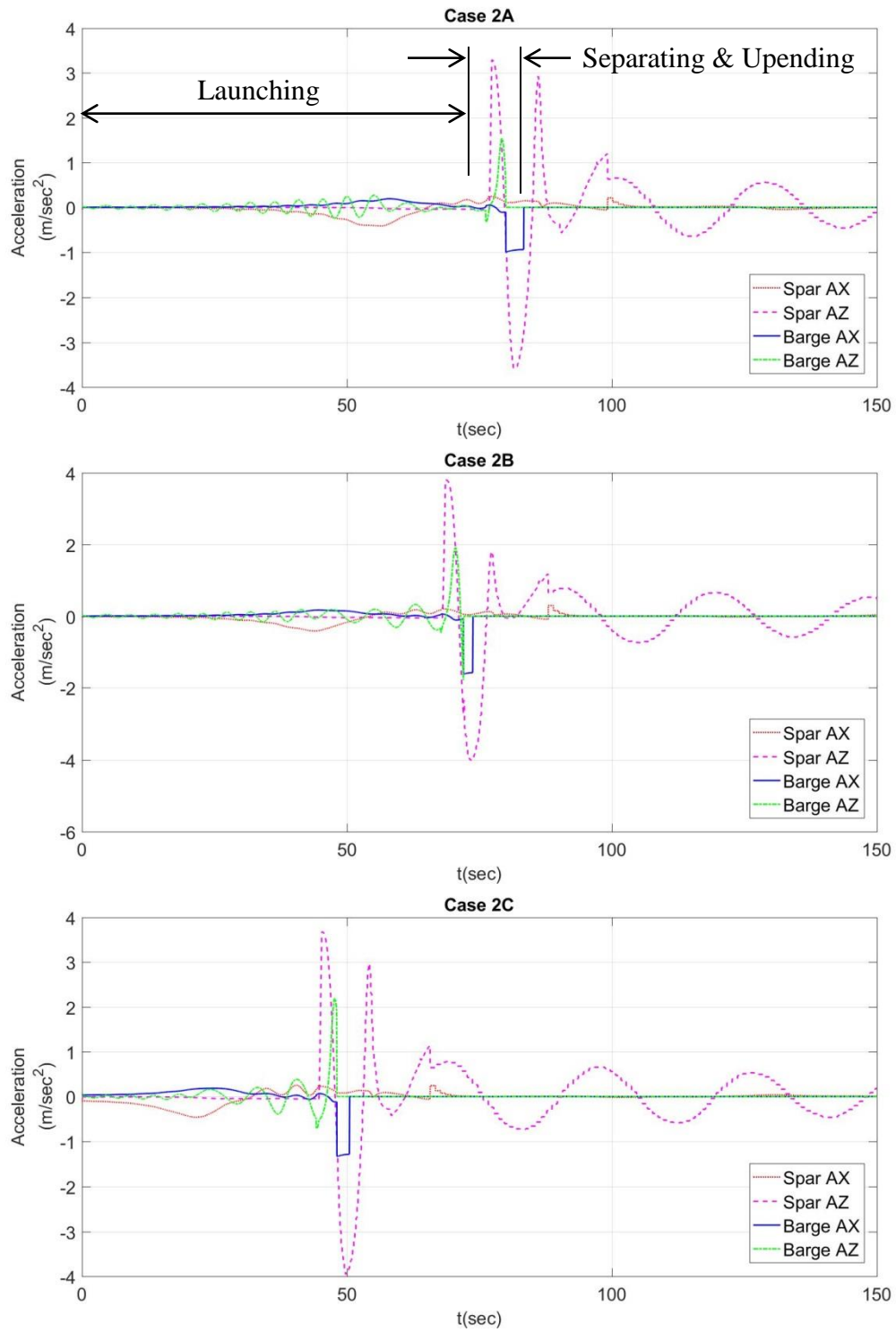


**Figure 37 Acceleration of spar hull and barge - Case study 2**

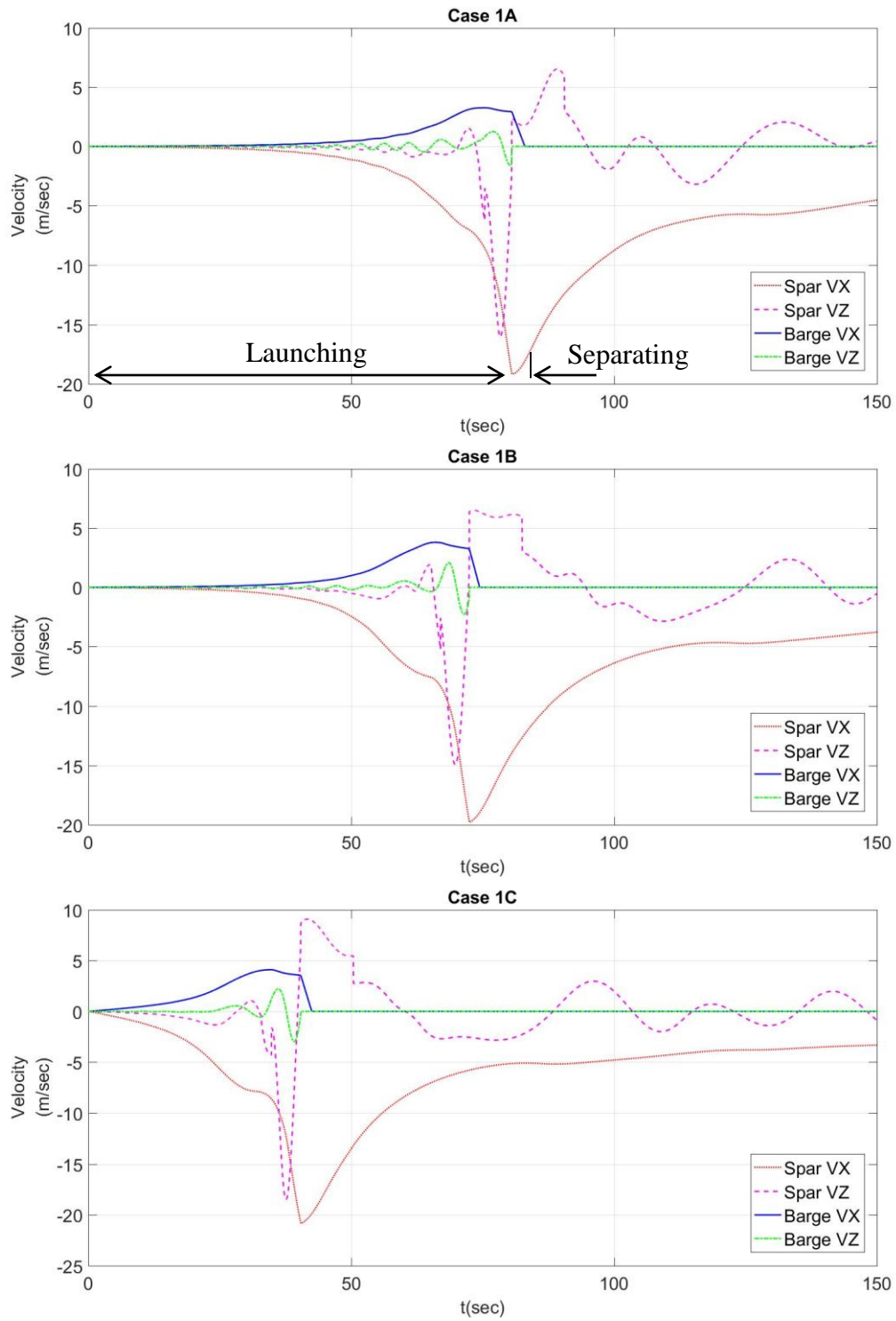
Figure 38 and Figure 39 show the velocity time series for the spar hull and barge. *Spar VX* and *Spar VZ* are the X-directional velocity and Z-directional velocity of the spar hull, respectively. *Barge VX* and *Barge VZ* are the X-directional acceleration and Z-directional acceleration of the barge, respectively.

The velocity is the key parameter to assess the risk of unexpected failure when launching a platform from a barge; very high velocity during launching can lead to an unexpected accident. The velocity trends in Figure 38 and 39 are similar to the accelerations discussed above. The X-directional velocity of the spar hull is increasing continuously in magnitude during launching and it will return to a static equilibrium state after reaching the negative peak. The X-directional velocity of the barge is increasing continuously during launching and it will return to a static equilibrium state after reaching the positive peak.

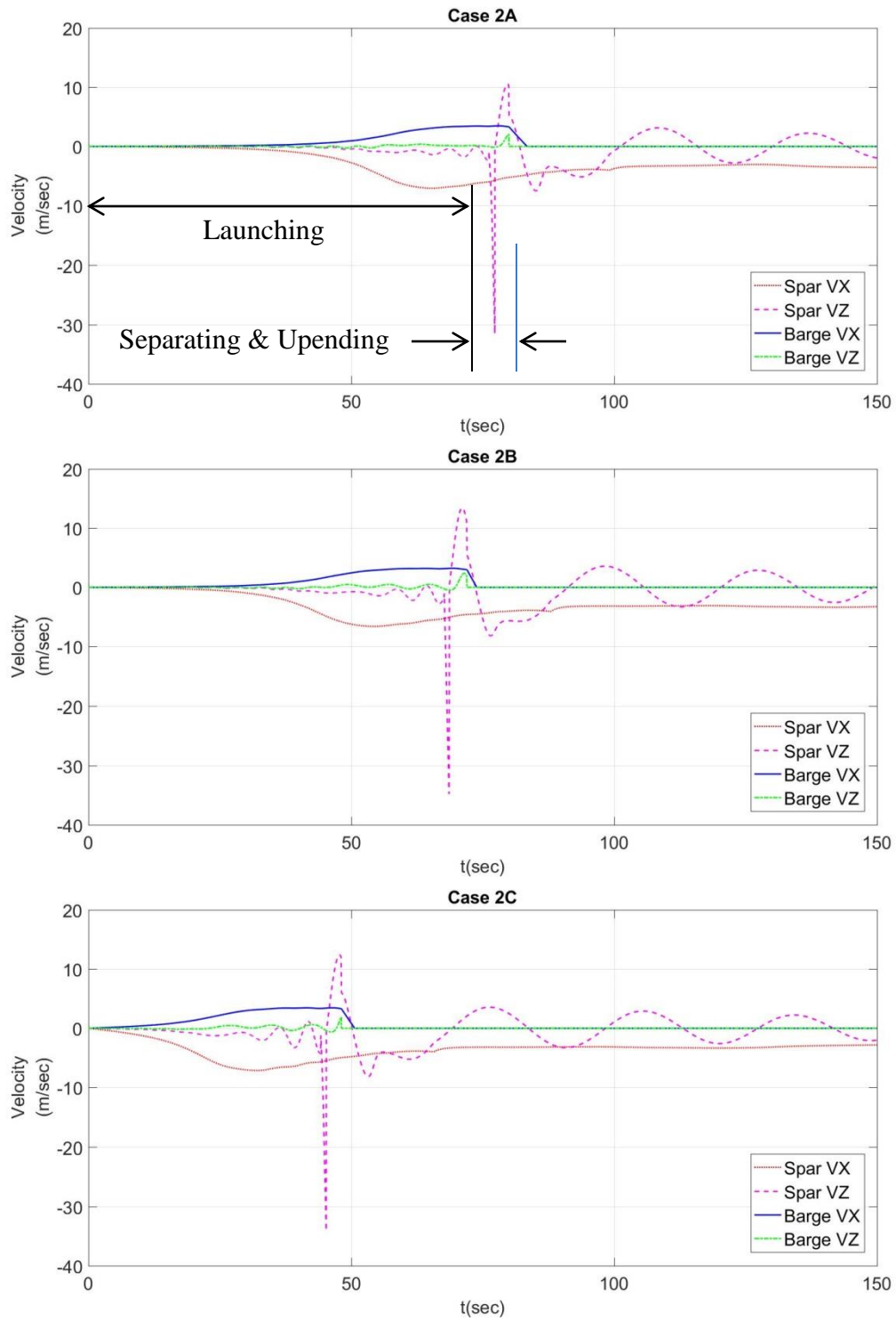
In Case study 1, the X-directional velocity and the Z-directional velocity are increasing dramatically during launching. The submerged depth of the spar hull is not deep when the CoG of the spar hull moves past the pivot point of each rocker arm, hence the buoyancy force on the spar is not large. The primary rocker arm and the secondary rocker arm will rotate with the spar hull at high rotational speed.



In Case study 2, the large buoyancy affects the spar hull before the CoG of the spar hull moves aft of the pivot point of the primary rocker arm. The primary rocker arm will rotate as the end of the spar hull surpasses the pivot point of the primary rocker arm. The Z-directional velocity of the spar hull peaks instantaneously due to the angular velocity when the spar separates from the barge and starts to upend. The X-directional velocity and Z-directional velocity of the spar hull are increasing steadily during launching.



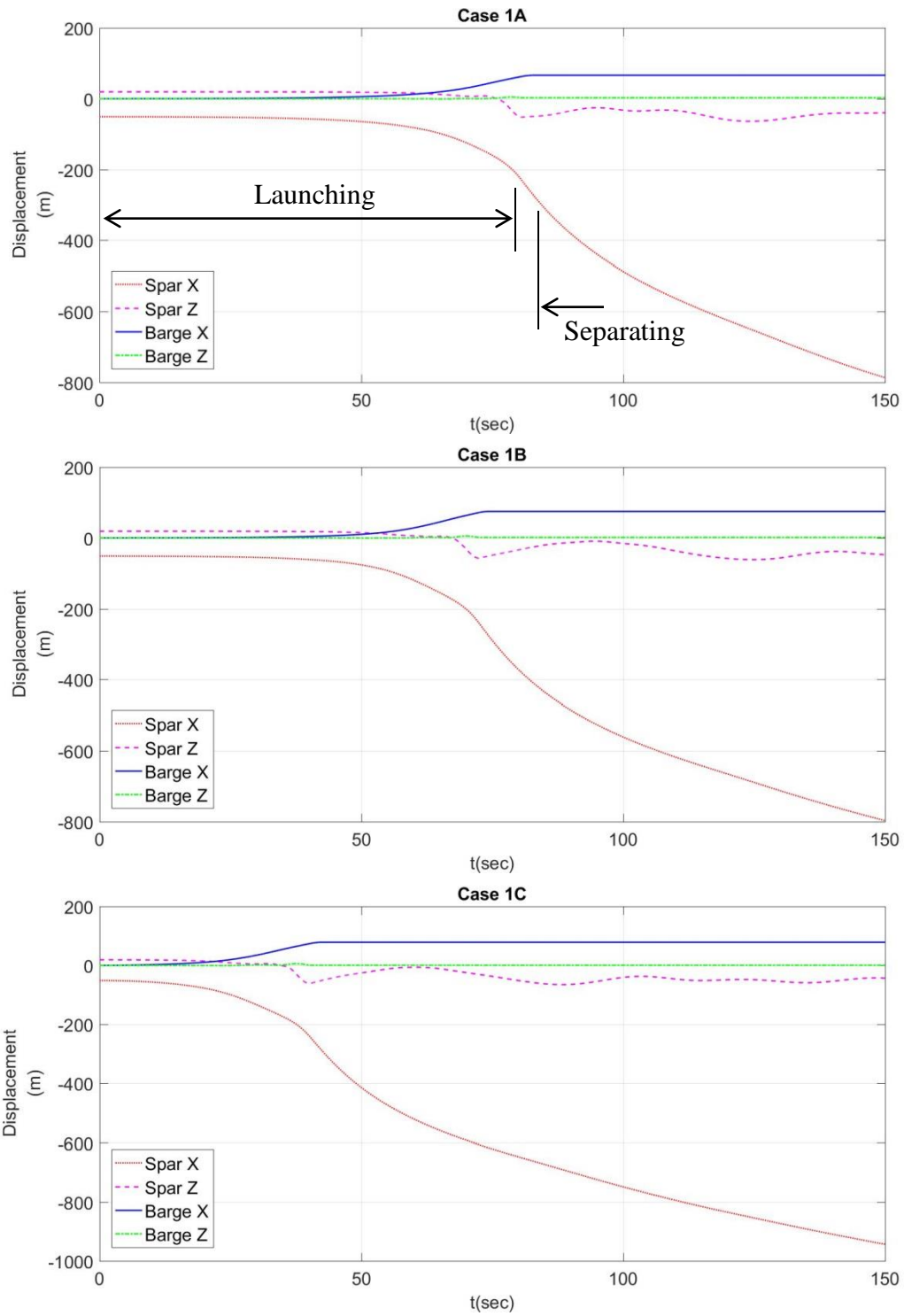
**Figure 38 Velocity for spar hull and barge - Case study 1**



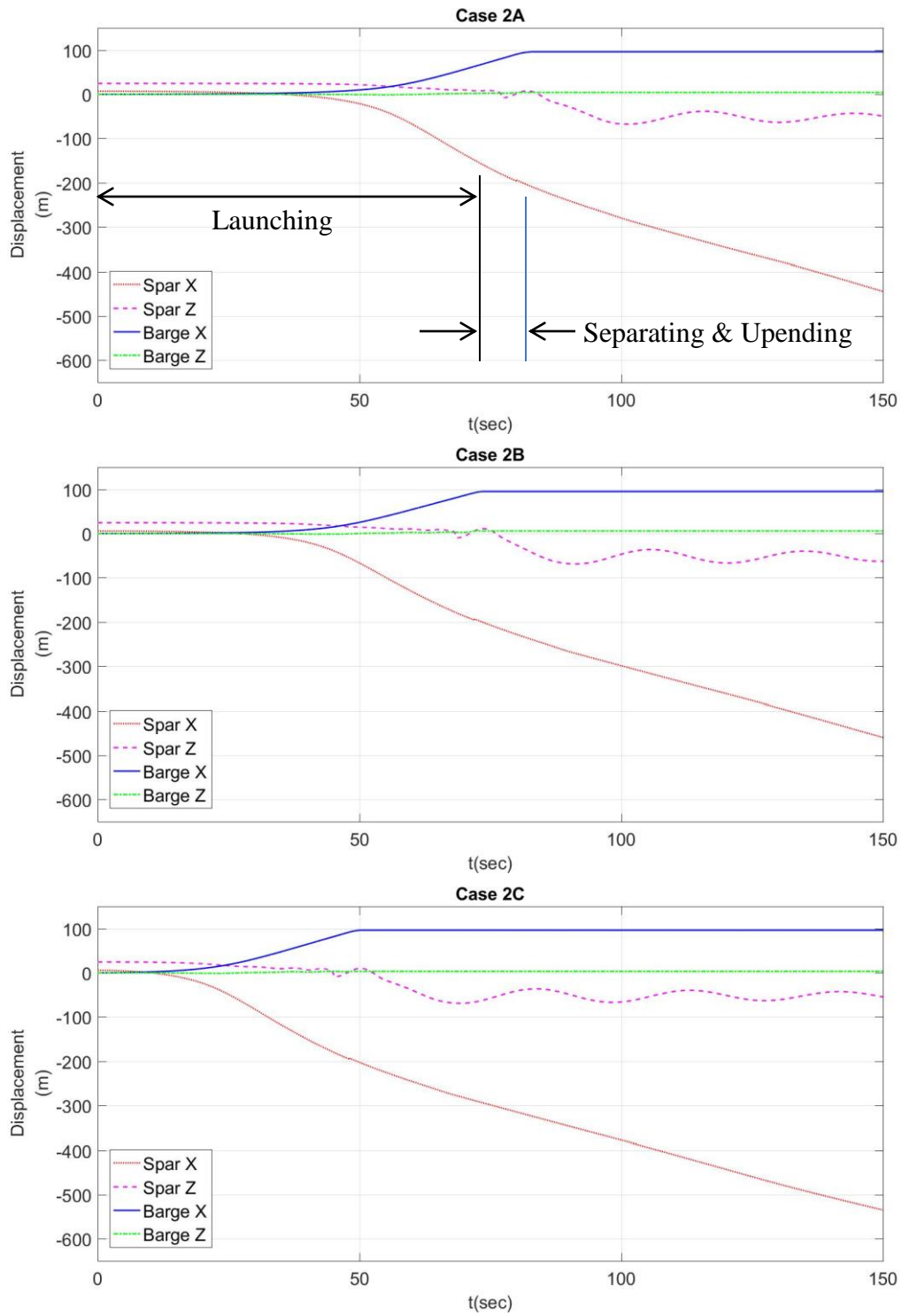
**Figure 39 Velocity for spar hull and barge - Case study 2**

Figure 40 and Figure 41 show the displacement of the spar hull and the barge during launching and upending. *Spar X* and *Spar Z* are the X-directional displacement and Z-directional displacement of the spar hull relative to the global origin, respectively. *Barge VX* and *Barge VZ* are the X-directional displacement and Z-directional displacement of the barge relative to the global origin, respectively. The global origin is the CoG of the barge at the initial position. The location of the spar hull at the initial time is the relative distance from the global origin.

We can deduce the displacement trajectories of each body with these figures. The spar hull moves quickly after separating from the barge. Ultimately, the spar hull will be stopped after oscillation due to the hydrodynamic viscous effect. As expected, the higher initial trim angle and lower kinetic friction coefficient associated with case studies 1C and 2C lead to greater depth of submergence of the spar CoG during launching.



**Figure 40 Displacement for spar hull and barge - Case study 1**



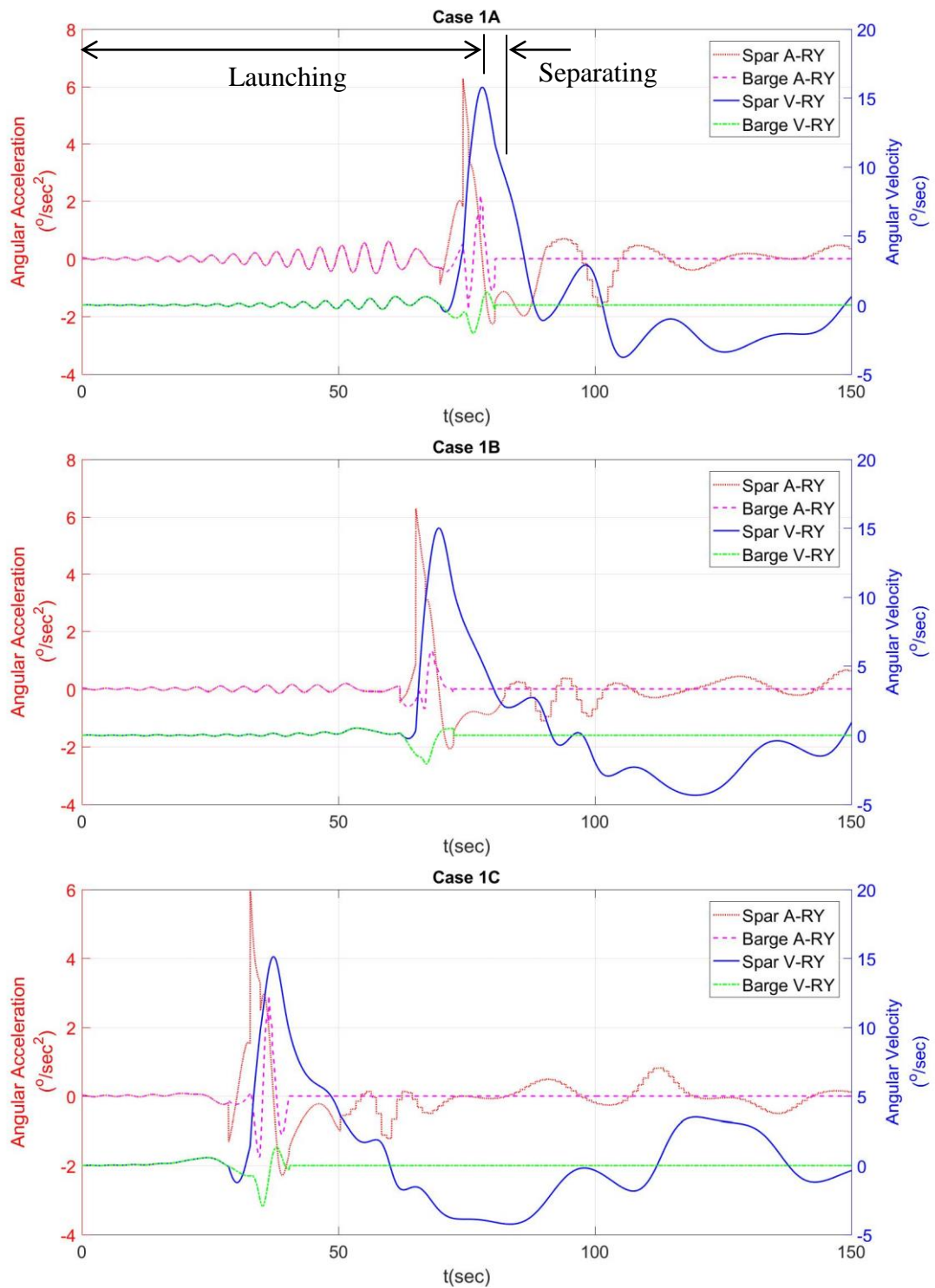
**Figure 41 Displacement for spar hull and barge - Case study 2**

Figure 42 and Figure 43 show the angular acceleration and velocity of the spar hull and the barge. *Spar A-RY* and *Barge A-RY* are the angular acceleration for the pitch trim angle of the spar hull and the barge, respectively. *Spar V-RY* and *Barge V-RY* are the angular velocity for the pitch trim angle of the spar hull and the barge, respectively. The angular acceleration is indicated by the left red color axis and the angular velocity is indicated by the right blue color axis.

In Case study 1, the angular acceleration and angular velocity are increasing dramatically during launching when the primary rocker arm and the secondary rocker arm rotate the spar hull.

In Case study 2, the angular acceleration and angular velocity are relatively stagnant during launching compared with Case study 1. This is because the large buoyancy acts on the spar hull and decreases the rotational acceleration of the spar hull with the opposite sign. The angular acceleration and the angular velocity are decreasing dramatically and become peak when the spar hull upends by itself after separating it from the barge.

The angular acceleration and the angular velocity are critical parameters to verify the proper operation of the rocker arms. When spar hull moves past the pivot point of each rocker arm, the barge can keep its stable motion by separating each tilting beam and rotating each rocker arm to safely guide the spar into the sea.



**Figure 42 Angular acceleration for spar hull and barge - Case study 1**



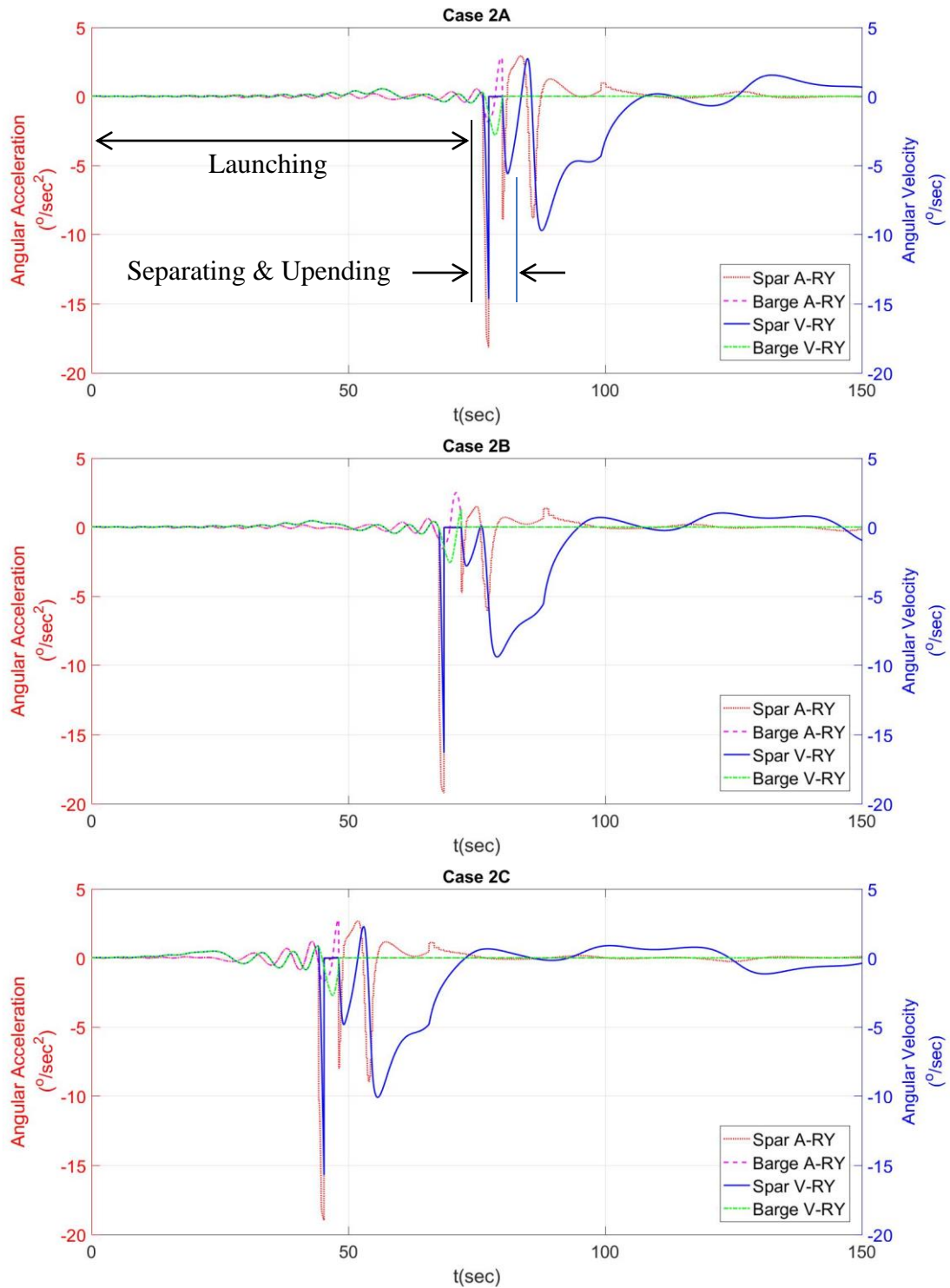


**Figure 43 Angular acceleration for spar hull and barge - Case study 2**

Figure 44 and Figure 45 show the pitch trim angle for the spar hull and the barge. The spar pitch trim angle is indicated by the left red color axis and the barge pitch trim angle is indicated by the right blue color axis.

The spar hull pitch trim angle increases with the same angle as the barge before the CoG of the spar hull is located at the pivot point of the primary rocker arm.

In Case study 1, after the CoG of the spar hull moves past the pivot point of the rocker arm while the rocker arm rotates, the spar pitch trim angle increases and the barge pitch trim angle decreases. After the spar hull separates from the barge, the barge will be restored to a stable condition and the spar hull will undergo damped oscillations until reaching a stable upright position.

In Case study 2, the spar pitch trim angle increases over a limited range due to the large buoyancy of the spar hull. After the spar hull separates from the barge, the spar pitch trim angle decreases as it upends itself while the barge is restored to a stable condition.

In all cases the primary rocker arm will start to rotate at the peak of the barge pitch trim angle.

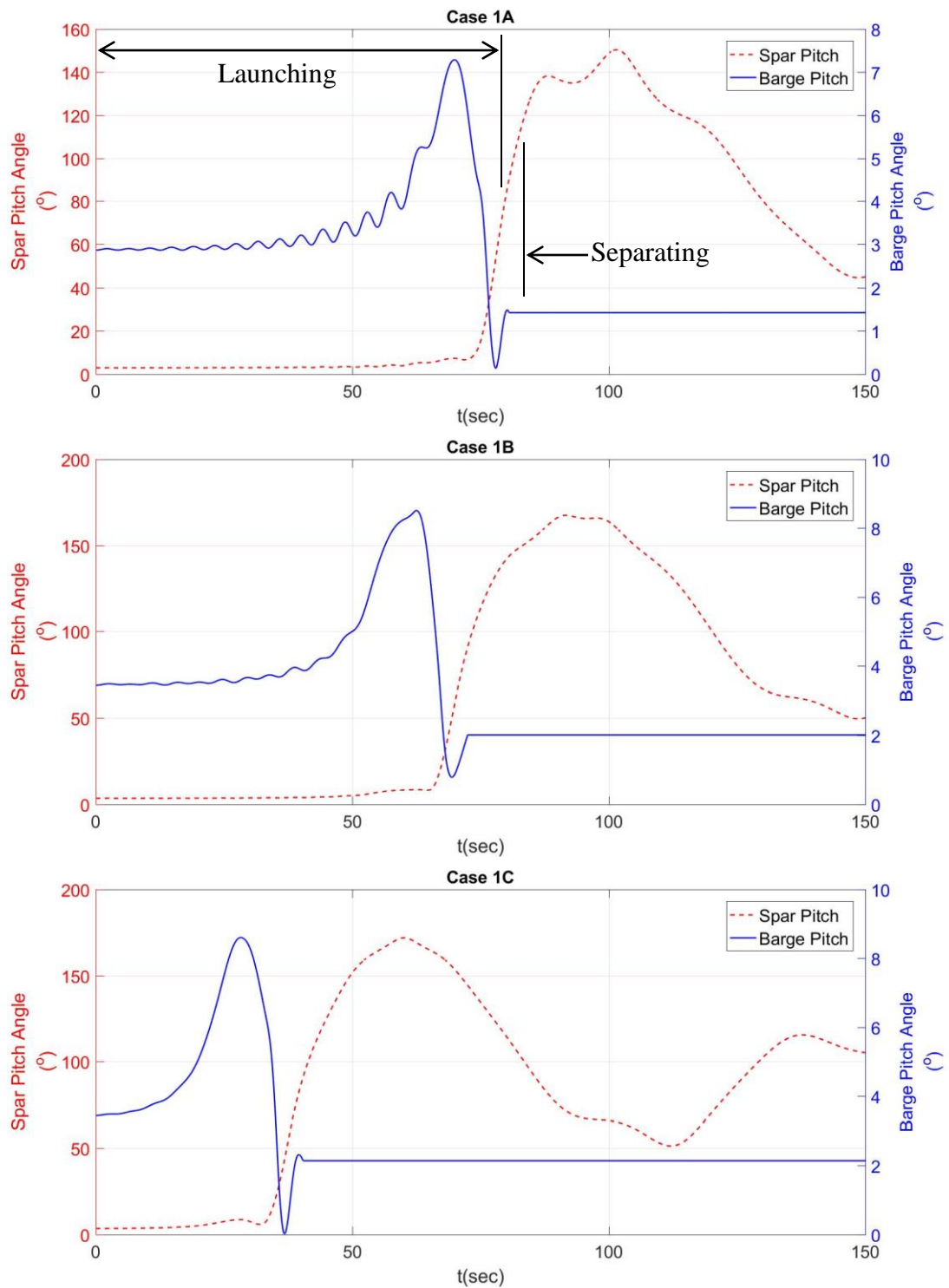
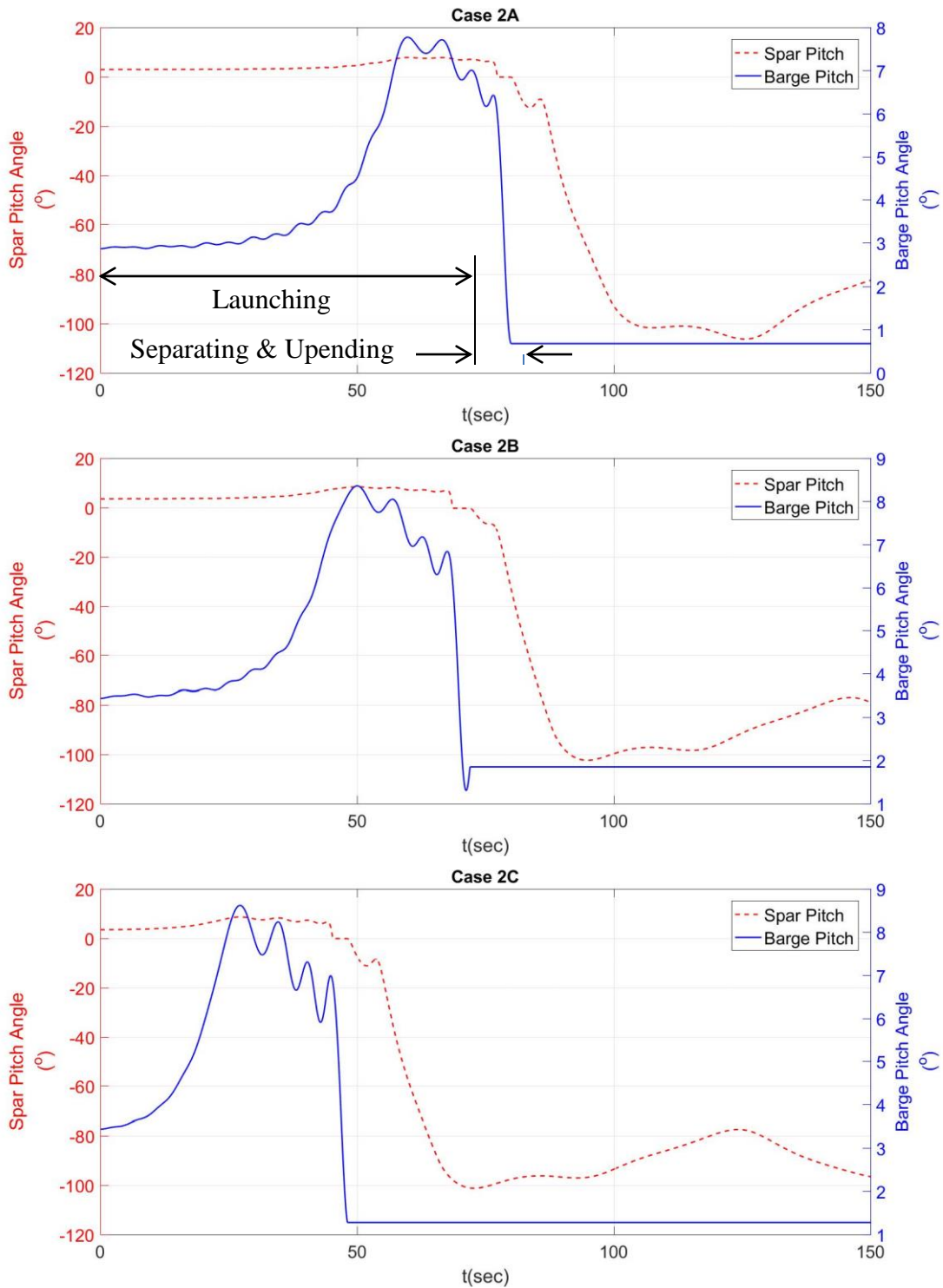


Figure 44 Pitch angle for spar hull and barge - Case study 1



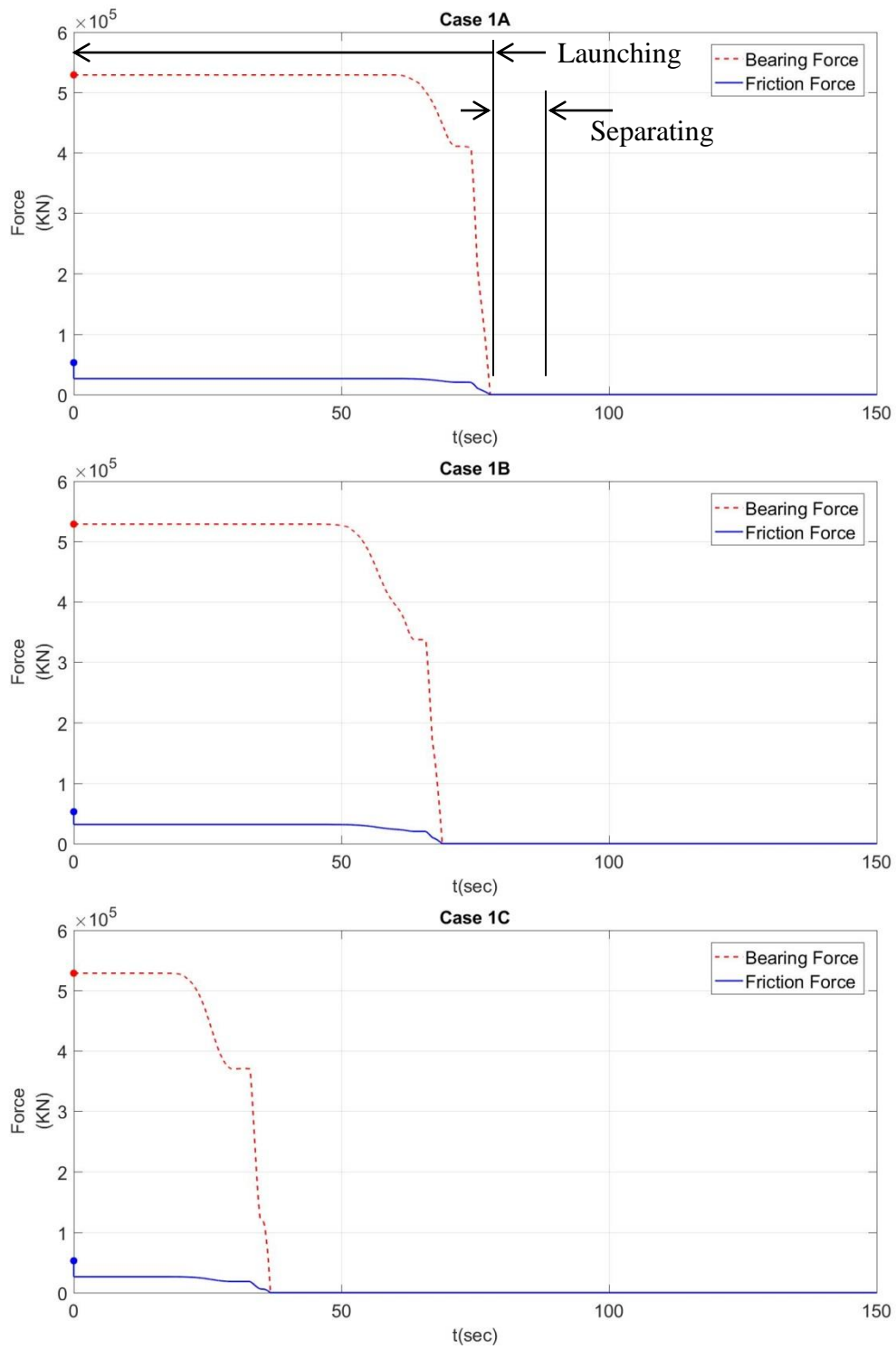
**Figure 45 Pitch angle for spar hull and barge - Case study 2**

Figure 46 and Figure 47 show the change of the coupling forces between the spar hull and the barge. The hydraulic jacks are applied to overcome the static friction force and initiate sliding of the spar hull. Then, the spar hull moves with its gravitational weight. When the spar hull starts to move, the kinetic friction coefficient is applied. The friction force trend is reflected by the bearing force because the forces are linearly proportional to each other (with the friction coefficient as the constant of proportionality).

In the both study cases, the coupling forces decrease dramatically as the rocker arm rotates. Then, the coupling forces become zero after the spar hull separates from the barge.

In Case study 2, there is some occurrence of oscillations of the bearing force as the barge pitch trim angle oscillates due to the large buoyancy of the barge.

The coupling force trends are similar to those for the pitch trim angle because of the dominating effect of the spar's weight on the bearing force.



**Figure 46 Coupling forces - Case study 1**

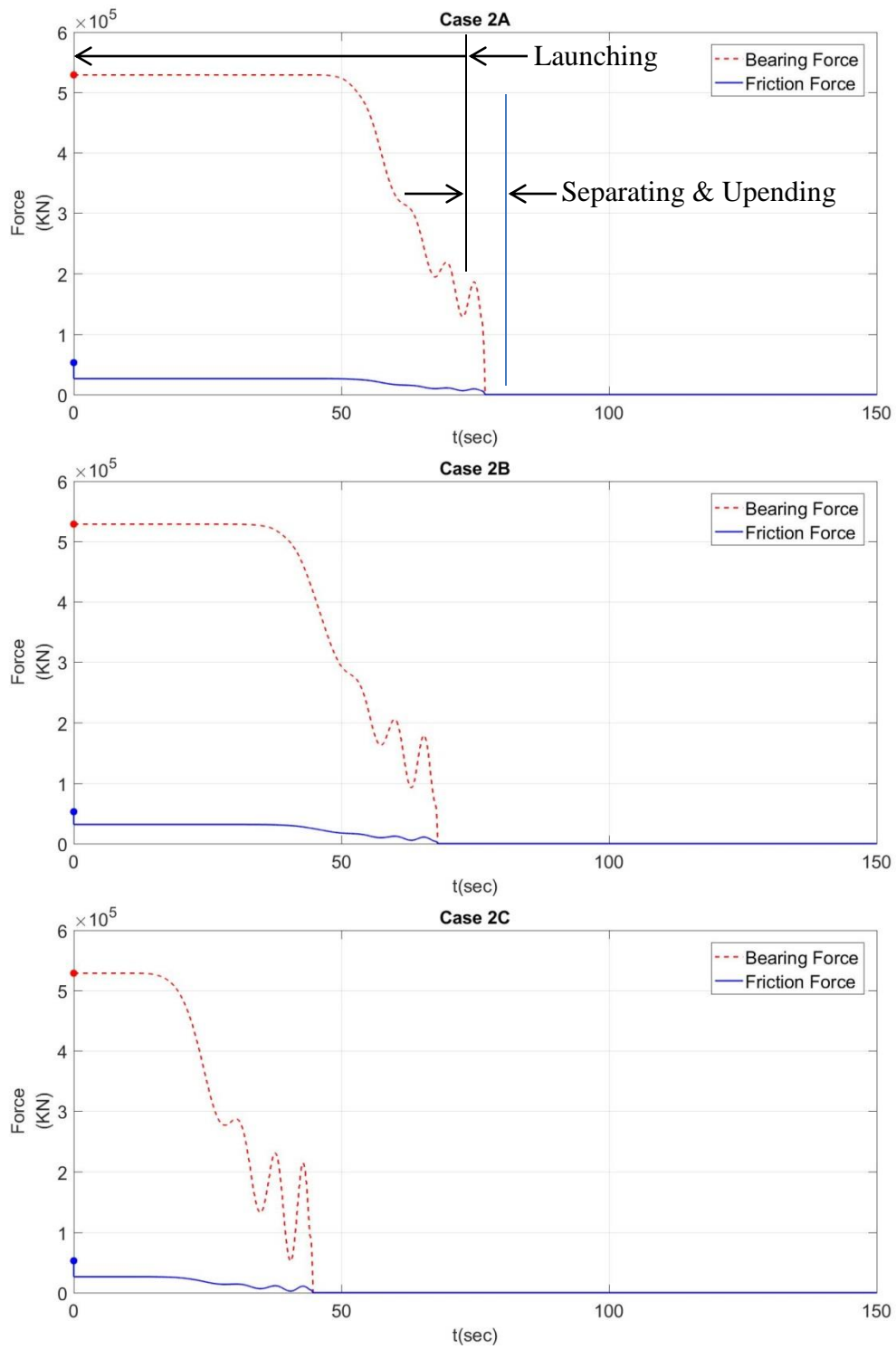


**Figure 47 Coupling forces - Case study 2**

Figure 48 and Figure 49 show the hydrodynamic forces for the spar hull.  $Hydro_x$  and  $Hydro_z$  are the X-directional hydrodynamic force and Z-directional hydrodynamic force, respectively. When the spar hull enters into the water, the hydrodynamic force is applied.

The drag force is influenced by the X-directional velocity, Z-directional velocity and the angular velocity of the spar hull.

In Case study 1, the hydrodynamic force reaches a peak value when the secondary rocker arm is rotated completely and the pitch trim angle is  $90^\circ$ . At this point the spar hull is accelerating into the water in a vertical orientation.

In Case study 2, the hydrodynamic force reaches a peak when the barge begins to oscillate before the primary rocker arm rotates. In the case of top launching, the CoG of the spar hull is initially located further from the rocker arm pivot point, the submerged volume of the spar becomes large before the primary rocker arm starts to rotate. For this reason, the hydrodynamic force is sensitive to the barge oscillation.

The hydrodynamic force of Case study 2 is smaller than that of Case study 1 because of the larger rate of increase of buoyancy which leads to a large rate of reduction of the spar hull velocity and acceleration.



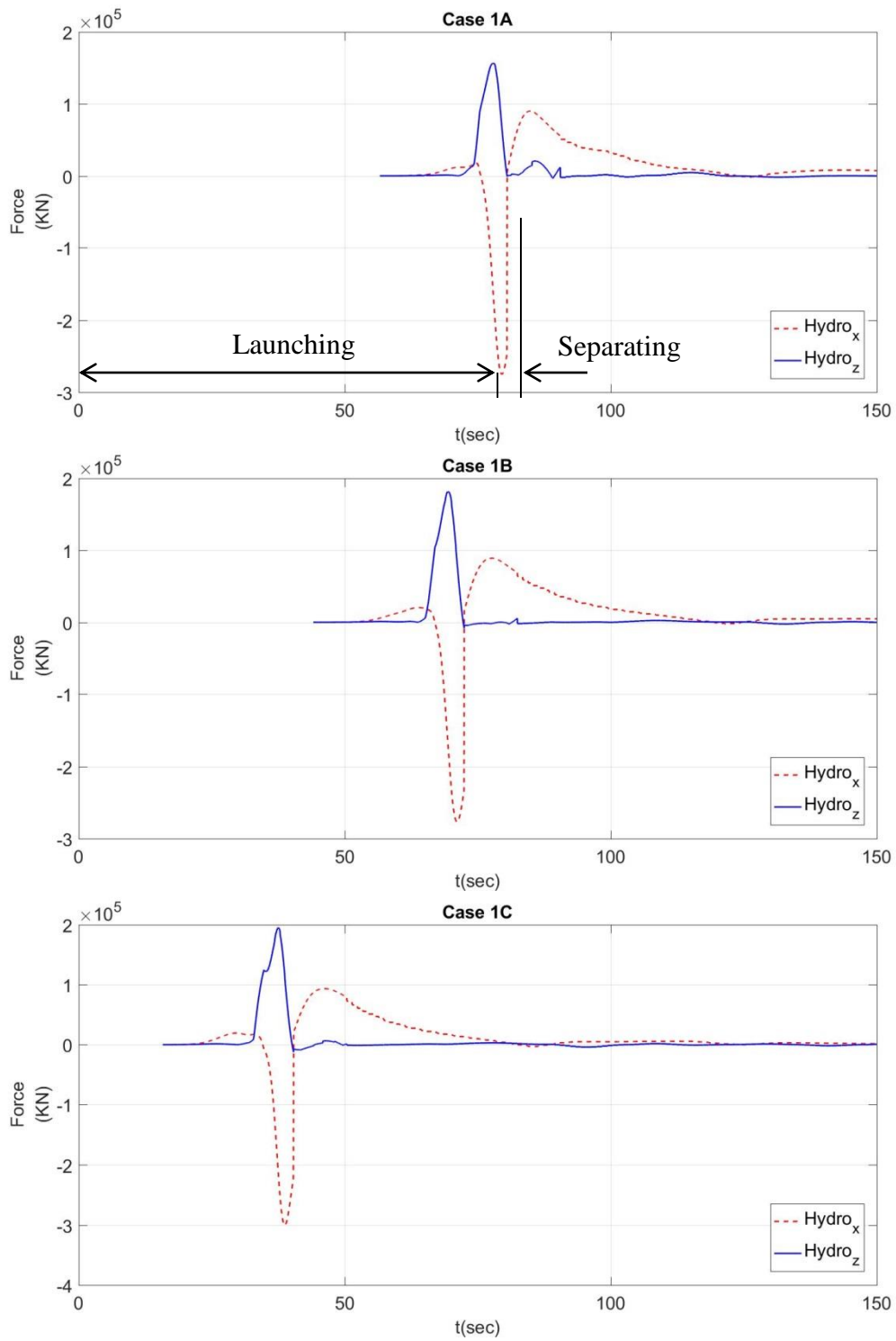


**Figure 48 Hydrodynamic force for spar hull - Case study 1**

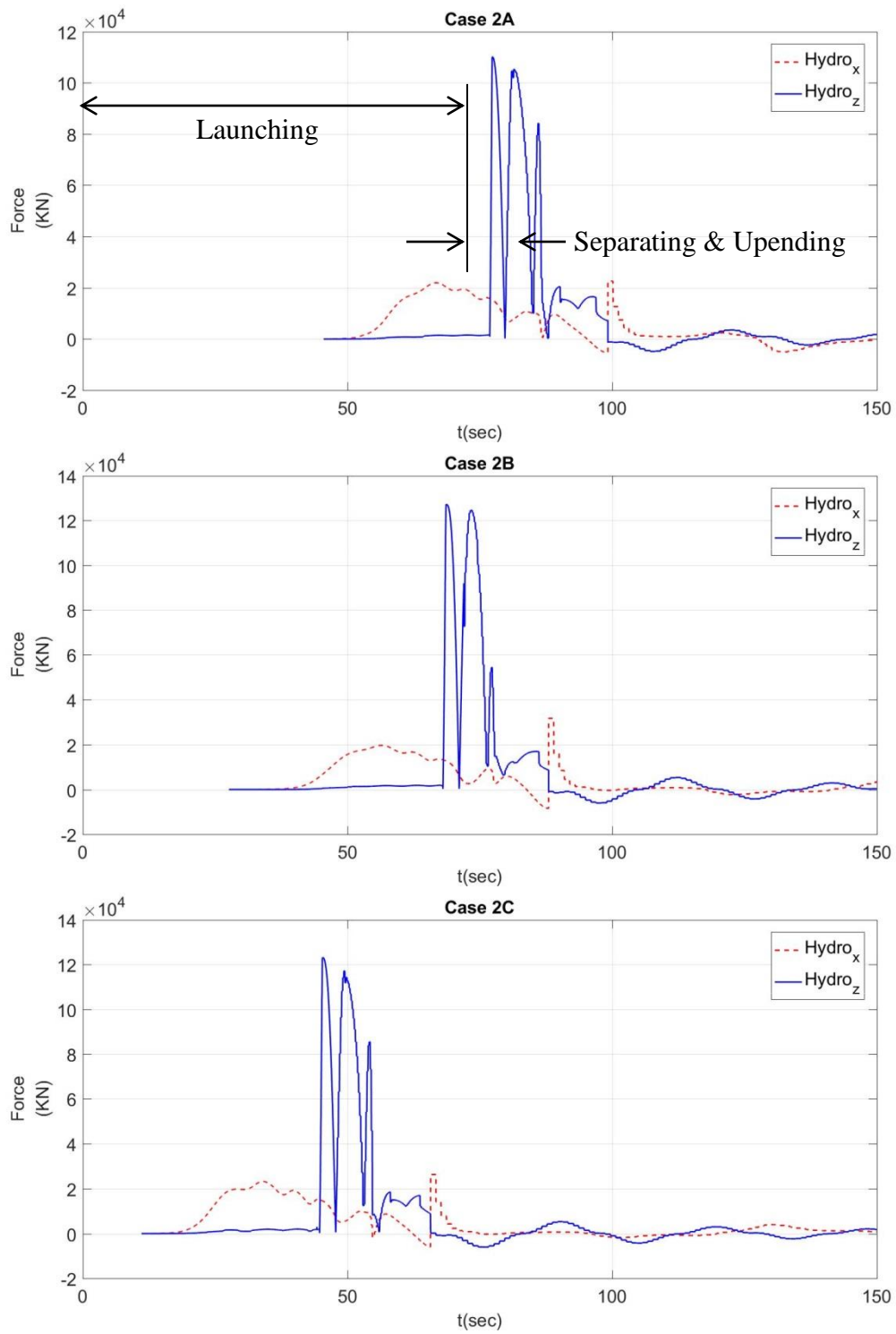
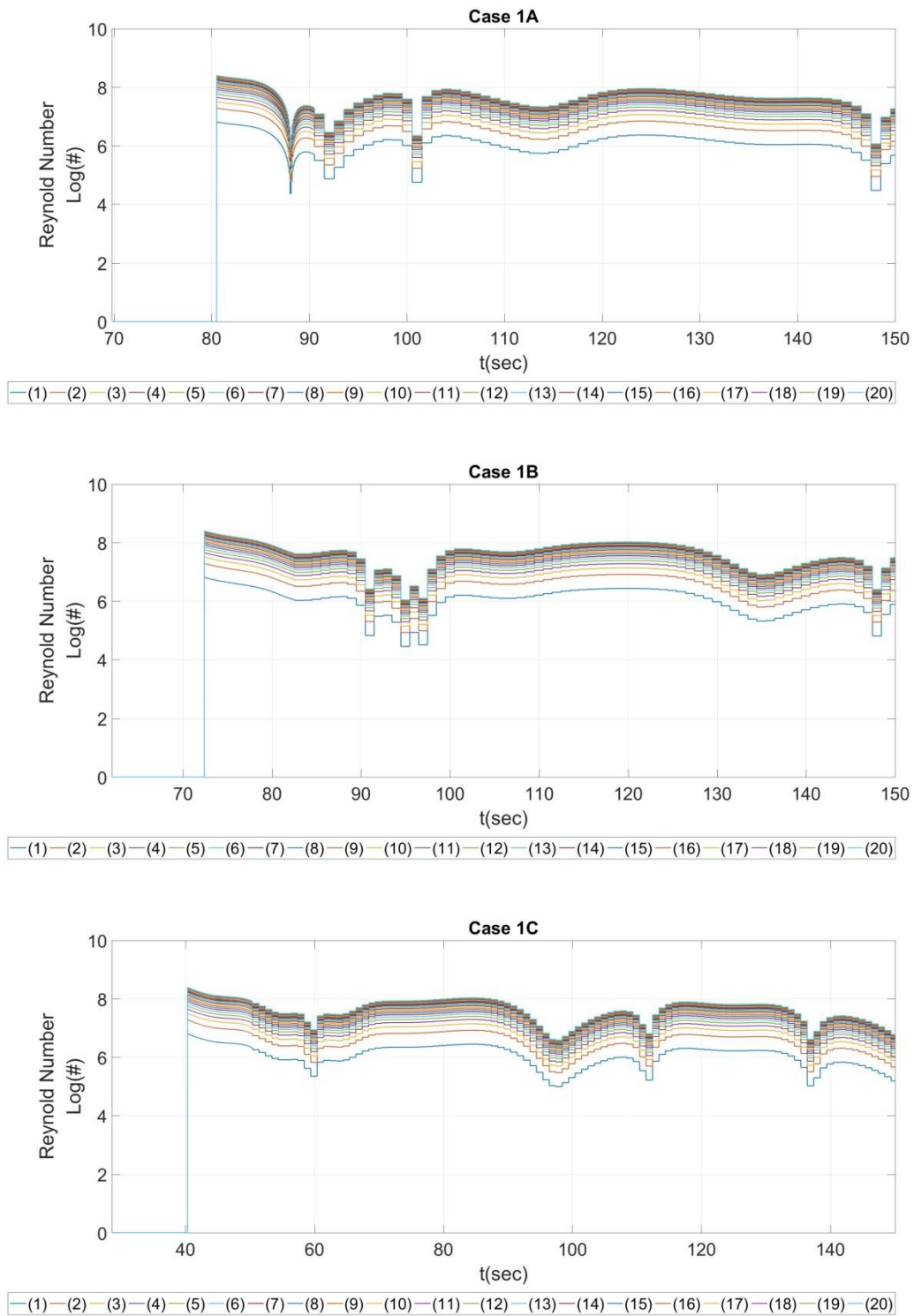


**Figure 49 Hydrodynamic force for spar hull - Case study 2**

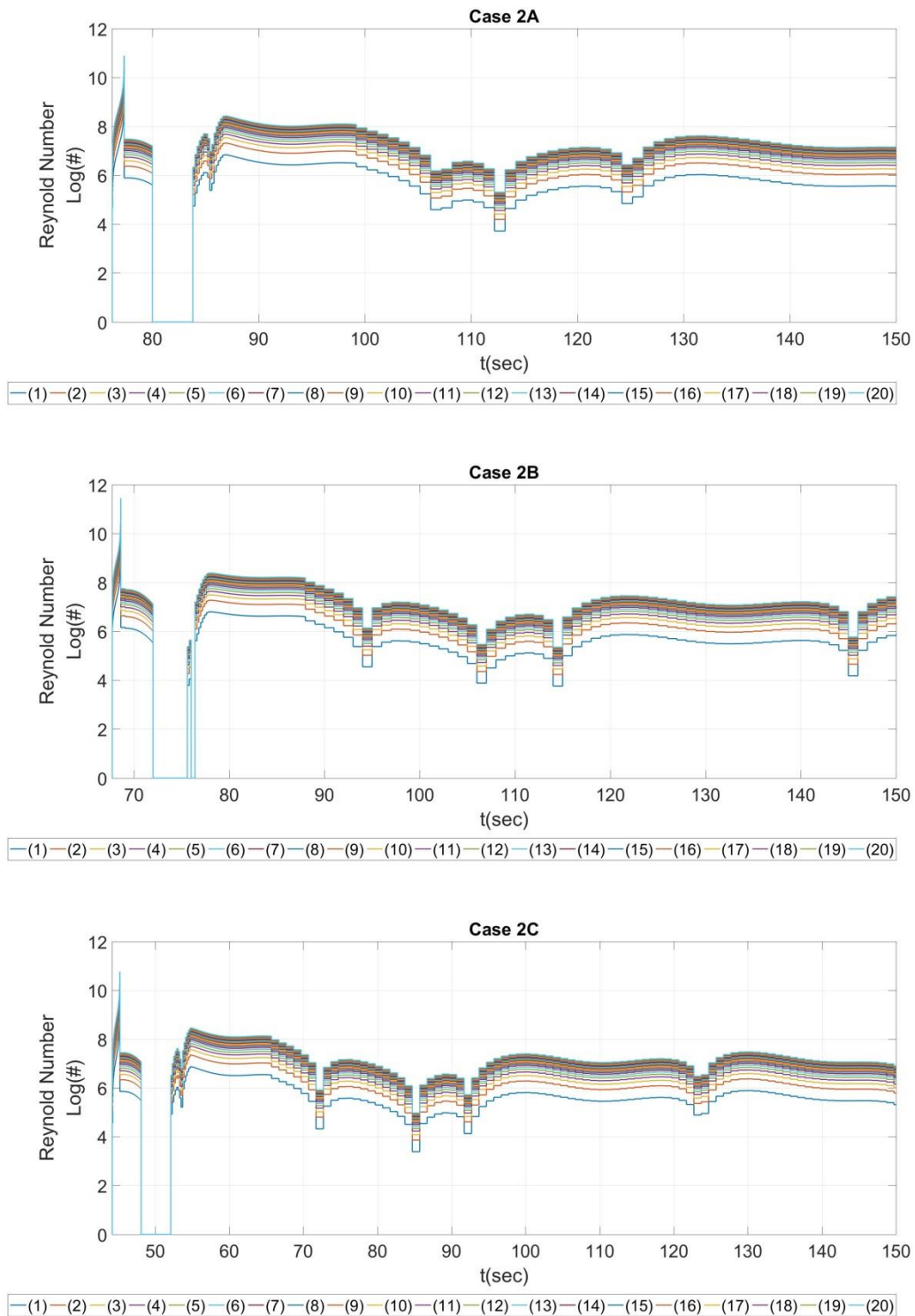
The drag force on the hull is calculated by dividing its length into discrete elements and evaluating the instantaneous normal velocity and the associated instantaneous Reynolds-number dependent drag coefficient for each element. The spar is divided into an upper and lower part above and below its CoG. The rotational pivot point is the CoG of the spar hull and it is illustrated in Figure 17. The upper part and lower part are each divided into twenty elements with equal interval height, respectively, and for each element the local velocity and the associated Reynolds number are calculated.

Figure 50 to Figure 53 show the time evolution of the location-dependent Reynolds number for the spar hull. When the spar hull rotates in the water, the Reynolds number is calculated considering the rotational velocity. Note that the Reynolds number in the figures is plotted on a logarithmic axis.

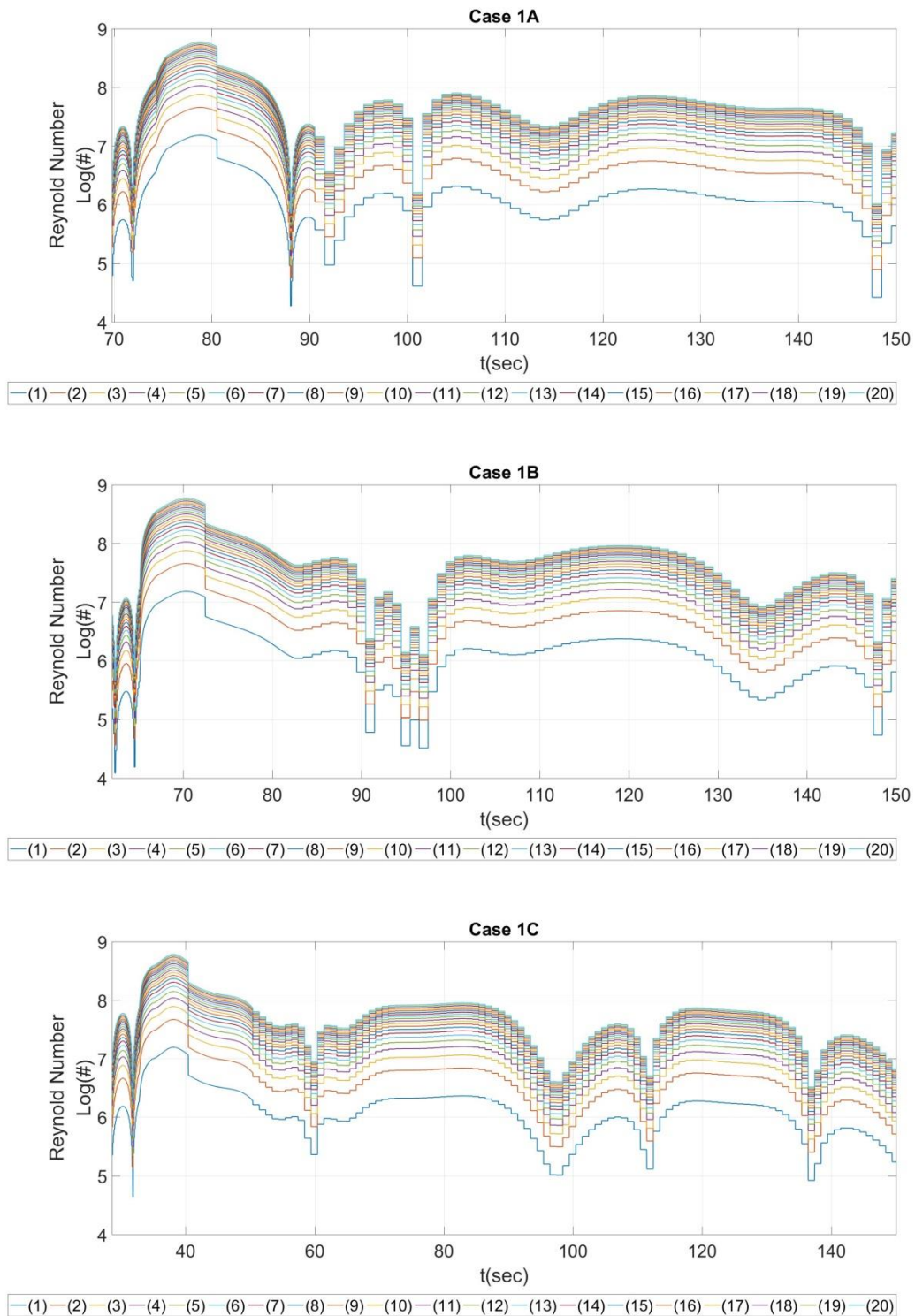
Figure 54 to Figure 57 show the associated time evolution of the local drag coefficients for the spar hull. The drag coefficients are determined according to Figure 3. Since the drag coefficient increases dramatically at low Reynolds numbers, the associated increase in the drag force plays an important role in slowing the drift velocity of the spar after launching.



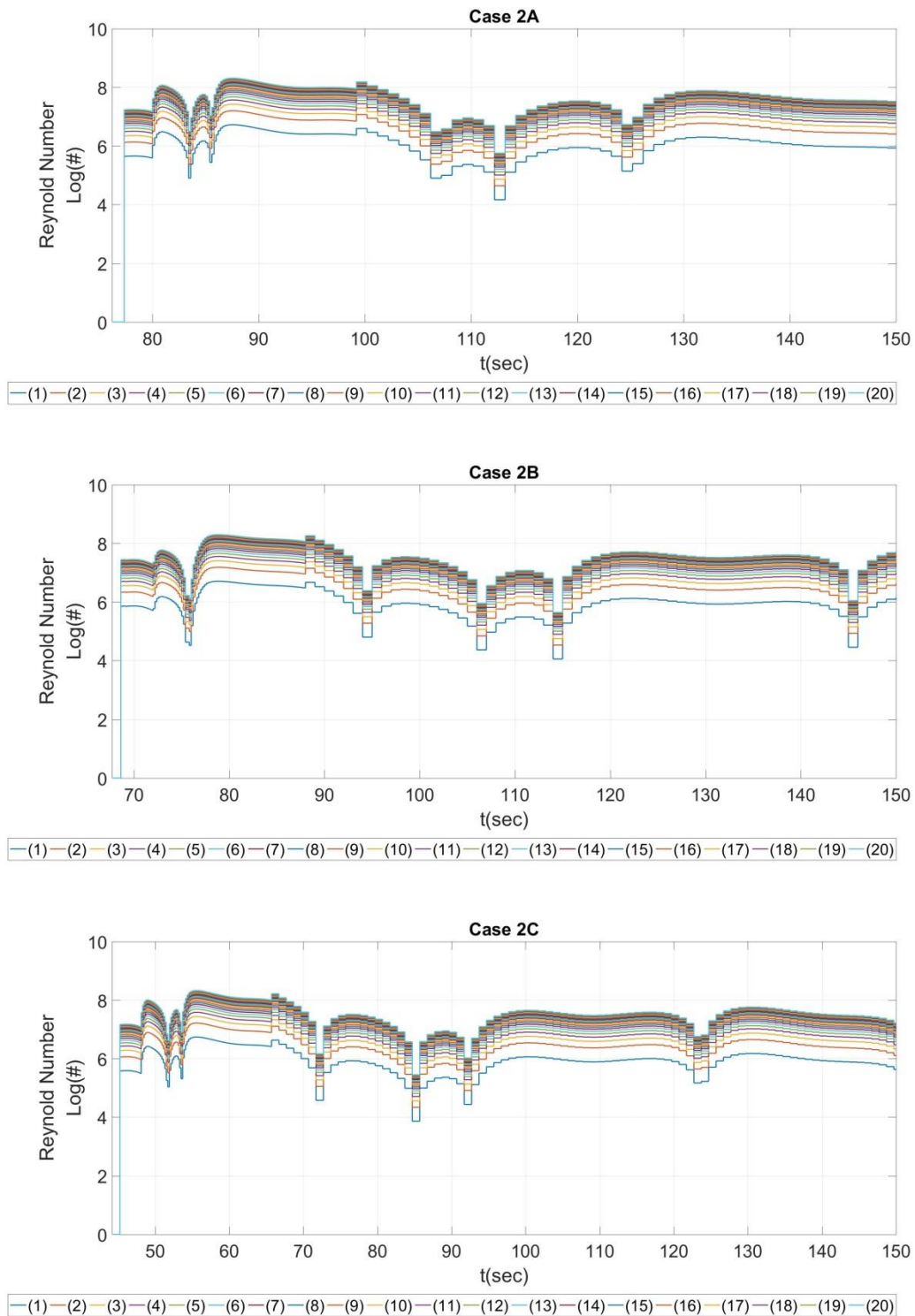
**Figure 50 Reynolds number for spar hull upper part- Case study 1**



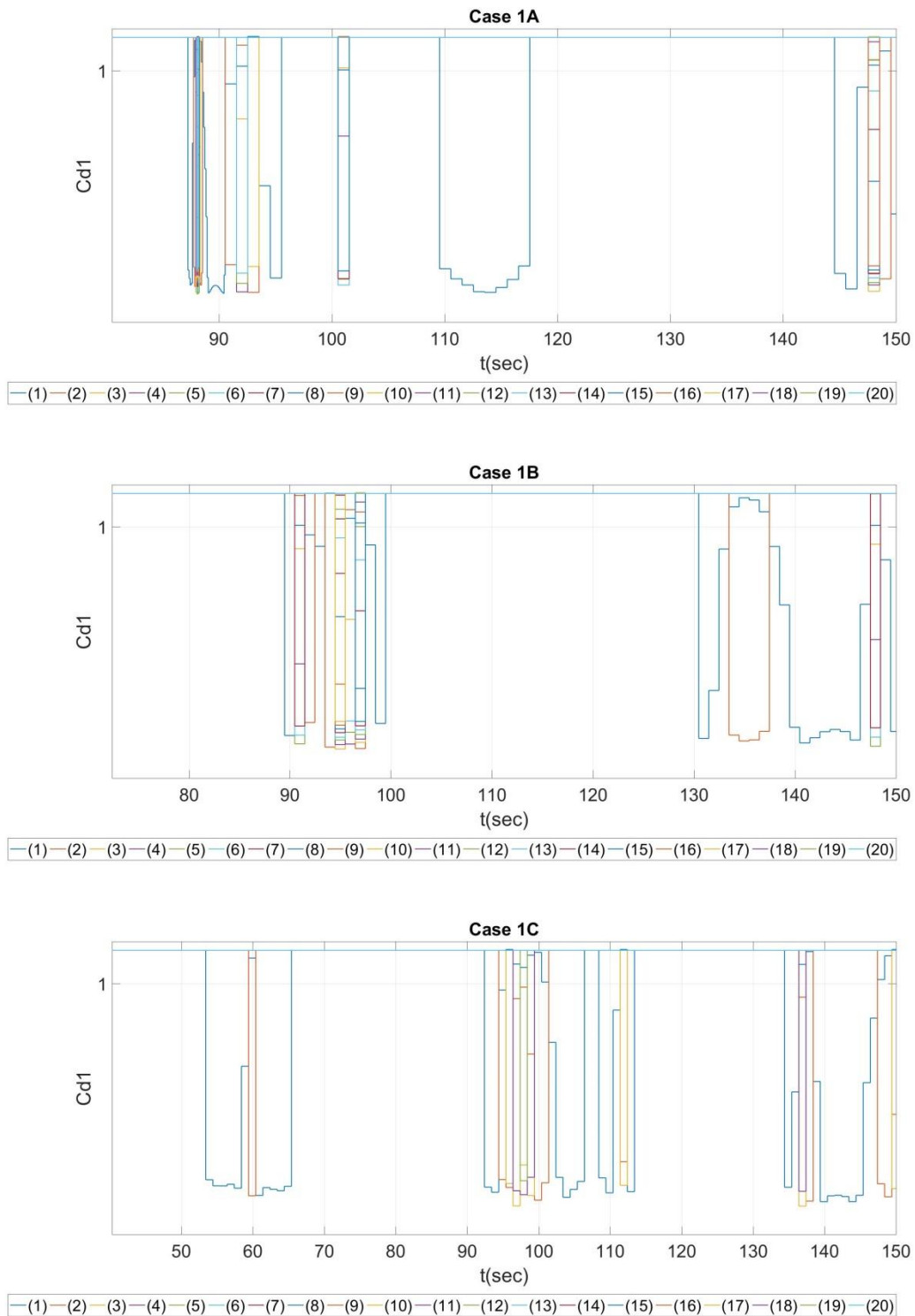
**Figure 51 Reynolds number for spar hull upper part - Case study 2**



**Figure 52 Reynolds number for spar hull lower part - Case study 1**

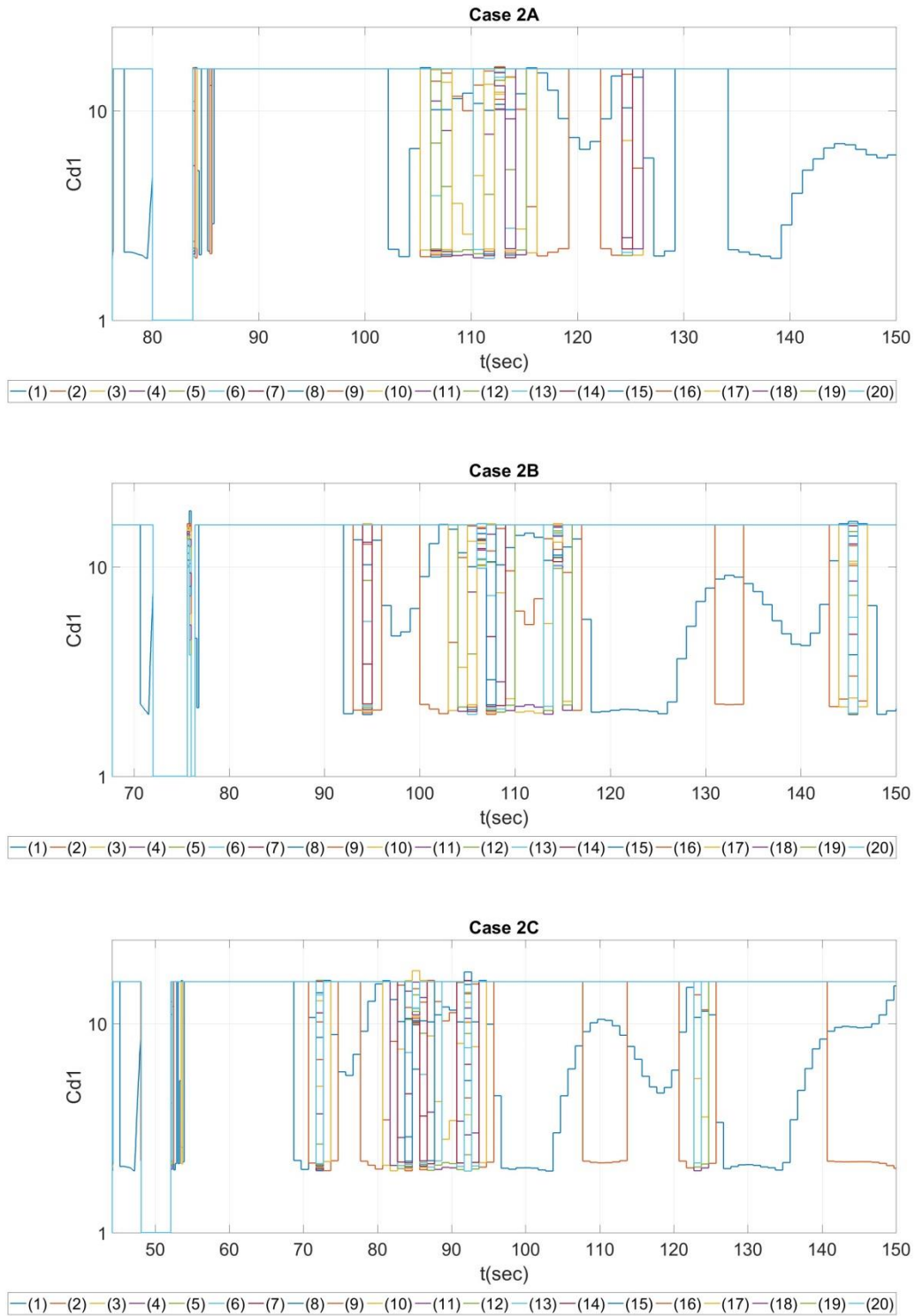


**Figure 53 Reynolds number for spar hull lower part - Case study 2**

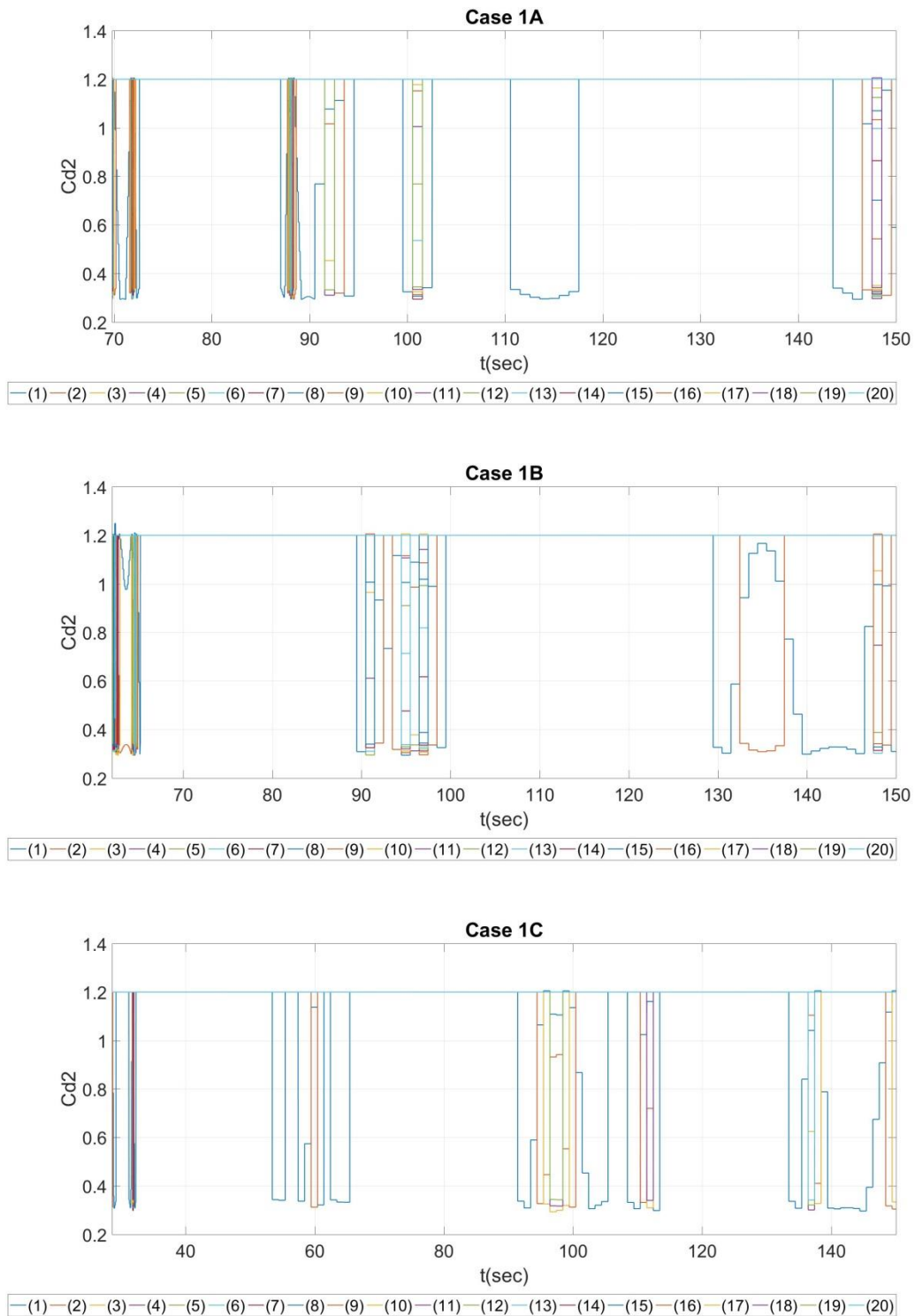


**Figure 54 Drag coefficient for spar hull upper part - Case study 1**

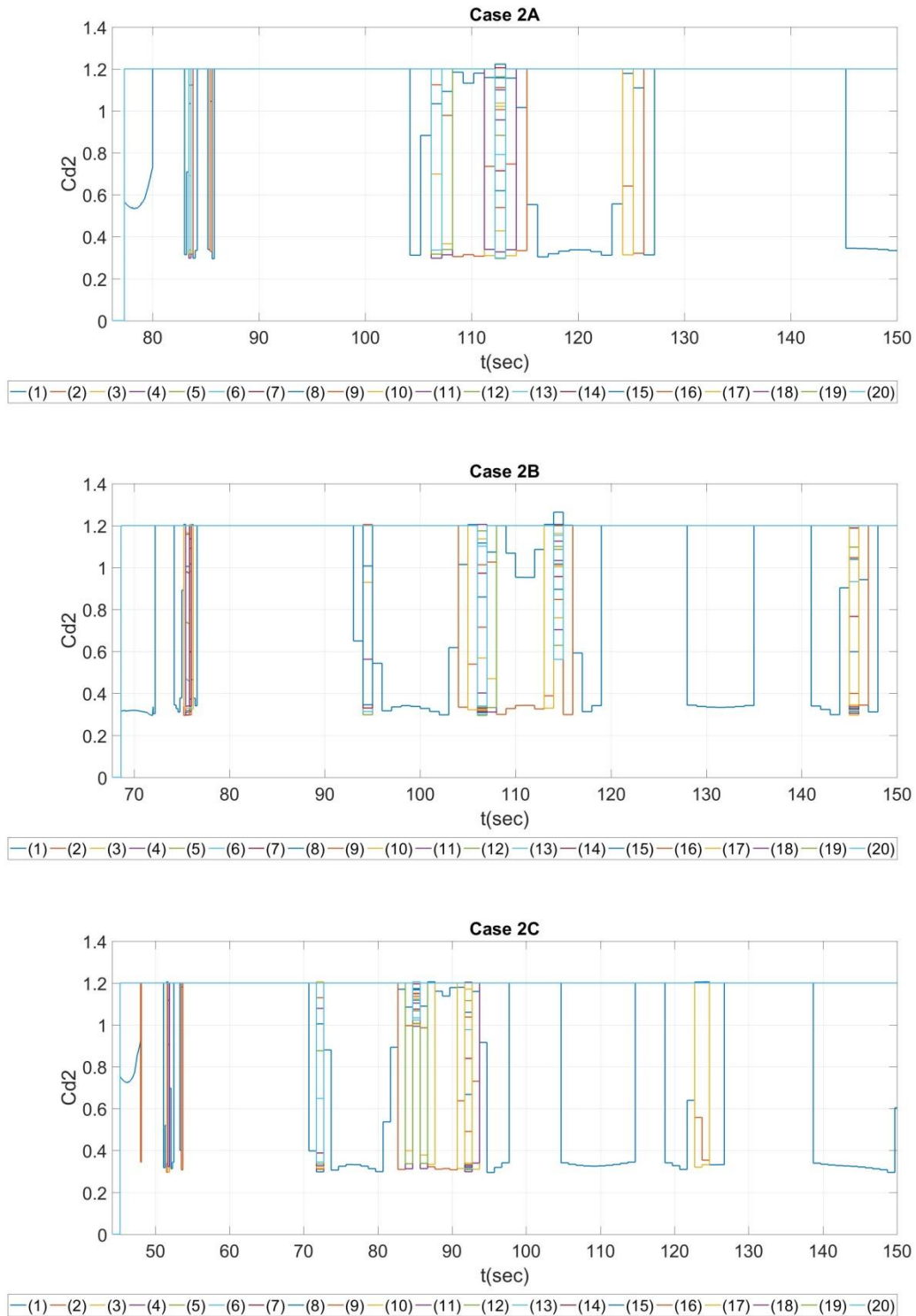




**Figure 55 Drag coefficient for spar hull upper part - Case study 2**



**Figure 56 Drag coefficient for spar hull lower part - Case study 1**



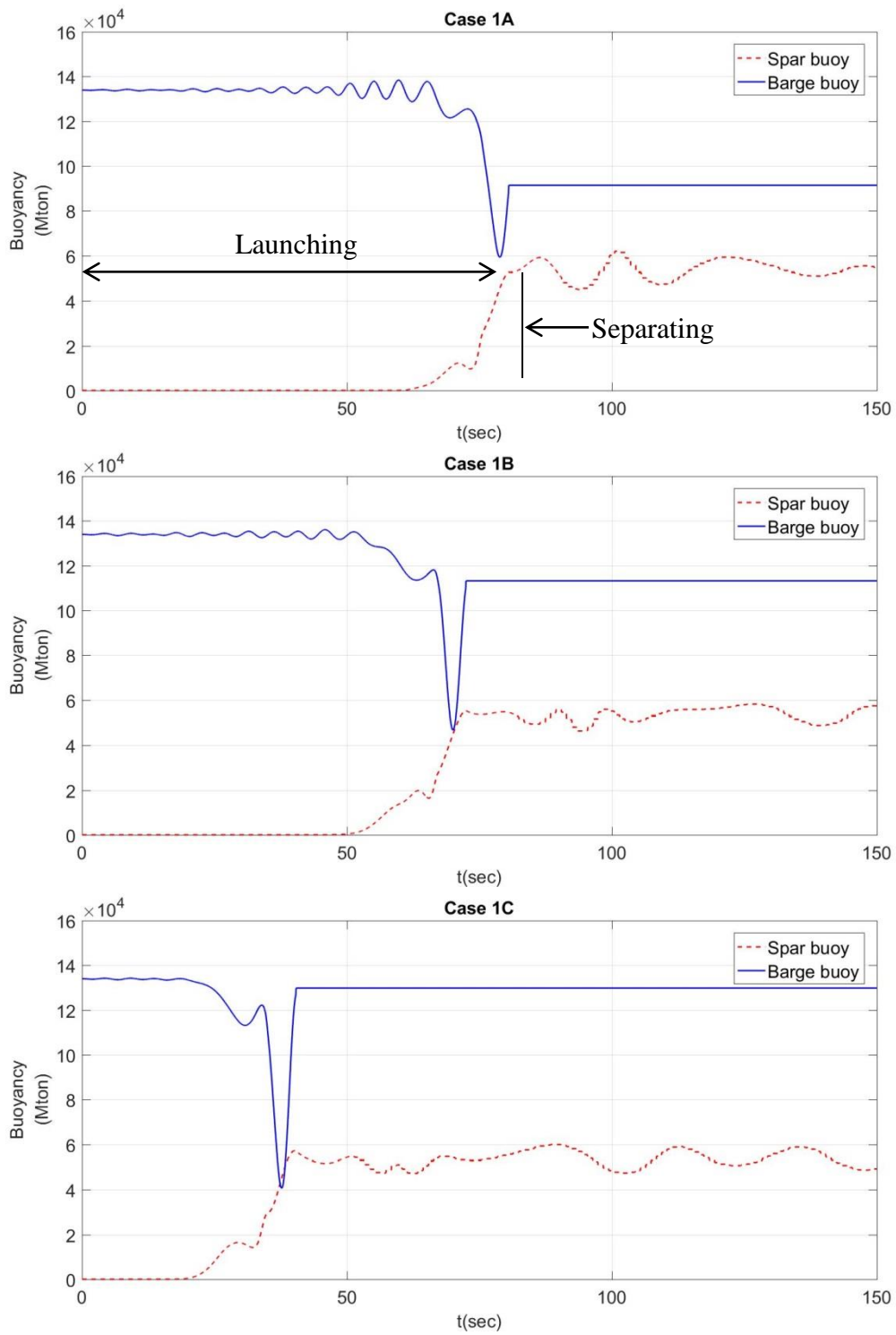
**Figure 57 Drag coefficient for spar hull lower part - Case study 2**

Figure 58 and Figure 59 show the time evolution of the buoyancy of the spar hull and barge. Figure 60 and Figure 61 show the time evolution of the center of buoyancy of the spar hull and the barge. The X and Z coordinates of the center of the buoyancy are indicated as distances in the global frame of reference relative to the CoG of each body. The center of buoyancy for the spar hull is far away from the CoG when the body is inclined with the larger submerged volume.

The spar buoyancy reaches a peak at the end of the launching when the spar hull starts to separate from the barge.

The spar hull center of buoyancy is far away from the CoG of the spar hull when the spar enters into the water. The barge center of buoyancy is far away from the CoG of the barge when the spar hull separates from the barge.

After the spar separates from the barge, the variation in the buoyancy and center of buoyancy mirror the oscillations of the spar hull.



**Figure 58 Buoyancy of spar hull and barge - Case study 1**

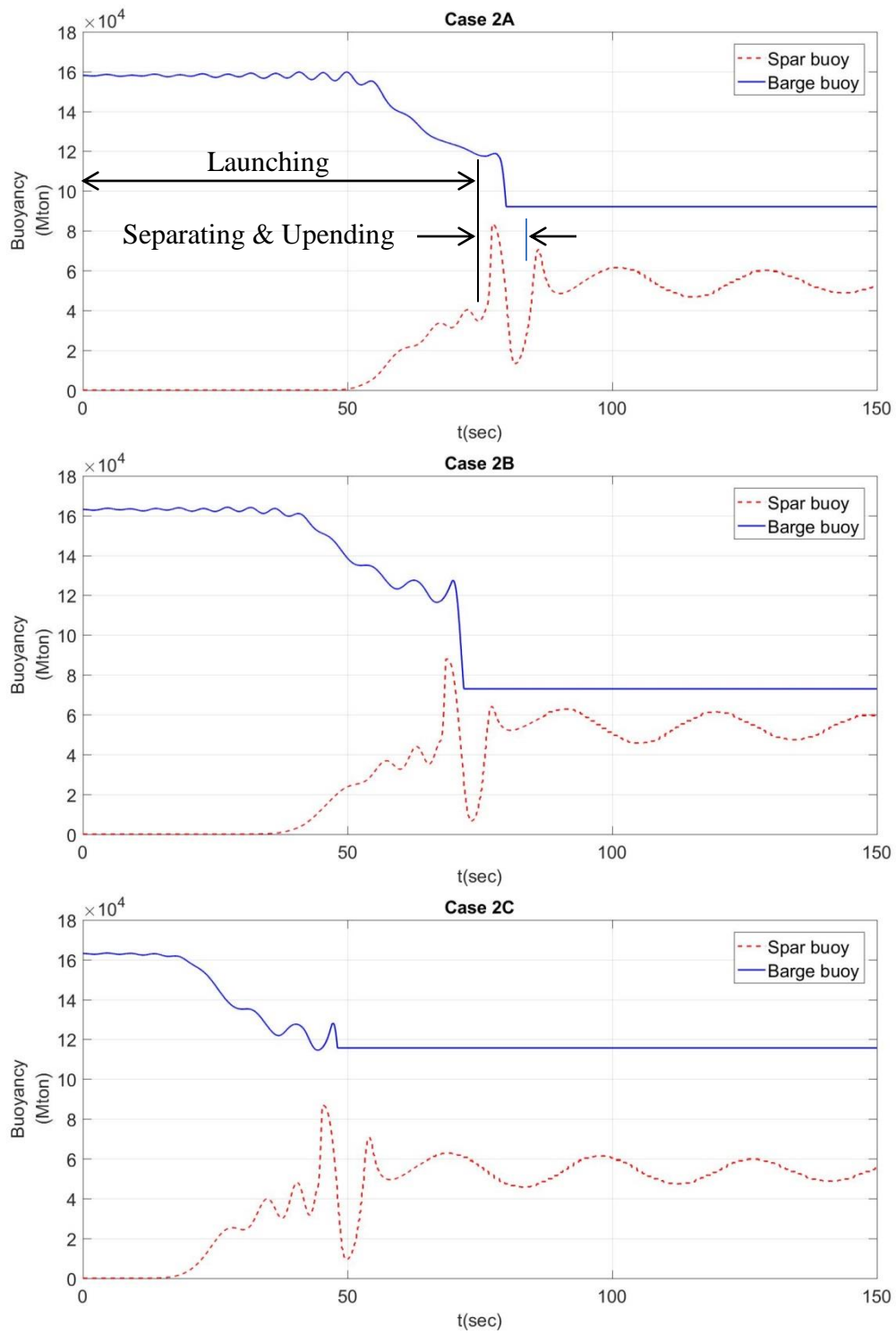


**Figure 59 Buoyancy of spar hull and barge - Case study 2**

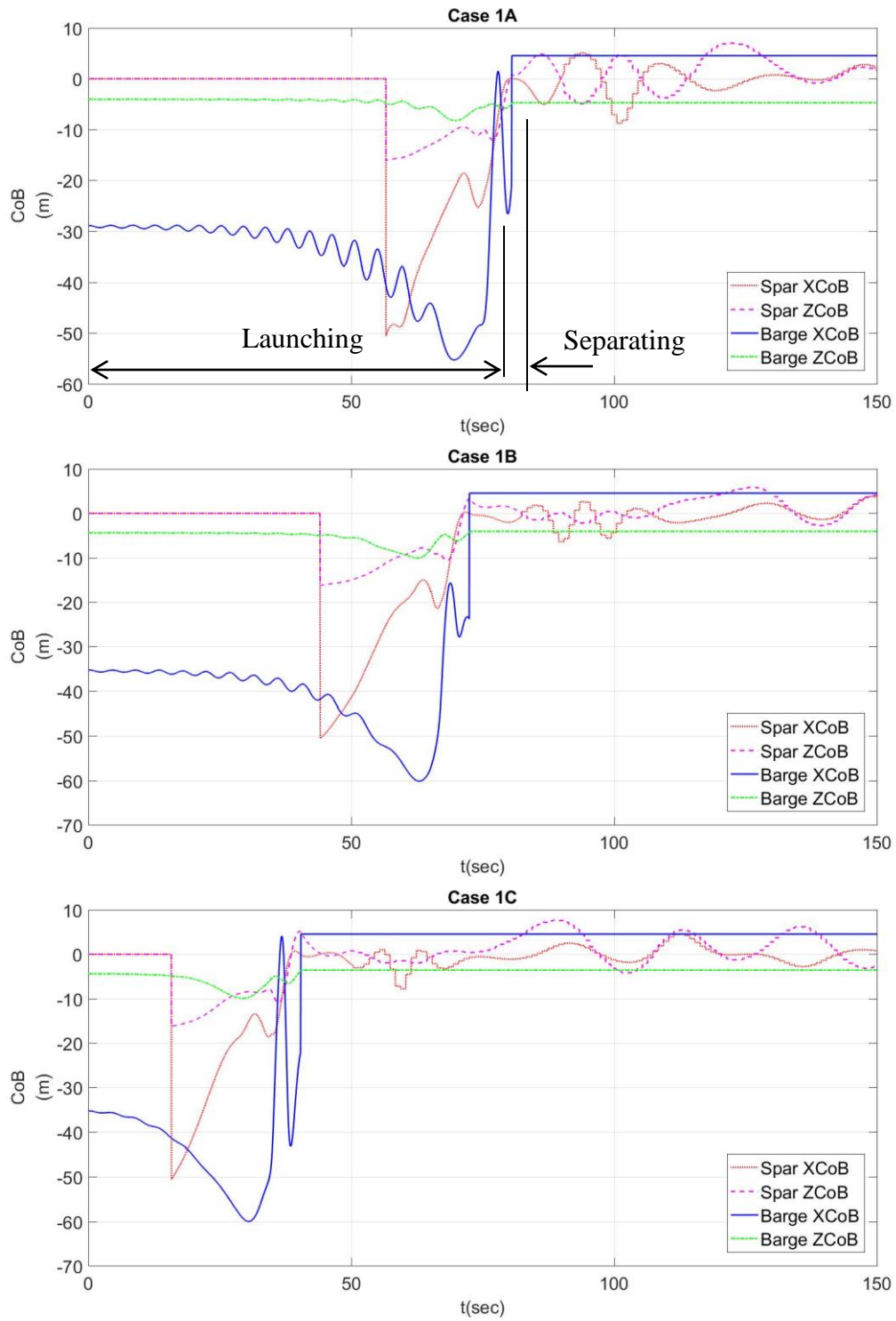


**Figure 60 Center of buoyancy of spar hull and barge - Case study 1**

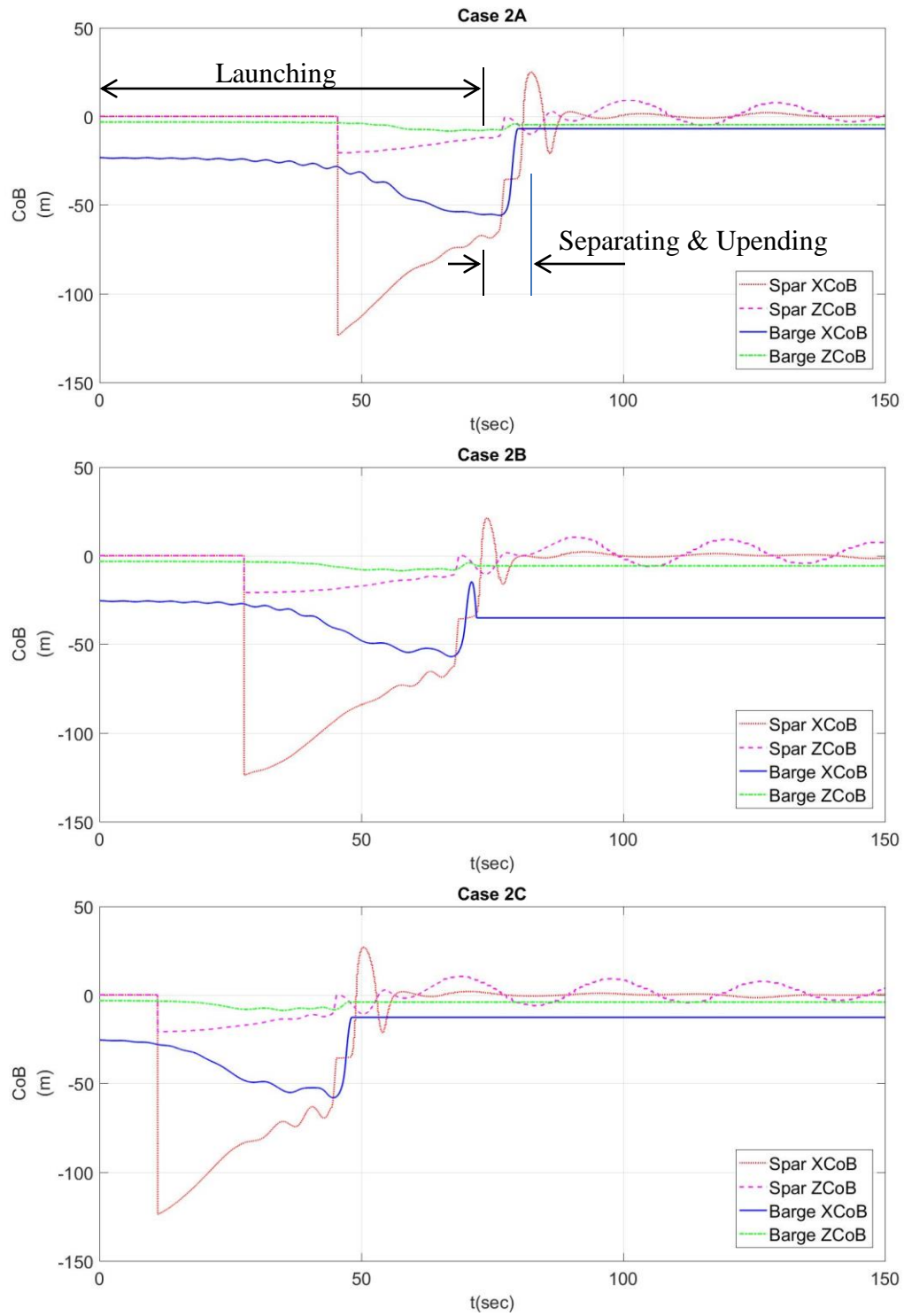


**Figure 61 Center of buoyancy of spar hull and barge - Case study 2**



### 5.3 Feasibility of Launching a Spar

For purposes of the numerical simulations, the kinetic friction coefficient should be set equal to the barge pitch trim angle (in radians) to ensure continuously smooth sliding of the spar hull. With two launch scenarios, this research investigated the sensitivity to pitch trim angle (0.05 and 0.06 radians) with the same friction coefficient (0.05 and 0.06) and an additional investigation was carried out on the pitch trim angle 0.06 radians with a friction coefficient 0.05. When lubricating oil is used, we can set the proper pitch trim angle at the start of the launching sequence with reference to the simulation model which is pretty rigorous and complete.

The essential differences between top launching and bottom launching are the initial condition and the X-direction velocity of the spar hull during launching. The initial trim angle (which affects the kinetic friction coefficient) controls the X-direction velocity which in turn affects the launching speed of the spar hull.

In the case of bottom launching, the primary rocker arm and the secondary rocker arm rotate methodically when the spar hull center of the gravity goes past the pivot point. In the case of top launching, due to the counter-moment from the spar buoyancy, the primary rocker arm and the secondary rocker arm will rotate when the end of the spar hull goes past each rocker arm pivot point. For the three top launch scenarios investigated herein, the secondary rocker arm did not rotate as the rotation of the primary rocker arm did not reach its 15-degree limit.

Although both top launching and bottom launching scenarios appear to be feasible, considering the launching velocity in Figure 38 and Figure 39, the top

launching scenario appears to be the preferred option to realize this advanced installation method.

## 6. CONCLUSIONS AND RECOMMENDATIONS

The aim of this research was to simulate the trajectories and analyze the relative parameters to assess the feasibility of barge-launching a spar hull. Two case studies were performed to investigate the optimization of the proper condition. The first case study is to launch a spar hull from the bottom. The second case study is to launch a spar hull from the top.

A rigorous mathematical model was developed based on formulation of the fundamental coupled equations of motion for the spar and barge. Numerical simulations of the two launch scenarios were conducted based on time integration of the equations of motion assuming a calm water condition. The simulated trajectories and time evolution of the forces on the spar and barge were examined in detail to verify consistency and assess critical transition points.

Launching operations start from the pre-launch condition by filling water into ballast tanks of the launch barge in order to trim the barge. The trim angle is equal to the coefficient of kinetic friction coefficient and a spar hull rests on the barge deck since the static friction is greater than the tangential component of the spar hull weight. Hydraulic jacks are commonly used in the launching of jacket-type offshore structures, and they are proposed here to push the spar hull on the barge deck and initiate the launch, as we'll as to avoid unfortunate accident due to the heavy weight of the spar hull. The hydraulic jack is used at the initial time for a short span of time to overcome the static friction and transition to kinetic friction.

Once the spar hull begins to move, the launch will proceed without any assistance. The spar hull will move continuously and the rocker arms will operate properly at the appropriate stage depending on the method of launching (top first or bottom first). After the spar hull separates from the rocker arms, the coupling forces are no longer in play and the spar hull will undergo damped oscillations before coming to rest floating in the upright position.

All six scenarios simulated herein resulted in a smooth and successful launching operation. It therefore appears that both top launching and bottom launching scenarios may be feasible. However considering the higher velocities associated with the bottom launching scenarios, the top launching method appears to be the preferred option. Other factors that need to be considered on a case-by-case basis but were not addressed herein include structural strength issues for the ballasted spar during launching, the construction yard capabilities, the offshore circumstances at the installation site, and the load-out and transportation of the spar from the construction yard to the installation site.

Further work is needed to refine and validate the modeling procedure developed in this thesis research. This could include extension of the model to three dimensional analyses to obtain more accurate results for the motions on the spar hull and barge, as well as experimental model testing to validate the numerical analyses. In addition, to realize this proposed installation method, global and local structure strength checks are needed considering in-service condition, pre-service condition and construction condition.

## REFERENCES

- Bhattacharyya, S. K., V.G. Idichandy & N. R. Joglekar (1985), "On experimental investigation of load-out, launching and upending of offshore steel jackets", Applied Ocean Research, Vol. 7, No.1, pp. 24 - 34
- Bentley (2013), H851, Library of Vessels, Ultramarine, <http://bentley.ultramarine.com/hdesk/tools/vessels/lbarges/h851.htm>
- Chakrabarti, S. K. (1994), "Scale effects on a unique launch sequence of a gravity-based structure", Applied Ocean Research 17, 33-41
- Edwards, Ken (2016), "Inclined cylinder volume calculation", LMNO Engineering, Research and software, Ltd., Ohio, USA, <http://www.lmnoeng.com/index.shtml>
- Faltinsen, O. M. (1990), "Sea loads on ships and offshore structures", Cambridge Ocean Technology Series, Cambridge University Press, Cambridge, New York
- Greenhow, M. (1988), "Water-entry and -exit of a horizontal circular cylinder", Applied Ocean Research, 1988, Vol. 10, No. 4, pp. 191-198.
- Greenhow, M. & Li, Y. (1987), "Added mass for circular cylinders near or penetrating fluid boundaries - review, extension and application to water-entry, -exit and slamming.", Ocean Engineering, 1987, Vol. 14, No 4, pp. 325-348.
- Hambro, L. (1982), "Jacket launching simulation by differentiation of constraints", Applied Ocean Research, Vol 4 Issue 3, July 1982, p 151-159
- Harris, John W. & Horst Stöcker (1998), "Handbook of mathematics and computational science", Springer, New York, 1998
- Jo, C. H., K. S. Kim & S. H. Lee (2001), "Parametric study on offshore jacket launching", Technical Note, Ocean Engineering, An International Journal of Research and Development, Vol 29 (2002) 1959-1979
- Koehler, B. R. & Kettleborough, C. F. (1977), "Hydrodynamic impact of a falling body upon a viscous incompressible fluid", Journal of Ship Research, Vol. 21, No. 3, pp. 165-181.
- Miloh, T. (1981), "Wave slam on a sphere penetrating a free-surface", Journal of Engineering Mathematics, Vol. 15, No. 3, pp. 221-240.

Morison, J. R., M. P. O'Brien, J. W. Johnson & S. A. Schaaf (1950), "The force exerted by surface waves on piles", U.C Berkeley, California, Petroleum Transactions, Aime, Vol. 189, 1950

Noble Denton & Associates Inc. (2009), Technical Policy Board, "Guidelines for the transportation and installation of steel jackets", 0025/ND, [www.nobledenton.com](http://www.nobledenton.com)

Press, William H., Saul A. Teukolsky, William T. Vetterling & Brian P. Flannery (2007), "Numerical recipes - The art of scientific computing", 3rd Edition, Cambridge University Press, Cambridge, UK, Cambridge, New York, USA

Vasicek , Daniel & C. H. Lu (1979), "Launch and flotation analysis of offshore structures part 2 - barge and jacket interaction on launch analysis", Petroleum Engineer International, May 1979, No. 6, vol. 51, pp. 10-16

Verhagen, J. H. G. (1967), "The impact of a flat plate on a water surface", Journal of Ship Research, Vol. 11, No. 4, pp. 211-223

Von Karman, T. (1929), "The impact of seaplane floats during landing", NACA, Technical Note 321, Aerodynamical Institute of the Technical High School, Aachen, Washington DC

WAMIT User Manual Version 7.0 (2013), WAMIT, Inc., Chestnut Hill, MA, USA, [www.wamit.com](http://www.wamit.com)

APPENDIX A - BALLASTING PLAN TABLE

**Table A 1 Ballast plan for Case 1A**

Ballasting plan for Case study 1A					
Tank No.	Weight (Mton)	XCoG (m) From Barge Origin	YCoG (m)	ZCoG (m) From Keel	Filled Ratio
psc1	221.9766	129.89	10.50	0.38	0.05
sbc1	221.9766	129.89	-10.50	0.38	0.05
psc2	201.7969	110.51	15.75	0.38	0.05
sbc2	201.7969	110.51	-15.75	0.38	0.05
psw2	201.7969	110.51	26.25	0.38	0.05
sbw2	201.7969	110.51	-26.25	0.38	0.05
psc3	403.5937	85.51	10.50	0.38	0.05
sbc3	403.5937	85.51	-10.50	0.38	0.05
psw3	201.7969	85.51	26.25	0.38	0.05
sbw3	201.7969	85.51	-26.25	0.38	0.05
psc4	403.5937	60.51	10.50	0.38	0.05
sbc4	403.5937	60.51	-10.50	0.38	0.05
psw4	201.7969	60.51	26.25	0.38	0.05
sbw4	201.7969	60.51	-26.25	0.38	0.05
psc5	403.5937	35.51	10.50	0.38	0.05
sbc5	403.5937	35.51	-10.50	0.38	0.05
psw5	201.7969	35.51	26.25	0.38	0.05
sbw5	201.7969	35.51	-26.25	0.38	0.05
psc6	201.7969	10.51	15.75	0.38	0.05
sbc6	201.7969	10.51	-15.75	0.38	0.05
psw6	201.7969	10.51	26.25	0.38	0.05
sbw6	201.7969	10.51	-26.25	0.38	0.05
pso6	201.7969	10.51	5.25	0.38	0.05
sbo6	201.7969	10.51	-5.25	0.38	0.05
psc7	201.7969	-14.49	15.75	0.38	0.05
sbc7	201.7969	-14.49	-15.75	0.38	0.05
psw7	3326.1655	-14.49	26.25	6.18	0.8241
sbw7	3326.1655	-14.49	-26.25	6.18	0.8241

psc8	403.5937	-39.49	10.50	0.38	0.05
sbc8	403.5937	-39.49	-10.50	0.38	0.05
psw8	201.7969	-39.49	26.25	0.38	0.05
sbw8	201.7969	-39.49	-26.25	0.38	0.05
psc9	403.5937	-64.49	10.50	0.38	0.05
sbc9	403.5937	-64.49	-10.50	0.38	0.05
psw9	1737.6965	-64.49	26.25	3.23	0.4306
sbw9	1737.6965	-64.49	-26.25	3.23	0.4306
psc10	5650.3125	-89.49	10.50	5.25	0.7
sbc10	5650.3125	-89.49	-10.50	5.25	0.7
psw10	201.7969	-89.49	26.25	0.38	0.05
sbw10	201.7969	-89.49	-26.25	0.38	0.05
psc11	171.5273	-112.61	15.75	0.38	0.05
sbc11	171.5273	-112.61	-15.75	0.38	0.05
psw11	171.5273	-112.61	26.25	0.38	0.05
sbw11	171.5273	-112.61	-26.25	0.38	0.05
c11	343.0547	-112.61	0	0.38	0.05
Total	31376.935	-38.57	0	3.68	

**Table A 2 Ballast plan for Case 1B & 1C**

Ballasting plan for Case study 1B & 1C					
Tank No.	Weight (Mton)	XCoG (m) From Barge Origin	YCoG (m)	ZCoG (m) From Keel	Filled Ratio
psc1	221.9766	129.89	10.50	0.38	0.05
sbc1	221.9766	129.89	-10.50	0.38	0.05
psc2	201.7969	110.51	15.75	0.38	0.05
sbc2	201.7969	110.51	-15.75	0.38	0.05
psw2	201.7969	110.51	26.25	0.38	0.05
sbw2	201.7969	110.51	-26.25	0.38	0.05
psc3	403.5937	85.51	10.50	0.38	0.05
sbc3	403.5937	85.51	-10.50	0.38	0.05
psw3	201.7969	85.51	26.25	0.38	0.05
sbw3	201.7969	85.51	-26.25	0.38	0.05
psc4	403.5937	60.51	10.50	0.38	0.05



sbc4	403.5937	60.51	-10.50	0.38	0.05
psw4	201.7969	60.51	26.25	0.38	0.05
sbw4	201.7969	60.51	-26.25	0.38	0.05
psc5	403.5937	35.51	10.50	0.38	0.05
sbc5	403.5937	35.51	-10.50	0.38	0.05
psw5	201.7969	35.51	26.25	0.38	0.05
sbw5	201.7969	35.51	-26.25	0.38	0.05
psc6	201.7969	10.51	15.75	0.38	0.05
sbc6	201.7969	10.51	-15.75	0.38	0.05
psw6	201.7969	10.51	26.25	0.38	0.05
sbw6	201.7969	10.51	-26.25	0.38	0.05
ps06	201.7969	10.51	5.25	0.38	0.05
sbo6	201.7969	10.51	-5.25	0.38	0.05
psc7	201.7969	-14.49	15.75	0.38	0.05
sbc7	201.7969	-14.49	-15.75	0.38	0.05
psw7	201.7969	-14.49	26.25	0.38	0.05
sbw7	201.7969	-14.49	-26.25	0.38	0.05
psc8	403.5937	-39.49	10.50	0.38	0.05
sbc8	403.5937	-39.49	-10.50	0.38	0.05
psw8	201.7969	-39.49	26.25	0.38	0.05
sbw8	201.7969	-39.49	-26.25	0.38	0.05
psc9	403.5937	-64.49	10.50	0.38	0.05
sbc9	403.5937	-64.49	-10.50	0.38	0.05
psw9	201.7969	-64.49	26.25	0.38	0.05
sbw9	201.7969	-64.49	-26.25	0.38	0.05
psc10	3228.7500	-89.49	10.50	3.00	0.4
sbc10	3228.7500	-89.49	-10.50	3.00	0.4
psw10	844.5337	-89.49	26.25	1.57	0.2093
sbw10	844.5337	-89.49	-26.25	1.57	0.2093
psc11	2058.3281	-112.61	15.75	4.50	0.6
sbc11	2058.3281	-112.61	-15.75	4.50	0.6
psw11	2530.7257	-112.61	26.25	5.53	0.7377
sbw11	2530.7257	-112.61	-26.25	5.53	0.7377
c11	4802.7656	-112.61	0	5.25	0.7
Total	31450.457	-65.71	0	3.10	

**Table A 3 Ballast plan for Case 2A**

Ballasting plan for Case study 2A					
Tank No.	Weight	XCoG	YCoG	ZCoG	Filled Ratio
		(m) From Barge Origin	(m)	(m) From Keel	
psc1	221.9766	129.89	10.5	0.38	0.05
sbc1	221.9766	129.89	-10.5	0.38	0.05
psc2	201.7969	110.51	15.75	0.38	0.05
sbc2	201.7969	110.51	-15.75	0.38	0.05
psw2	201.7969	110.51	26.25	0.38	0.05
sbw2	201.7969	110.51	-26.25	0.38	0.05
psc3	403.5937	85.51	10.5	0.38	0.05
sbc3	403.5937	85.51	-10.5	0.38	0.05
psw3	201.7969	85.51	26.25	0.38	0.05
sbw3	201.7969	85.51	-26.25	0.38	0.05
psc4	403.5937	60.51	10.5	0.38	0.05
sbc4	403.5937	60.51	-10.5	0.38	0.05
psw4	201.7969	60.51	26.25	0.38	0.05
sbw4	201.7969	60.51	-26.25	0.38	0.05
psc5	403.5937	35.51	10.5	0.38	0.05
sbc5	403.5937	35.51	-10.5	0.38	0.05
psw5	201.7969	35.51	26.25	0.38	0.05
sbw5	201.7969	35.51	-26.25	0.38	0.05
psc6	201.7969	10.51	15.75	0.38	0.05
sbc6	201.7969	10.51	-15.75	0.38	0.05
psw6	201.7969	10.51	26.25	0.38	0.05
sbw6	201.7969	10.51	-26.25	0.38	0.05
pso6	201.7969	10.51	5.25	0.38	0.05
sbo6	201.7969	10.51	-5.25	0.38	0.05
psc7	201.7969	-14.49	15.75	0.38	0.05
sbc7	201.7969	-14.49	-15.75	0.38	0.05
psw7	201.7969	-14.49	26.25	0.38	0.05
sbw7	201.7969	-14.49	-26.25	0.38	0.05
psc8	403.5937	-39.49	10.5	0.38	0.05
sbc8	403.5937	-39.49	-10.5	0.38	0.05
psw8	201.7969	-39.49	26.25	0.38	0.05
sbw8	201.7969	-39.49	-26.25	0.38	0.05

psc9	403.5937	-64.49	10.5	0.38	0.05
sbc9	403.5937	-64.49	-10.5	0.38	0.05
psw9	3802.3883	-64.49	26.25	7.07	0.9421
sbw9	3802.3883	-64.49	-26.25	7.07	0.9421
psc10	7910.4375	-89.49	10.5	7.35	0.98
sbc10	7910.4375	-89.49	-10.5	7.35	0.98
psw10	2030.7668	-89.49	26.25	3.77	0.5032
sbw10	2030.7668	-89.49	-26.25	3.77	0.5032
psc11	3156.1031	-112.61	15.75	6.90	0.92
sbc11	3156.1031	-112.61	-15.75	6.90	0.92
psw11	3156.1031	-112.61	26.25	6.90	0.92
sbw11	3156.1031	-112.61	-26.25	6.90	0.92
c11	6449.4281	-112.61	0	7.05	0.94
Total	55480.448	-74.80	0	5.79	

**Table A 4 Ballast plan for Case 2B & 2C**

Ballasting plan for Case study 2B & 2C					
Tank No.	Weight	XCoG	YCoG	ZCoG	Filled Ratio
		(m) From Barge Origin	(m)	(m) From Keel	
psc1	221.9766	129.89	10.5	0.38	0.05
sbc1	221.9766	129.89	-10.5	0.38	0.05
psc2	201.7969	110.51	15.75	0.38	0.05
sbc2	201.7969	110.51	-15.75	0.38	0.05
psw2	201.7969	110.51	26.25	0.38	0.05
sbw2	201.7969	110.51	-26.25	0.38	0.05
psc3	403.5937	85.51	10.5	0.38	0.05
sbc3	403.5937	85.51	-10.5	0.38	0.05
psw3	201.7969	85.51	26.25	0.38	0.05
sbw3	201.7969	85.51	-26.25	0.38	0.05
psc4	403.5937	60.51	10.5	0.38	0.05
sbc4	403.5937	60.51	-10.5	0.38	0.05
psw4	201.7969	60.51	26.25	0.38	0.05
sbw4	201.7969	60.51	-26.25	0.38	0.05
psc5	403.5937	35.51	10.5	0.38	0.05

sbc5	403.5937	35.51	-10.5	0.38	0.05
psw5	201.7969	35.51	26.25	0.38	0.05
sbw5	201.7969	35.51	-26.25	0.38	0.05
psc6	201.7969	10.51	15.75	0.38	0.05
sbc6	201.7969	10.51	-15.75	0.38	0.05
psw6	201.7969	10.51	26.25	0.38	0.05
sbw6	201.7969	10.51	-26.25	0.38	0.05
pso6	201.7969	10.51	5.25	0.38	0.05
sbo6	201.7969	10.51	-5.25	0.38	0.05
psc7	201.7969	-14.49	15.75	0.38	0.05
sbc7	201.7969	-14.49	-15.75	0.38	0.05
psw7	201.7969	-14.49	26.25	0.38	0.05
sbw7	201.7969	-14.49	-26.25	0.38	0.05
psc8	403.5937	-39.49	10.5	0.38	0.05
sbc8	403.5937	-39.49	-10.5	0.38	0.05
psw8	201.7969	-39.49	26.25	0.38	0.05
sbw8	201.7969	-39.49	-26.25	0.38	0.05
psc9	1614.3750	-64.49	10.5	1.50	0.2
sbc9	1614.3750	-64.49	-10.5	1.50	0.2
psw9	3304.5385	-64.49	26.25	6.14	0.8188
sbw9	3304.5385	-64.49	-26.25	6.14	0.8188
psc10	7937.8819	-89.49	10.5	7.38	0.9834
sbc10	7937.8819	-89.49	-10.5	7.38	0.9834
psw10	3809.6958	-89.49	26.25	7.08	0.9439
sbw10	3809.6958	-89.49	-26.25	7.08	0.9439
psc11	3163.9934	-112.61	15.75	6.92	0.9223
sbc11	3163.9934	-112.61	-15.75	6.92	0.9223
psw11	3163.9934	-112.61	26.25	6.92	0.9223
sbw11	3163.9934	-112.61	-26.25	6.92	0.9223
c11	6463.8364	-112.61	0	7.07	0.9421
Total	60565.027	-82.38	0	6.36	

## APPENDIX B - VITA

Sanghun Son was born on June 30, 1980 in Busan, South Korea. In February of 2007 he was awarded his B.S. degree in Naval Architecture and Ocean Engineering from Inha University. From January of 2007 he started working in the offshore structure basic design and engineering department of the offshore division of Hyundai Heavy Industries Co. Ltd. in South Korea until August of 2014 when he enrolled the graduate program at Texas A&M University in September 2014. His last position was the lead structure engineer for DSO project of Chevron Co.

In 2009, he successfully completed the development of Local Scantling Calculation Check Program to evaluate double hull tankers with Common Structural Rules and he is the one of inventors for a patent titled “Database Design Method for Shipped Structure Weight Data” which was registered in South Korea in 2014 when he worked in Hyundai Heavy Industries, Co. Ltd.

From February of 2017 he started working as a manager in the energy and shipbuilding materials solution marketing department of POSCO, which is the largest leading steel manufacturer in the world, in South Korea.

His permanent address is 45, Cheongnyong-ro 53beon-gil, Namsan-dong, Geumjeong-gu, Busan, 46217, South Korea. His email is worldbestson@gmail.com.